2019

Land change and carbon dynamics in the Colombian Amazon

BOSTON UNIVERSITY

GRADUATE SCHOOL OF ARTS AND SCIENCES

Dissertation

LAND CHANGE AND CARBON DYNAMICS IN THE COLOMBIAN AMAZON

by

PAULO ARTURO ARÉVALO ORDUZ

B.Sc., Pontificia Universidad Javeriana, 2010

Submitted in partial fulfillment of the

requirements for the degree of

Doctor of Philosophy

2019

Approved by

First Reader

Pontus Olofsson, Ph.D.
Research Associate Professor of Earth and Environment

Second Reader

Mark A. Friedl, Ph.D.
Professor of Earth and Environment

Third Reader

Lucy Hutyra, Ph.D.
Associate Professor of Earth and Environment

Fourth Reader

Richard A. Houghton, Ph.D.
Senior Scientist
George M. Woodwell Chair for Global Ecology
Woods Hole Research Center

DEDICATION

To my loving family. My heart is with all of you, always.

Dedicado a mi familia. Mi corazón está con ustedes, siempre.

ACKNOWLEDGMENTS

I have had the immense privilege of working with, learning from and being inspired by many people during my time at Boston University. I would like to thank all the faculty members that taught me so much and exposed me to so many fascinating research topics, and especially my committee members for their feedback and guidance to make this work possible. Special thanks to Chris Holden for his technical guidance, the countless things I learned from him and the code that greatly facilitated my work. To Eric Bullock for his constant help, for his company in these five years and the great times we have had that made this experience so much more enriching and special.

I would also like to thank all my colleagues and staff for their advice, especially the members of my research group. Thanks to Xiaojing Tang for his contributions, particularly in the last stages of my dissertation. To Valerie Pasquarella for her help and the inspiring conversations. Thanks to Betsy Cowdery and Radost Stanimirova for all the support and help, to Alexey Shiklomanov and Andrew Trlica for sharing this journey together, and to all of my department colleagues. Also, thanks to Alissa Beideck, Frederick George III and Matthew Dicintio for the help in navigating university procedures and making it all work smoothly behind the scenes.

To my family for their support over the years, I would not be here without their help, their patience and understanding. Especially to my mom, Fabiola Orduz, for her dedication and sacrifice.

My time as a PhD student at Boston University was the most exciting and enriching time of my adult life so far, but it was also marked by periods of significant

hardship. I am grateful for all the people that whose supportive presence contributed to the completion of this dissertation. Thanks to Jeb Taylor for his love and support during these years. To Brad Conner for his constant presence, especially in the most difficult times. To my friends Paul Fahey and Jared Katz, who accompanied me in key moments of this journey. And to my friend Liz Murcia, her encouragement and positive influence is always there, even in the distance.

Finally, a special note of gratitude for my advisors Pontus Olofsson and Curtis Woodcock. My time at Boston University exceeded all expectations in great part thanks to their thoughtful guidance, their constant support, their approach to provoking questions and planting new seeds of academic curiosity. I thank Pontus for opening the doors to so many enriching experiences that have greatly contributed to my personal and professional development. And I am forever grateful with Curtis for his patience, his mentoring, and his incredible support and understanding in the most challenging times.

LAND CHANGE AND CARBON DYNAMICS IN THE COLOMBIAN AMAZON

PAULO ARTURO ARÉVALO ORDUZ

Boston University Graduate School of Arts and Sciences, 2019

Major Professor: Pontus Olofsson, Ph.D.
Research Associate Professor of Earth and Environment

ABSTRACT

Tropical deforestation is a significant source of CO_2 emissions to the atmosphere. Quantifying land use changes and associated emissions is critical for reporting and reducing emissions of greenhouse gases. In the Colombian Amazon, areas of forest conversion estimated at biennial intervals using a combination of dense time series of Landsat observations and statistical estimators based on reference data indicate that deforestation is modest (87 kha $year^{-1}$) relative to surrounding countries and regions. Other land cover and change areas can also be estimated at biennial intervals, including a land cover class representing regrowing secondary forest, which is on average five times larger than the forest-to-pasture conversion. Areas of gain and loss of secondary forest are very small for this region relative to deforestation.

Errors in the detection of change negatively impact the precision of the land change area estimates. New methods estimate the uncertainty associated with maps of land change, represented as probability maps of omission and commission of change. These probabilities are higher in the deforestation frontier of the study area, where the fine spatial scale of the disturbances and the low temporal data density make it challenging to detect the changes accurately. The presented methods improve our ability

to integrate uncertainty into applications that make use land change maps, such as spatial carbon models.

Methods to estimate emissions based on bias-adjusted areas of land change show that net carbon emissions average 10 Tg $year^{-1}$ (0.22 Mg ha^{-1} $year^{-1}$) in the entire study area, and can be further disaggregated by the land cover contributing to the emissions or removals. This dissertation shows that the conversion from forest to pastures has been the largest forest loss pathway in the Colombian Amazon for almost two decades. While there is a small carbon offset due to sequestration by regrowing forests, conversion to pasture is also the main source of carbon emissions associated with land change. The methods and results presented in this dissertation demonstrate the potential of the Landsat archive to enable the quantification of land changes, their uncertainty, and their associated carbon emissions, even in areas with relatively infrequent cloud-free observations.

TABLE OF CONTENTS

LIST OF TABLES

LIST OF FIGURES

LIST OF ABBREVIATIONS

AGB .....Aboveground Biomass

BFAST ..... Breaks For Additive Season and Trend

CCDC.....Continuous Change Detection and Classification

CODED.....Continuous Degradation Detection

EROS..... Earth Resources Observation and Science

ESPA.....EROS Science Processing Architecture

ETM+..... Enhanced Thematic Mapper

FREL..... Forest Reference Emission Level

GFOI .....Global Forest Observation Initiative

IDEAM.....Instituto de Hidrología, Meteorología y Estudios Ambientales.

IPCC..... Intergovernmental Panel on Climate Change

MODIS.....Moderate Resolution Imaging Spectroradiometer

MRV ..... Monitoring, Reporting and Verification

NIR.....Near Infrared

OLI.....Operational Land Imager

OLS..... Ordinary Least Squares

REDD.....Reducing Emissions from Deforestation and forest Degradation

RMSE..... Root-Mean-Square Error

SWIR.....Short Wave Infrared

UNFCCC..... United Nations Framework Convention on Climate Change

USGS..... United State Forest Service

WRS2..... World Reference System-2

YATSM..... Yet Another Time Series Model

CHAPTER 1: INTRODUCTION

Tropical deforestation accounts for 7 - 14% of the CO_2 emissions released into the atmosphere by human activities (Achard et al., 2014; Goetz et al., 2015; Harris et al., 2012). Terrestrial ecosystems currently act as a net sink of carbon despite land use and land cover change-related carbon emissions (Le Quéré et al., 2009), but the net flux of carbon between land and atmosphere due to land use and land cover change is the most uncertain term in the global carbon budget (Houghton et al., 2012). This uncertainty is mostly due to inadequate data on carbon density of forests and regional rates of deforestation (Baccini et al., 2012a), inadequate methods for monitoring of forest degradation (Bullock et al., 2018), inadequate characterization of post-disturbance landscapes including processes like regeneration and shifting cultivation (Arneth et al., 2017), and inadequate treatment of errors and bias in maps derived from remote sensing data (Olofsson et al., 2013). The research presented in this dissertation aims to advance the monitoring of forests and terrestrial carbon by implementing new and exciting approaches to satellite data analysis and statistical inference. Recent methods based on analysis of time series of satellite data have the potential to improve our understanding of land change by providing information that allow us to reconstruct the land history at the pixel level. These kinds of approaches enable a more comprehensive analysis of the landscape including the mapping and monitoring of dynamic and transitional land processes like vegetation regrowth and degradation, which are inherently difficult to map but may result in substantial carbon emissions and/or removals from the atmosphere

(Pearson et al., 2017; Poorter et al., 2016). Temporally consistent maps of land cover and land change created with time series methods can be used in conjunction with statistical methods and reference data to accommodate classification errors and provide bias-adjusted area estimates of land change with quantified uncertainties. Area estimation is a key component to determine the historical carbon fluxes associated with land change, and it is typically conducted in conjunction with an accuracy assessment of the land cover classes (or changes) being evaluated.

1.1 Time series analysis of remote sensing data

The opening of the Landsat archive in 2008 (Woodcock et al., 2008) has enabled the development of new algorithms that rely on dense time series of Landsat observations to analyze changes on the land surface. These algorithms use a variety of statistical techniques to detect signals that represent a change on Earth's surface in the form of change in land cover, land use and management, or land condition (referred to land change throughout this dissertation). Two general approaches have been used to process and extract information for remote sensing time series. First, composite-based approaches use a statistic (e.g. median) for a fixed number of observations, or the "best" images according to some criterion (e.g. cloud cover) (Griffiths et al., 2014; Huang et al., 2010; Kennedy et al., 2010). The main advantage of compositing is the avoidance of clouds and a reduction of data to be analyzed, which enables large-scale mapping (Hansen et al., 2013; Kim et al., 2014) but at the expense of losing intra-annual information (e.g. seasonality, phenology, etc.). The second category include approaches that use all

available observations. Such approaches are more computationally expensive and require detailed cloud and cloud shadow screening, but enable the study of phenology and seasonality, as well as a more detailed analysis of landscapes that experience rapid change (GFOI, 2016). Examples include BFAST (DeVries et al., 2015; Verbesselt et al., 2010a), CCDC/YATSM (Holden, 2016a; Zhu and Woodcock, 2014a) and CODED (Bullock et al., 2018). Furthermore, high frequency observations allow the characterization of intra-annual trends and changes, helping distinguish long-term trends from short-lived disturbances, or even noise (Verbesselt et al., 2010b; Zhu, 2017). Such methods have enabled the separation of spectrally similar land cover classes that differ in their seasonal patterns, improving the mapping of forest types and ecosystem state and dynamics (Pasquarella et al., 2018, 2016). Time series analysis allows the continuous tracking of land change activities, which enables a more comprehensive characterization of the land history –such as the detection of subtle transitions like forest recovery and forest degradation (Bullock et al., 2018; Kennedy et al., 2010) – compared to traditional mapping methods. In addition, the use of temporal segments allows for the creation of temporally consistent land cover maps that are less subject to the spectral variability in the data. Temporally consistent maps are important for the continuous monitoring of land cover classes, as they facilitate the comparisons of maps over time. The use of temporal segments also opens the possibility to characterize carbon dynamics at the pixel level. While these methods have been tested and proven useful in many locations around the world, few published articles have applied time series algorithms that use all the available

observations in a tropical region, where the lower historical data availability and the higher incidence of clouds may hamper their utility.

1.2 Area estimation

Even with modern image-processing techniques and high quality remote sensing data, maps created using remote sensing data will always exhibit some degree of error. Errors arise from imperfections in the input data, training data and the mapping process, and from the inherently complex task of classifying continuously varying landscape features, often without clear boundaries, into discrete map classes. Because the effect of classification errors, estimating the area of a specific map class by methods that sum pixel values for map units assigned to that class (referred to as "pixel-counting") is a biased procedure that produces erroneous area estimates because the effects of classification errors are ignored (GFOI 2016). To accommodate the effects of map classification errors, areas of landscape features require estimation by application of an unbiased estimator to sample data (Olofsson et al., 2014). The use of unbiased estimators is therefore crucial for applications that require reliable values of land change area and their uncertainty, such as those related to carbon emission reporting. The uncertainty in area estimates is expressed as a confidence interval that is estimated using the variance estimator corresponding to the sample design. The sampling design should be chosen to take into account the specific objectives and priorities of the analysis (e.g. estimation of stable or change area, or map accuracy). Several designs are available but stratified random sampling is commonly used as it satisfies multiple designs criteria (Olofsson et

al., 2014). Once the sample is generated, reference land conditions are recorded at each sample unit. Recommendations, examples and good practices for estimating the area of land change are available in the literature (Olofsson et al., 2014), and have become standard practice for reporting of map accuracies and estimating areas of change. The body of literature applying these principles as well as time series algorithms is ample (Table 1-1.). However, most of these studies have been conducted in the United States with relatively few examples from REDD+ countries, with the exception of those pertaining to the Mexican carbon monitoring system (Gebhardt et al., 2014) and the Peruvian forest monitoring system (Potapov et al., 2014).

Article	**Algorithm**	**Mapping frequency**	**Sampling design**	**Area estimation**	**LCC**	**Scale**
(Cohen et al., 2016)	TimeSync only	Annual, 1985-2012	Two stage cluster sampling. Stratified by ecoregion. Interpreted annually.	Annual, sample based	Forest disturbance by type	CONUS
(Masek et al., 2013)	VCT	Annual, 1985-2005	Stratified random, based on forest types	Annual, sample based	Forest disturbance by type	CONUS
(Hansen et al., 2014)	Multi-temporal spectral metrics	2006-2010	Stratified sampling (bare cover, forest cover)	One period with CI's. Annual, probably from maps.	Forest cover	CONUS
(Hansen et al., 2013)	Multi-temporal spectral metrics	Annual, 2000-2015	Stratified random for accuracies and errors.	Annual, map based	Forest gain and loss	Global
(DeVries et al., 2015)	BFAST	Annual, 1999–2013	No sampling	Annual, map based	Forest loss and regrowth	Peru, two path/rows

Article	Algorithm	Mapping frequency	Sampling design	Area estimation	LCC	Scale
(Olofsson et al., 2016)	CCDC	One period, 1986-2011	Stratified random, based on map classes	One period, sample based	Multiple land cover classes	New England
(Sleeter et al., 2013)	NLCD	1973–2000, 4 change intervals of ~7 years	Stratified random based on ecoregions	Annual, but based in the ~7 year period	Multiple land cover classes	CONUS
(Griffiths et al., 2014)	Multi-method	1985-2010 at 5 year intervals	Stratified random, frequency not clear.	Per mapping period	Forest disturbance and recovery	Carpathian ecoregion
(Gebhardt et al., 2014)	Multi-temporal spectral metrics	1993–2008 at ~3 year intervals	Stratified random area-weighted sampling, based on previous LC map. Timing unclear.	Per mapping period	Multiple land cover classes	Mexico
(Potapov et al., 2014)	Multi temporal spectral metrics	2000-2011, single period	Two stage stratified random cluster sampling	Single period with map based annual values	Forest loss	Peruvian amazon
(Yin et al., 2014)	LandTrendr (MOD-Trendr)	2000-2011, Annual	Disproportionate stratified estimator.	Validation only.	Multiple land cover classes	Inner Mongolia
(Kennedy et al., 2012)	LandTrendr	1985-2008, Annual	Random	Validation only	Forest disturbance by type	NW USA

Table 1-1. Previous studies that use time series methods and statistical sampling to derive area estimates.

1.3 REDD+, the IPCC and greenhouse gas emissions reporting

REDD+ is an international mechanism created by the parties of the United Nations Framework Convention on Climate Change (UNFCCC) in 2005 that seeks to mitigate climate change by curbing carbon emissions from land change. Originally, REDD

(Reducing Emissions from Deforestation and forest Degradation) was designed to create a financial value for the carbon stored in forests, offering monetary incentives for tropical countries to reduce their rates of forest loss (UN-REDD, 2016). The "plus" sign was added to extend the reach of REDD to include sustainable forest management, conservation of forests and enhancement of carbon sinks (the full name of REDD+ is [REDD] *and the role of conservation, sustainable management of forests and enhancement of forest carbon stocks in developing countries*). Countries that participate in REDD+ are responsible for submitting a national forest reference emission level (FREL) that constitutes their carbon emissions baseline, usually based on historical trends. Future payments to the country are tied to their ability to demonstrate a reduction of emissions over a given period relative to their FREL. For this reason, methodologies to estimate both the reference levels and the subsequent emissions need to be consistent and transparent, and estimates unbiased and with known uncertainty. The ability to provide uncertainty estimates is only possible if uncertainties are quantified for changes in carbon stock and land area. Two main approaches have been identified to provide systematic and periodical estimates of carbon emissions and removals for REDD+ reporting: the stock change, and the gain/loss approach. The former requires estimates of standing carbon at times 1 and 2, which typically require forest inventories, whereas the latter is based on the product of *emission factors* (i.e. carbon content per unit area per land cover type) and *activity data* (i.e. estimated areas of REDD activities that cause carbon emissions or removals – synonymous with land change) (GFOI, 2016). Because of a lack of long-term national forest inventories and the need to account for other land cover classes besides

forest, methods to estimate carbon emissions and removals in the tropics typically rely on the gain/loss approach. The Intergovernmental Panel on Climate Change (IPCC) guidelines provide three tiers of approaches to estimate emissions and removals. Tier 1, or the "default method", relies on default emission factors; Tier 2 requires country-specific emission factors; whereas Tier 3 includes higher-order methods with estimates of carbon emissions and removals being tracked in space and time, often through the use of models (GFOI, 2016). Higher tiers are desirable because they can provide estimates of greater certainty than lower tiers when properly implemented, but they come at the cost of an increase in their complexity. Therefore, the selection of an initial tier must be done considering the country circumstances.

Similarly, for representation of land, the IPCC provides three approaches: Approach 1 does not include any direct data on land change but simply country-scale area estimates of stable land categories; Approach 2 requires a land change matrix but without a spatial representation; whereas Approach 3 requires a spatially and temporally explicit representation of land categories and conversions (GFOI, 2016). Similar to the multiple tiers for estimation of carbon emissions and removals, higher-level approaches are desirable because they provide a more accurate and precise representation of a country's land change trajectories, which is essential to estimate emissions associated with them, particularly in developing countries.

Regardless of the tier or approach, central to a country's REDD+ reporting is a MRV (Monitoring, Reporting and Verification) system, which aims at communicating mitigation procedures and estimation approaches (Cancun COP). The MRV system of a

country includes approaches for national forest monitoring in accordance with the IPCC Tier system (IPCC, 2006). At the core of a robust and transparent MRV system is the concept of *good practice*, which requires that national greenhouse gas inventories should not *neither over- nor under-estimates as far as can be judged* and *uncertainties reduced as far as is practicable* (IPCC, 2006). As explained in Section 1.2, statistical methods are available for the quantification and reduction of uncertainty, particularly for the estimation of areas of change. However, estimates of area bias and accuracy pertain to the entire study area, and do not provide information at the pixel level. The result is a mismatch between higher-level tier methods that rely on spatially explicit, often pixel-level, and methods for accommodation of bias and uncertainty. To overcome this mismatch, approaches are needed that inform issues of bias and uncertainty at the pixel-level in order for Tier 3 methods to comply with the IPCC reporting criteria.

1.4 Study area

The study area corresponds to the Colombian Amazon region as defined by the Sinchi Amazonic Institute of Scientific Research (Instituto Amazónico de Investigaciones Científicas) (Figure 1-1). The area, which is mostly covered by tropical rainforest, makes up more than two thirds of the forest area of Colombia (Galindo et al. IDEAM, 2014). The Colombian Amazon contains substantial carbon stocks and is one of the most biodiverse regions in the world (Asner et al., 2012; Duivenvoorden, 1996; Olson and Dinerstein, 2002; Orme et al., 2005).

Figure 1-1. Study area and Landsat scenes processed. The Landsat WRS-2 path and row are displayed for each scene. The total area of study region is 46,822 kha

Multiple studies have attempted to identify general patterns of land use in this area. Sánchez-Cuervo et al. (2012) documented vegetation recovery in the Andes and a

significant loss of woody vegetation in the northern boundary of the Amazon region between 2001 and 2010. Sy et al. (2015) attributed smallholder crop and mixed agriculture as the main drivers of deforestation, and underlined the importance of other wooded lands in the process. Armenteras et al. (2006) and Etter et al. (2006b) identified colonizing agriculture (*colonización agrícola*) in the Colombian Amazon, characterized by pasture establishment and cattle ranching along the deforestation frontier as the main cause of ecosystem change in the region. Etter et al. (2006a) found that areas that experienced deforestation were partially offset by regenerating vegetation between 1999 and 2002, which was further corroborated by Aide et al. (2013), again, emphasizing the separation of primary and secondary forest, and the monitoring of post-disturbance landscapes. These practices increase the forest fragmentation and make land cover patterns more "patchy", spontaneous and unplanned than those documented in the neighboring countries of Brazil and Ecuador (Armenteras et al., 2006). The relationship between fires and forest fragmentation has also been studied (Armenteras et al., 2017). These studies have improved our understanding of the drivers of change and overall changes in the Colombian Amazon, but no regional maps of the dynamics and patterns of conversion between multiple land categories over time have been produced. Estimates of carbon emissions exist but only for deforestation in irregularly spaced periods, and their uncertainty has not been reported (Ramírez-Delgado et al., 2018; Yepes et al., 2011). The national forest and carbon monitoring system, led by the National Institute of Hydrology, Meteorology and Environmental Studies (IDEAM), has a strong remote sensing component. Its development has vastly improving the country's capabilities to report

areas of forest and forest loss at biennial intervals, as well as their associated carbon emissions. However, the focus on accurate detection of forest and forest loss has translated into less attention to changes between more detailed land cover classes, particularly those that may contribute to carbon removals such as regrowing secondary forests. While the rate of deforestation is less than in Brazil and Ecuador (FAO, 2010), the presence of more complex spatio-temporal dynamics of clearing, abandonment and regrowth, make the Colombian Amazon a relevant landscape to analyze.

1.5 Structure of this dissertation

This dissertation explores the use of dense time series of Landsat observations to improve the understanding of land change in the Colombian Amazon for the last eighteen years, particularly as it relates to carbon emissions and the REDD+ reporting process. It builds on current techniques to demonstrate the continuous estimation of areas for multiple land change activities and the carbon fluxes resulting from them, and provides guidance and recommendations for future similar studies. It also explores the use of methods to measure uncertainty in the detection of change in time series of Landsat observations.

1.5.1 Continuous monitoring of land change activities and post-disturbance dynamics from Landsat time series: A test methodology for REDD+ reporting

The provision of credible evidence of reductions in the extent of land change activities that release carbon to the atmosphere is a key component to the success of REDD+. With the rates of land change typically being very small relative to the total study area, sampling-based approaches for estimation of annual or biennial areas have proven problematic, especially when comparing area estimates over time. In this chapter, I present a methodology for monitoring and estimating areas of land change activity at high temporal resolution that is compliant with international guidelines. I also provide a set of recommendations and lessons learned that could improve similar efforts in the future, helping make the reporting required for REDD+ more feasible.

1.5.2 Spatial representation of the probability of errors in maps of land change

Remote sensing-based maps provide spatially explicit information that is of importance in many subsequent analyses, for example, estimation of carbon emissions and evaluation of biodiversity. The classification errors in these maps limits their use for such analysis without accounting for their negative impacts. While sampling techniques can accommodate the effects of classification errors, the sampling-based estimates of bias and uncertainty provide no information about individual pixels. Available methods that aim to quantify classification uncertainty at the pixel-level do not account for uncertainty in the detection of changes. Approaches that provide spatial information on uncertainty in

change maps are therefore needed but are with a few exceptions nonexistent in the literature. In this chapter, a method is presented for estimation of pixel-level probability of omission and commission of change in maps produced using the CCDC algorithm. The relationship between error probabilities and the actual incidence of omission and commission errors is analyzed.

1.5.3 Carbon emissions associated with land conversions and recovery of disturbed landscapes

Previous efforts to characterize the carbon dynamics in the Colombian Amazon have focused on estimating the average emissions over irregular periods due to deforestation activities and without reporting their uncertainty. In this chapter, I present the results from applying two approaches for estimating carbon fluxes in the study area using the areas calculated from "pixel counting" (biased) and estimated areas (bias-adjusted) of land change for each biennial period, calculated as explained in Chapter 2. Net and gross carbon fluxes per period and land change class are reported, as well as the instantaneous and delayed emissions from different pools, obtained from one of two approaches applied. I also present time-aggregated estimates of carbon fluxes with reduced uncertainties and discuss future avenues for a more accurate representation of processes such as carbon removals due to secondary forest regrowth.

CHAPTER 2: CONTINUOUS MONITORING OF LAND CHANGE ACTIVITIES AND POST-DISTURBANCE DYNAMICS FROM LANDSAT TIME SERIES

2.1 Introduction

Current tropical deforestation has been estimated to account for 7-14% of the annual CO_2 emissions released into the atmosphere by human activities whereas intact tropical primary forests sequester an equal amount (Achard et al., 2014; Goetz et al., 2015; Harris et al., 2012; Houghton et al., 2012). However, recent research suggests that a reduction in carbon density of tropical primary forest due to disturbance exceeds the emissions from deforestation, with the result that tropical forests are becoming a net source of carbon to the atmosphere (Baccini et al., 2017). The need for a reduction of emissions is thus more urgent than ever. Efforts to reduce global deforestation have led to the establishment of international frameworks like the (UN-REDD, 2016) that stipulate financial incentives to countries for reducing carbon emissions from tropical deforestation and forest degradation. For such frameworks to be successful, robust approaches that provide estimates of carbon emissions and removals with proper uncertainty metrics are required (IPCC, 2003). As mentioned in Section 1.3, methods to estimate carbon emissions and removals in the tropics typically rely on a gain/loss approach. Three tiers, from lower to higher complexity, are provided by the IPCC for the estimation of emission and removals. Similarly, the IPCC provides three approaches for the representation of land, with higher approaches increasing in complexity and leading to a spatial representation of land categories and conversions. Following the Cancun

Agreement of the United Nations Framework Convention on Climate Change (UNFCCC), countries that wish to report carbon emissions and removals under the requirements of IPCC guidelines need to create a system for Measurement, Reporting and Verification (MRV) for communication of the mitigation procedures and estimation approaches (UNFCCC, 2018). The national MRV system includes approaches for national forest monitoring in accordance with the IPCC Tier system (IPCC, 2006).

While tropical deforestation and associated carbon emissions have been extensively studied during the last three decades (Achard et al., 2002; Baccini et al., 2012a; Brown, 1997a; DeFries et al., 2002; FAO, 1993; Hansen et al., 2013), the last couple of years have witnessed remarkable developments in environmental remote sensing. The opening of the Landsat archive in 2008 (Woodcock et al., 2008) has allowed for production of global maps of forest cover change (Hansen et al., 2013; Kim, 2010) and time series analysis of satellite data to study changes on the land surface (see for example Kennedy et al., 2010; Verbesselt et al., 2010; Zhu and Woodcock, 2014). New missions with global acquisition strategies and free data policies are already in orbit (Sentinel-2A, -2B and Landsat-8) and more are forthcoming (Landsat-9, -10 and Sentinel-2C, -2D). In addition, statistical protocols for unbiased estimation of area have become an integral part of forest and land cover monitoring (McRoberts, 2011; Olofsson et al., 2013; Stehman, 2013). Together, these advancements enable a more comprehensive analysis of land change that meets the highest requirements of IPCC for land representation. Still, there are relatively few studies in the scientific literature focused on the use of these methods for advancing operational forest monitoring in MRV systems. Notable exceptions are the

Guyana MRV system that conforms to the IPCC Approach 3 for multiple land cover classes (GFOI, 2014); the national forest monitoring system of Peru that employs Landsat-based time series analysis and unbiased estimation of forest cover change (Potapov et al., 2014); the PRODES system of Brazil (Instituto Nacional de Pesquisas Espaciais (INPE), 2016) based on manual interpretation of Landsat imagery; and the Mexican MAD-MEX system (Gebhardt et al., 2014) that uses time-series analysis, segmentation and approaches for statistical inference. Colombia has experienced an increase in forest monitoring capacity with a Government agency (Instituto de Hidrología, Meteorología y Estudios Ambientales, IDEAM) dedicated to the establishment of a forest monitoring system (IDEAM, 2016). The Colombian system is built upon good practices in remote sensing and sampling-based estimation, including stratified estimation and implementation of new algorithms that make use of the Landsat archive. The aforementioned forest monitoring systems are impressive and have provided valuable information on the state of tropical forests. Still, what is missing is a system that tracks the conversions between the six IPCC land categories, including the dynamics of post-disturbance landscapes, at high temporal and spatial resolution, coupled with unbiased estimation protocols for provision of biennial estimates of activity data.

In this Chapter I test a methodology for continuous monitoring and estimation of areas of land cover and land change that is compliant with IPCC Approach 3 for representation of land. The methodology builds on recent advancements in the field of environmental remote sensing, using algorithms for time series analysis (Zhu and Woodcock, 2014a) and estimation protocols (Olofsson et al., 2013; Stehman, 2013). The

performance of the methodology is tested for the Colombian Amazon (Study area, section 1.4) between 2001 and 2016.

2.2 Methodology

2.2.1 Time series analysis of land conversion

All available terrain-corrected (L1T), surface reflectance images from the TM, ETM+, and OLI sensors onboard Landsat-5, -7 and -8 with a cloud cover of less than 80% were downloaded from the EROS Center Science Processing Architecture (ESPA) website (USGS, 2010) for the 25 Landsat path and rows covering the study area (Figure 1-1). Because of a data gap around the mid-1990s (Figure 2-1), only data acquired after 1997 were used. This yielded a total of 5,184 images that were stacked chronologically to create time series of surface reflectance.

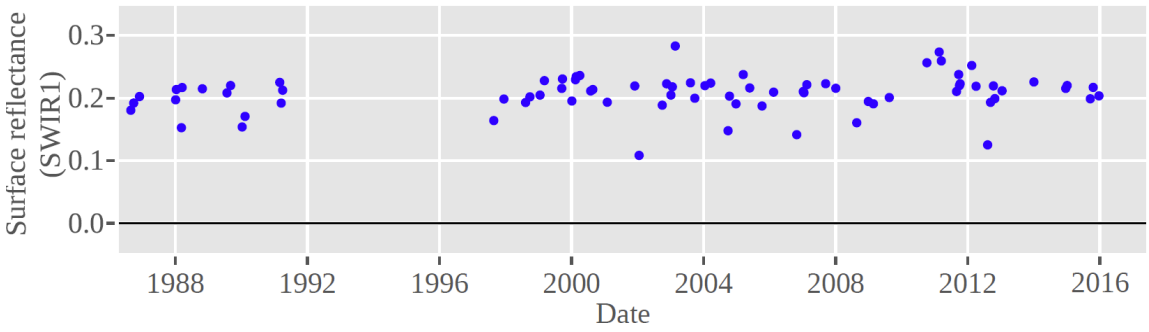

Figure 2-1. Time series of short-wave infrared observations (the SWIR1 band) acquired by Landsat -5-, 7 and -8 of a pasture in the Colombian Amazon. A clear gap in available observations can be seen between 1992 and 1997. Landsat WRS-2 path 7, row 59; coordinates 73.9290 W, 1.9687 N.

A Python implementation of the Continuous Change Detection and Classification (CCDC) algorithm was applied to each Landsat pixel in each of the 25 Landsat path and rows from 1997 to 2016. CCDC (and YATSM, the Python implementation used in this study) searches for "breaks" in a time series by monitoring for change in the residuals of the forecast from statistical models (Holden, 2016a; Zhu et al., 2012; Zhu and Woodcock, 2014a). The models predict the surface reflectance for any given date, and if the difference between observed and predicted reflectance across multiple bands is sustained for a certain number of consecutive observations, a change is flagged by the algorithm. After a change is detected, this process is repeated for the remaining observations in the time series iteratively. The time segments are subsequently classified in a supervised manner using a random forest classifier (Breiman, 2001) with time series model coefficients as input features, and training data. This approach enables identification of land categories before and after land change activities are detected. Two masking procedures were applied to reduce the number of cloudy observations in the data. The first procedure filters cloudy observations as flagged by Fmask (Zhu and Woodcock, 2012). The second procedure uses two multi-temporal methods similar to the Tmask procedure (Zhu and Woodcock, 2014b) that search for noise and remove it during the model-fitting phase.

Of importance to the stated objectives is the ability of the algorithm to track post-disturbance landscape dynamics; an example is provided in Figure 2-2, which shows a pixel located along the deforestation frontier of the Colombian Amazon. Figure 2-2

shows an example of colonizing agriculture which is common along the deforestation frontier: *Primary Forest*, present from the start of the time series, is converted to *Pasture* in 2005 which in turn is abandoned a year or two after its creation and *Secondary Forest* is allowed to regenerate. The regeneration is evident by the decreasing trend in the time series of shortwave infrared reflectance, but in 2011, the regenerated forest is again converted to *Pasture* which appears to be the prevailing land use until the end of the time series. The situation in Figure 2-2 is a rather common example of the landscape dynamics in the region. It is included to showcase the ability of the algorithm to detect the activities on the land surface including the timing, and importantly, to identify the condition of post-disturbance landscapes. It is important because: 1) these dynamics have a profound impact on the terrestrial carbon budget and will, if not identified correctly, result in erroneous estimates of carbon emissions and removals; and 2) many current forest monitoring systems in the tropics are limited to mapping and estimating forest loss and gain (Espejo and Jonckheere, 2017) without the ability to provide a complete picture of the landscape dynamics. An underlying hypothesis of the presented research is that CCDC, as illustrated in Figure 2-2, will be able to map land conversions and post-disturbance landscapes across the study area such that the resulting map data can be used to stratify the landscape in a way that allows for sufficiently precise estimation of activity data at annual or biennial frequency.

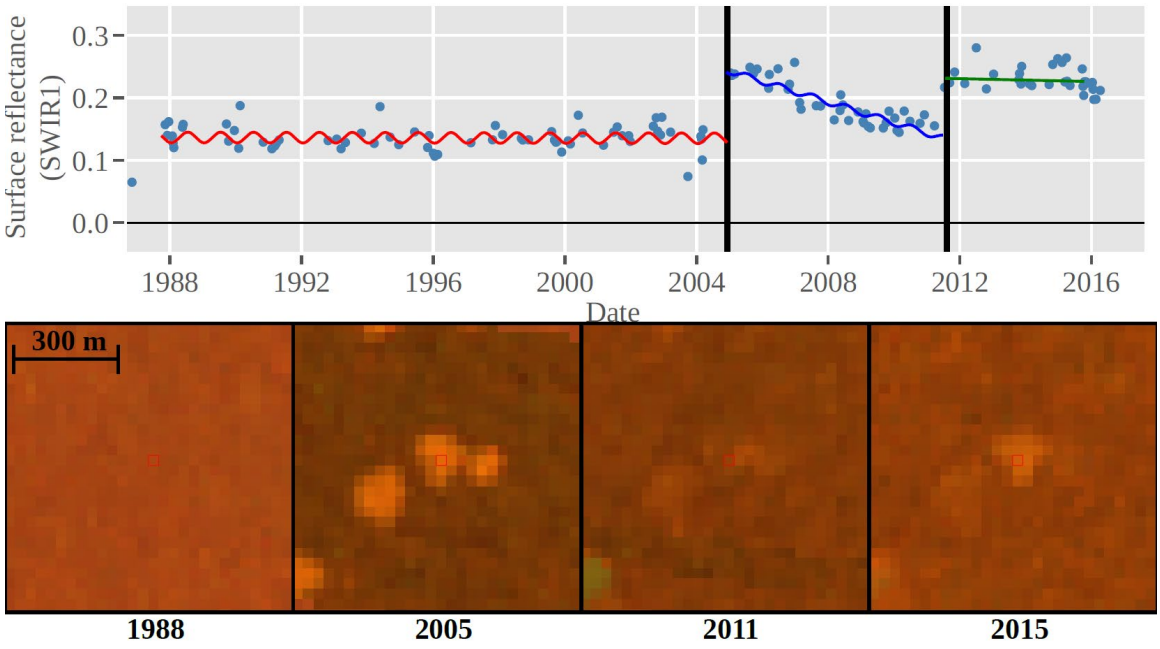

Figure 2-2. Time series of observations of SWIR1 surface reflectance measured by Landsat TM, ETM+, OLI band 5 (blue dots; upper) and snippets of Landsat composites in NIR-SWIR1-RED band combination (lower). CCDC predictions of surface reflectance are plotted as solid lines and detected breaks as vertical black lines. (Landsat path-row 6-59, pixel coordinates: 72.1795 W, 1.4725 N).

Given the low density of satellite data in the study area, only simplified time series models could be used for change detection. The time series models included one harmonic to account for annual variability, which is the only major seasonal fluctuation observed in this area. The Red, Near- and Infrared bands were used to detect changes in the time series. The time series segments were required to have at least nine valid observations, and five consecutive observations were required to flag a change when the prediction differed from the observed. Training data were collected manually over ten Landsat paths and rows to account for the natural variability in each of the land categories, particularly in the *Forest* category. Training data were identified using Landsat imagery and the TSTools plugin for QGIS (Holden, 2016b; QGIS Development

Team, 2009). In total, 420 training polygons were collected, with the total number of training pixels per land category being approximately proportional to the mapped area of the category, based on initial test maps produced and refined iteratively. Training data were obtained for the six IPCC land categories: *Forest*, *Grassland*, *Urban*, *Pastures/Crops*, *Water* and *Other* (mostly river sandbanks and rocky surfaces), plus a seventh category: *Secondary Forest.* The term *Secondary Forest* is used for the remainder of the manuscript to describe vegetation that exhibited a clear temporal pattern of regeneration but without having fully recovered to the state of a primary forest, as illustrated in Figure 2-3. It should be noted that even though I use the term "secondary", the forest might have been disturbed more than once. *Grassland* and *Pasture* were defined as separate map classes because the former is mostly natural while the latter is the result of direct human intervention and the most common post-deforestation land category. An additional map class denominated *All classes to unclassified* was assigned for pixels where the time series presented a break with a labeled segment prior to it, but no segment fitted afterwards. Training polygons labeled *Forest* were mostly collected in areas where the presence of stable primary forest with a closed homogenous canopy forest was evident and thus required no formal definition. This decision was corroborated by looking at the individual pixel time series, which displayed a stable, flat trend centered on surface reflectance around 0.15 in the Landsat SWIR1 band, as seen in Figure 2-4. Polygons labeled *Secondary Forest* were collected using a similar approach, only selecting pixels with segments that showed a clear negative slope with reflectance around 0.20 in the SWIR1 band following a disturbance event. A single classifier created from

the training dataset across the study area was applied to the time series segments for creation of land cover annual maps from 2001 to 2016 for each Landsat scene. This allowed for an initial training and stabilization period between the start of the time series in 1997 and the beginning of the analysis to find change, in 2001. Annual maps were mosaicked in sequential order from low to high WRS-2 path and row number (i.e. north to south, east to west), discarding the relatively small overlap zones of each previous scene in order to simplify the process.

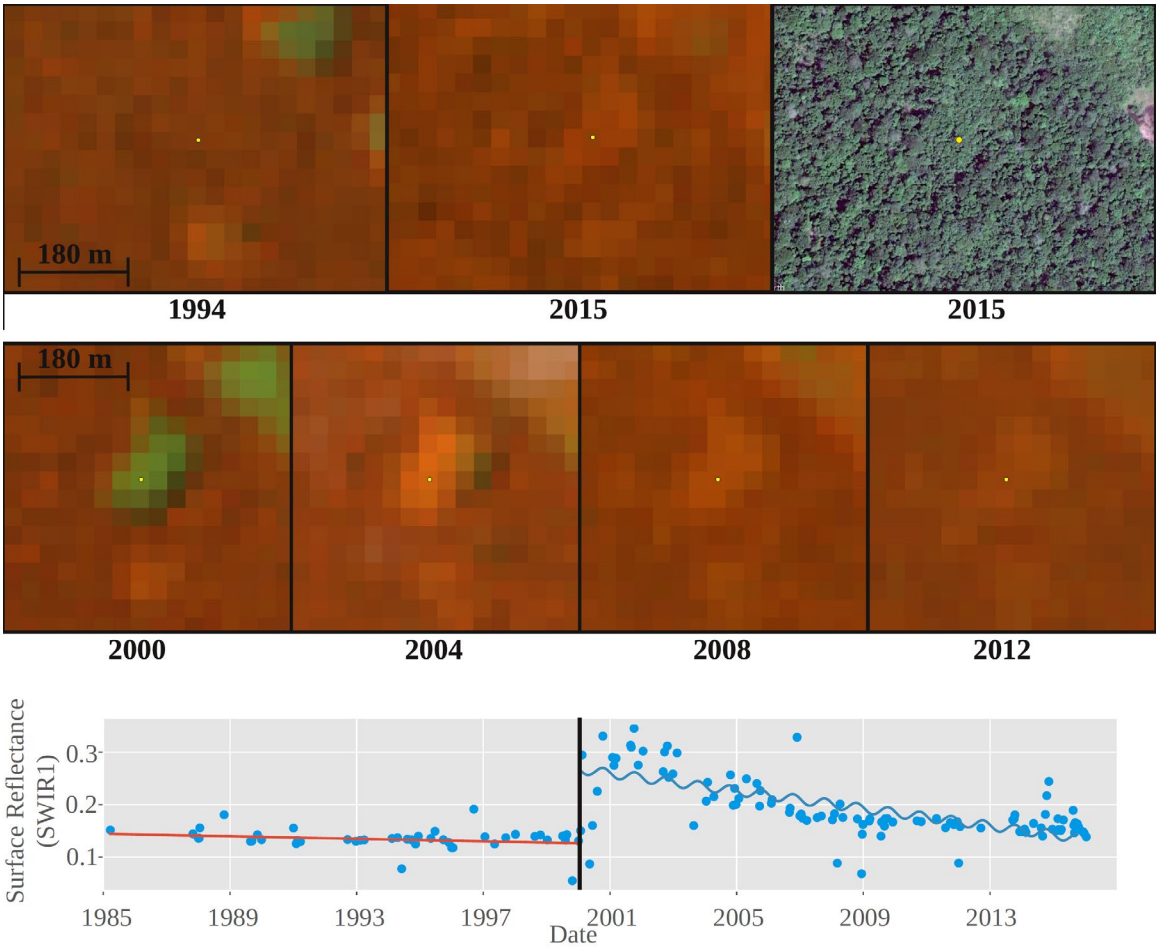

Figure 2-3. Example pixel showing the process of *Secondary Forest* regrowth after a short lived forest disturbance in the year 2000. The first row shows two images corresponding to the year 1994 and 2015. A comparison of only those two images would omit the ongoing vegetation recovery process. The second row shows the forest recovery over time, but classifying those images individually would result either in a *Pasture* label for the first two, or a *Forest* label for the last two. This example illustrates the importance of using dense time series of Landsat observations to accurately represent processes of vegetation recovery and regrowth. Landsat images are in RGB NIR-SWIR1-RED band combination. The most recent high resolution image was obtained from Google Earth. Latitude: 1.3458, Longitude: -71.8890

2.2.2 Area estimation

Areas retrieved by pixel-counting in maps will be incorrect because of classification errors. Therefore, areas and their confidence intervals need to be estimated by applying unbiased estimators to sample data of reference observations (GFOI, 2016;

Stehman, 2000). A sample-based approach to area estimation is emphasized by the IPCC Good Practice Guidelines for reporting within the UNFCCC treaty (IPCC, 2003, preface; GFOI 2014, p. 25): “inventories for the land use, land-use change and forestry sector that are neither over- nor underestimates so far as can be judged, and in which uncertainties are reduced as far as practicable”. In statistical terms, the first criterion is related to *bias*; an estimator is characterized as unbiased if it produces a parameter estimate such that the mean value taken over all possible samples is equal to the population parameter (Cochran 1977). Still, if several random samples are selected, the estimates obtained from each of the samples will be different because of the randomization of the selection, even if using an unbiased estimator. This uncertainty is characterized by construction of a confidence interval, which relates to the second IPCC criterion.

In this study, a stratified design and estimation approach (Cochran, 1977; Olofsson et al., 2013) were implemented. Stratified random sampling was chosen to target the sampling of areas exhibiting land change activity, which as informed by the maps, were a very small proportion of the study area. Further, the stratified estimator has proven efficient when applied to categorical observations (GFOI, 2016). The stratification contained six stable land strata and five land change strata representing mapped land dynamics between 2001 and 2016 (Table 2-1).). The *All-classes-to-unclassified* class was included in the stratification, but its area was not estimated. A buffer stratum corresponding to mapped forest in close proximity (< 90 m) to mapped transitions from *Forest-to-Pasture* was added to the stratification and used as a part of the sampling design to diminish the impact of omission errors. The buffer stratum was added

because the *Forest* stratum occupied 86% of the study area, and any pixels in this stratum identified in the reference classification as exhibiting land change activity (i.e. omission errors of change activities in the map) will carry a large area weight and dramatically reduce the precision in area estimates of land change activities.

The total sample size was determined using the stratified variance estimator solved for *n* as described in Cochran (Cochran, 1977) with a target standard error of 0.3% (equivalent of 1.6 Mha, or a 95% confidence interval of ± 3.1 Mha) of the *Forest-to-Pasture* class, which had a mapped area of 0.87% (4.5 Mha) of the total area between 2001 and 2016. In other words, the sample size was selected to achieve a margin of error of 60% if using the stratum area as an indication of the area estimate. While a margin of error (defined here as the half width of the 95% confidence interval divided by the estimate) of 60% seems high, it must be recognized that estimating an area that is assumed to be less than one percent of the study area is inherently difficult. For example, targeting a margin of error of 25% would have resulted in a sample size of almost 6,000 sampling units. Hence, the motivation behind these numbers was mainly practical and a compromise between precision and available human resources. Targeting a 60% margin of error gave a total sample size of 1,050 sample units that were allocated to strata following "good practices" for estimation of area of change (Olofsson et al., 2014): 50 and 75 units were allocated to the smaller strata and the remaining 400 units were allocated to the larger *Forest* stratum. The sampling assessment unit was a 30 m × 30 m Landsat pixel which was chosen to coincide with the minimum mapping unit.

A reference observation was provided for each unit in the sample by examining a time series of Landsat observations of surface reflectance using the TSTools plugin for QGIS (Holden, 2016b; QGIS Development Team, 2009). Examples of pixels labeled as forest in the reference sample can be seen in Figure 2-5. The legend of reference observations (Table 2-1) was based on the stratification legend to facilitate estimation of area, and was recorded along with time of change (if any). Multi-temporal very-high resolution imagery was used if available, and the following measures were taken to increase the interpretation confidence: the interpreters were carefully trained to understand and identify the land dynamics in the region; strata information was not made available to the interpreter during the collection of reference observations; and the reference label was assigned one of three levels of confidence. Labels with the lowest confidence, or labels on which interpreters disagreed, were double-checked at a later stage and modified. A stratified estimator was applied to the sample data for estimation of area with 95% confidence intervals following Olofsson et al. (2013). To assess the effectiveness of the buffer stratum to contain omission errors, areas with 95% confidence intervals were also estimated without using the buffer stratum (i.e. by combining the *buffer* and *Stable Forest* map classes and using the resulting class as the *Forest* stratum in the calculations). An overview of this workflow can be seen in Figure 2-4.

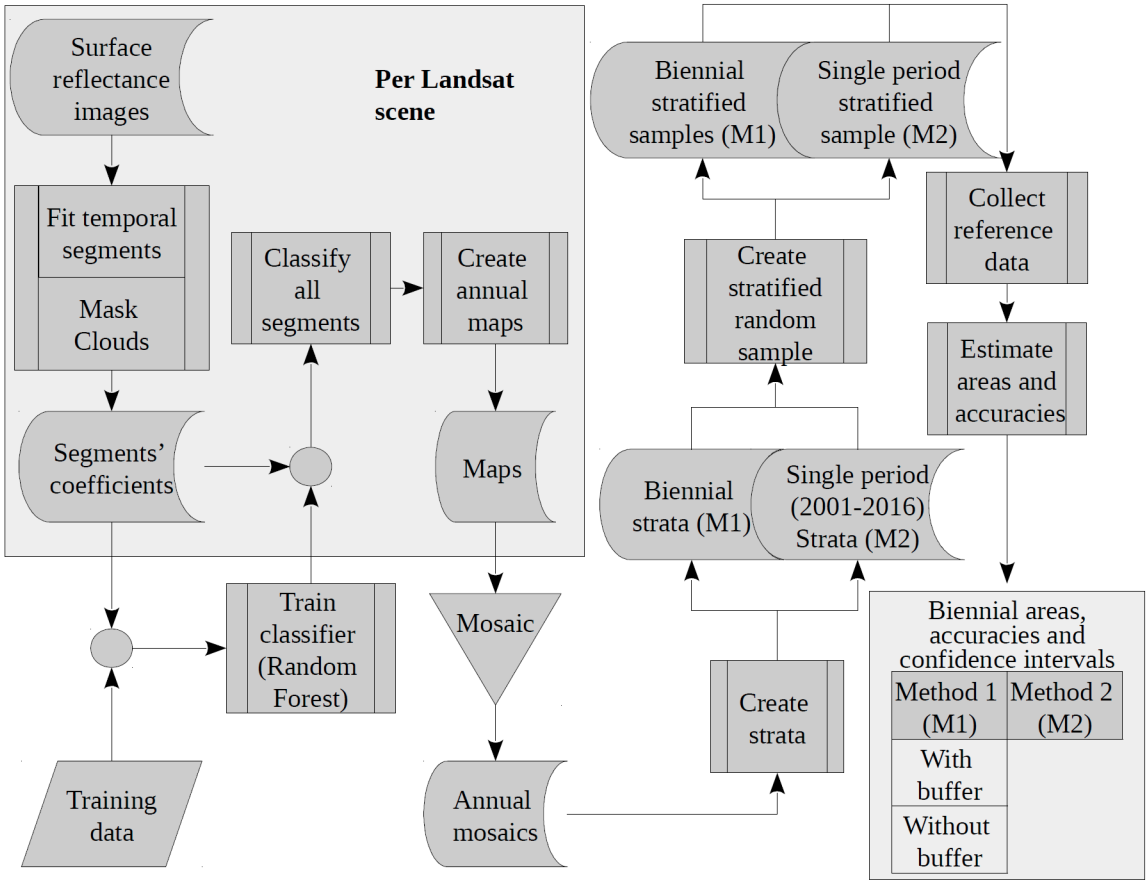

Figure 2-4. Overview of the workflow used to estimate areas, accuracies and uncertainty using maps created from time series of Landsat imagery as a source of stratification and manually collected reference data**.**

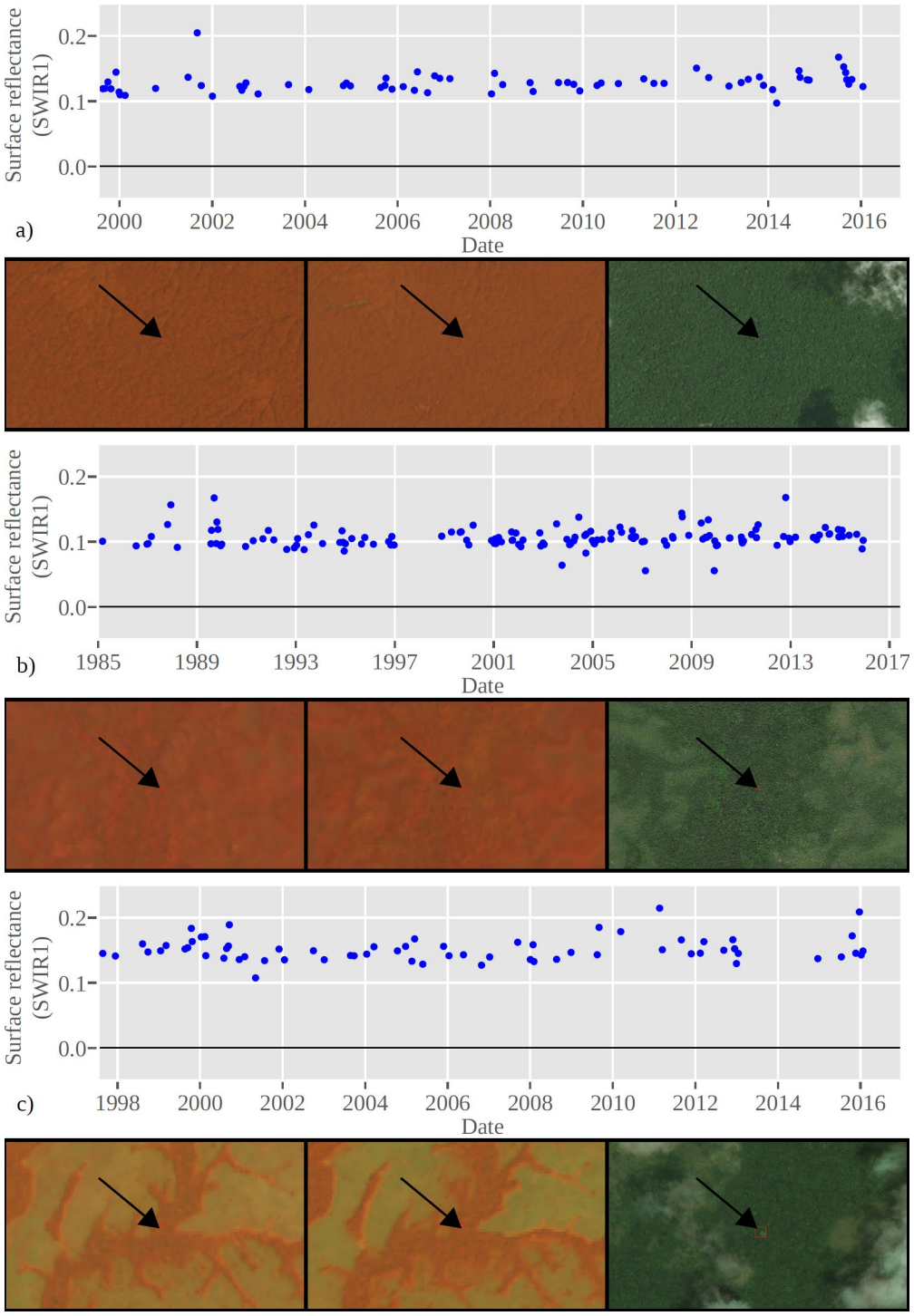

Figure 2-5. Examples of stable forest in time series of Landsat SWIR1 surface reflectance for a pixel in a) an area of intact primary forest, b) the edge between forest and shrublands and c) a riparian forest next to natural grasslands. Landsat subsets in RGB NIR-SWIR1-RED band combination are shown for dates near the beginning and end of the time series, respectively. High resolution imagery (zoomed) of the example pixels from Bing Maps are shown to the right of the Landsat images.

Stratum name	Description	W_h	n_h
Stable forest	Stable forest.	85.70	400
Stable grassland	Stable natural grassland.	2.81	75
Stable Urban + Stable other	Areas that show stable urban cover, as well as other bright surfaces like exposed rock and sand	0.08	50
Stable pasture-cropland	Stable human introduced pasturelands and croplands.	4.91	75
Stable secondary forest	Areas that show sustained vegetation regrowth over the course of two years or more.	1.06	50
Stable water	Stable water bodies.	1.29	50
Forest to pasture	Areas that experienced conversion from forest to pastures or croplands.	1.40	50
Forest to secondary forest	Areas that experienced a brief conversion to pastures or croplands that were abandoned shortly thereafter and display a regrowing trend.	0.26	50
Gain of secondary forest	Areas that experienced a conversion from pastures, grasslands, urban, water and other to secondary forest.	0.11	50
Loss of secondary forest	Areas of secondary forest that were converted to any other class (except to forest).	0.23	50
Other to other	Other transitions that are not relevant.	0.45	50
All to unclassified	Areas of classes other than forest and secondary forest that experienced a disturbance but have no class label afterwards.	0.35	50
Buffer	Areas of stable forest that were assigned to a 'buffer' stratum surrounding the *Forest to pasture* stratum.	1.37	50

Table 2-1. Strata names and their description, strata weight (Wh [%]) based on the map of stable and change classes between 2001 and 2016, and number of sample units allocated to strata (n_h). The areas of the *All to unclassified* and *Buffer* strata were not estimated. The term "stable" implies the presence of a single land cover class during the entire period being analyzed.

Central to reporting of trends in carbon emissions and removals from land surface activities is the ability to provide estimates at high temporal frequency. The UNFCCC requires reporting at annual or biennial time intervals (GFOI, 2016), which complicates the estimation of land change activities as the areas are often very small at such short

intervals. In this study, the most common activity was the conversion of forest to pastures, which was mapped as occupying 0.87% of the study area over 16 years. At annual intervals, the area of this activity would average less than a tenth of a percent. Even at biennial intervals, the area will be small from an estimation perspective. The situation of estimating small areas in the presence of large strata of stable land cover is a complicated issue in many national forest monitoring systems aimed providing area estimates of land change activity data for reporting within the REDD+ mechanism (Espejo and Jonckheere, 2017). To explore solutions and to provide better guidance on this issue, two approaches were investigated for area estimation. The first approach uses only one sample for all sixteen years of the study period that is analyzed such that area estimates are obtained for biennial intervals. The analysis is based on the construction of a ratio estimator and indicator functions as described in Stehman (2014); code and documentation are provided in a GitHub repository https://github.com/parevalo/workflow. While this approach requires only a single sample, it requires continuous reference observations for the entire 2001-2016 time period at each sample location. I introduce the term "continuous reference observations" to distinguish from observations at only one point in time or at shorter time interval. In this case, the reference observations were collected in biennial intervals. The second approach is based on the selection of a sample for each time interval for which area estimates are required; for biennial reporting, seven independent samples were required and obtained from each biennial strata map (annual reporting would have required fifteen samples which I did not have the resources to provide). Stratified estimators were constructed for each sample

such that independent estimates were provided for each two-year period. I selected seven samples of equal size and allocation by stratified random sampling using the design described above (i.e. 1,050 units allocated to the study area according to the recommendations in Olofsson et al. (2014) and shown in detail in Appendix B). I hypothesize that the single-sample-approach will save time and cost as the collection of sample data is often a time-consuming process but result in less precise estimates. I hypothesize a lesser precision because the stratification of the study area is based on the change map 2001-2016, which makes strata are less likely to correspond to the targeted land change activities at any given biennial interval. The result is an increased likelihood of having very few, or even zero, reference observations of land change activities (*Forest-to-Pasture* for example) for certain biennial intervals, especially in the beginning of the study period. Whether estimates obtained using the single-sample-approach have similar or better precision than those obtained from the multiple-samples-approach (i.e. smaller standard errors), and whether the single-sample-approach results in such large uncertainty that independent samples are required for each time interval, were key questions to be answered in this research.

2.3 Results

The products generated in this study were: (i) a map of land categories and conversions for the time period 2001-2016 (Figure 2-6); (ii) annual map products of the IPCC land categories and biennial maps of stable categories and their conversions; and

(iii) biennial area estimates with 95% confidence intervals of activity data, i.e. the IPCC land categories of the most prevalent activities involving conversions to and from *Forest*, *Secondary Forest* and *Pasture*.

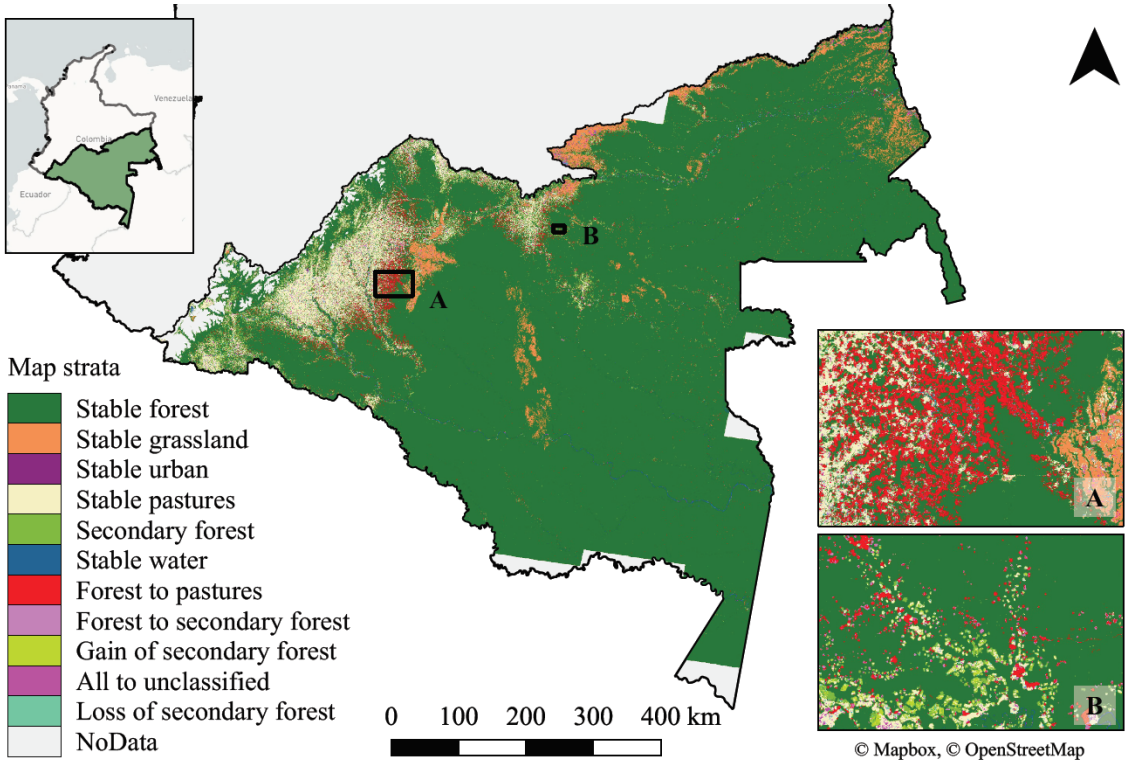

Figure 2-6. Map of IPCC land categories including conversions between 2001 and 2016 detailing: A) areas of conversion from forest to pasture, and B) areas with evidence of secondary forest and heterogeneous land changes.

Central to this study are the biennial area estimates with 95% confidence intervals of stable land categories and conversions shown in Figure 2-7. As expected, it was found that the multiple-samples-approach of collecting sample data that represented each time interval yielded more precise estimates than the single-sample-approach (Figure 2-9, Appendix A and C). With the single-sample-approach, several biennial area estimates of

land change activities were highly uncertain and at times not significantly different from zero (Appendix A and C). The margins of error, calculated as the half width of the 95% confidence interval divided by the area estimate (Figure 2-9 and Appendix C), were in general smaller with the multiple-samples-approach for the area estimates of the land change activities. Although a few individual area estimates were not significantly different from zero even with biennial sample data, the precision of estimates was considerably higher and sufficient to construct temporal trajectories of the more important and prevalent activities, including *Forest-to-Pasture* and *Forest-to-Secondary Forest*. Note however that even with the multiple-samples-approach, the *Forest-to-Pasture* estimate for 2003-2005 was highly uncertain and the 2001-2003 and 2009-2011 periods were not significantly different from zero. To complement these figures, the *Forest-to-Pasture* and *Forest-to-Secondary-Forest* classes were combined to estimate a join *Deforestation* class, show in Figure 2-8, for which all the biennial estimates are different from zero.

The use of a buffer stratum was highly effective at diminishing the impact of omissions of observed deforestation activities present in the *Forest* stratum. For example, the standard error of the biennial area estimates of Forest-to-Pasture decreased between 54% and 98%. The effect on other land change activities, which were also substantial with the exception of *Gain-of-Secondary-Forest,* can be seen in Table 2-2. Note the use of a buffer stratum does not decrease the precision in area estimates.

	Forest to pasture		Forest to sec. forest		Gain of sec. forest		Loss of sec. forest	
Period	No buffer	Buffer	No buffer	Buffer	No buffer	Buffer	No buffer	Buffer
2001 - 2003	316	104	184	104	0.8	0.8	11.8	11.8
2003 - 2005	355	53	36	36	12.3	12.3	0.5	0.5
2005 - 2007	327	7	130	4	1.3	1.3	12.8	12.8
2007 - 2009	272	10	241	8	49.2	49.2	92.6	13.7
2009 - 2011	223	103	159	15	36.4	36.4	98.4	36.7
2011 - 2013	285	10	157	6	2.7	2.7	2.3	2.3
2013 - 2015	255	15	128	9	5.6	5.6	6.3	6.3

Table 2-2. Comparison of standard error of areas in kha per period for the change strata, with and without the buffer stratum.

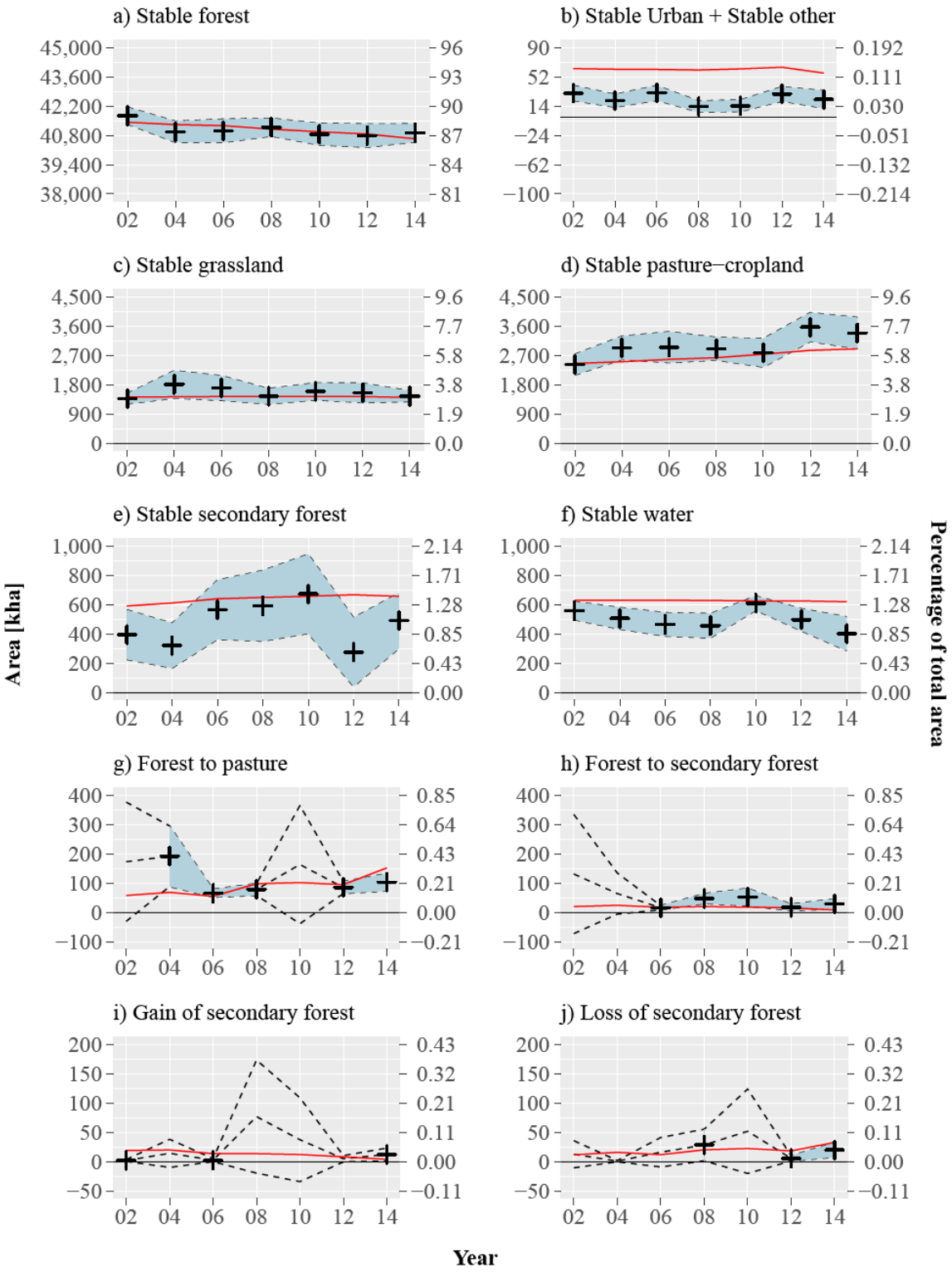

Figure 2-7. Biennial area estimates with 95% confidence intervals (dashed lines) for stable and change classes, estimated from the reference data using the multiple-samples-approach. Cross markers represent

values that are statistically different from zero (i.e. confidence interval does not include zero). Colored areas represent consecutive periods with confidence intervals that do not contain zero. The red continuous line represent areas obtained directly from the map by pixel-counting. The years on the x-axes represent the middle of each biennial period for visualization purposes (02 for 2002, 04 for 2004 and so on). The y-axes were set to aid in the visualization of the areas (but kept similar in rows where the same scale was sensible) given the large differences in magnitude. The panel for the Other-to-other class was removed, as it did not contain any relevant information

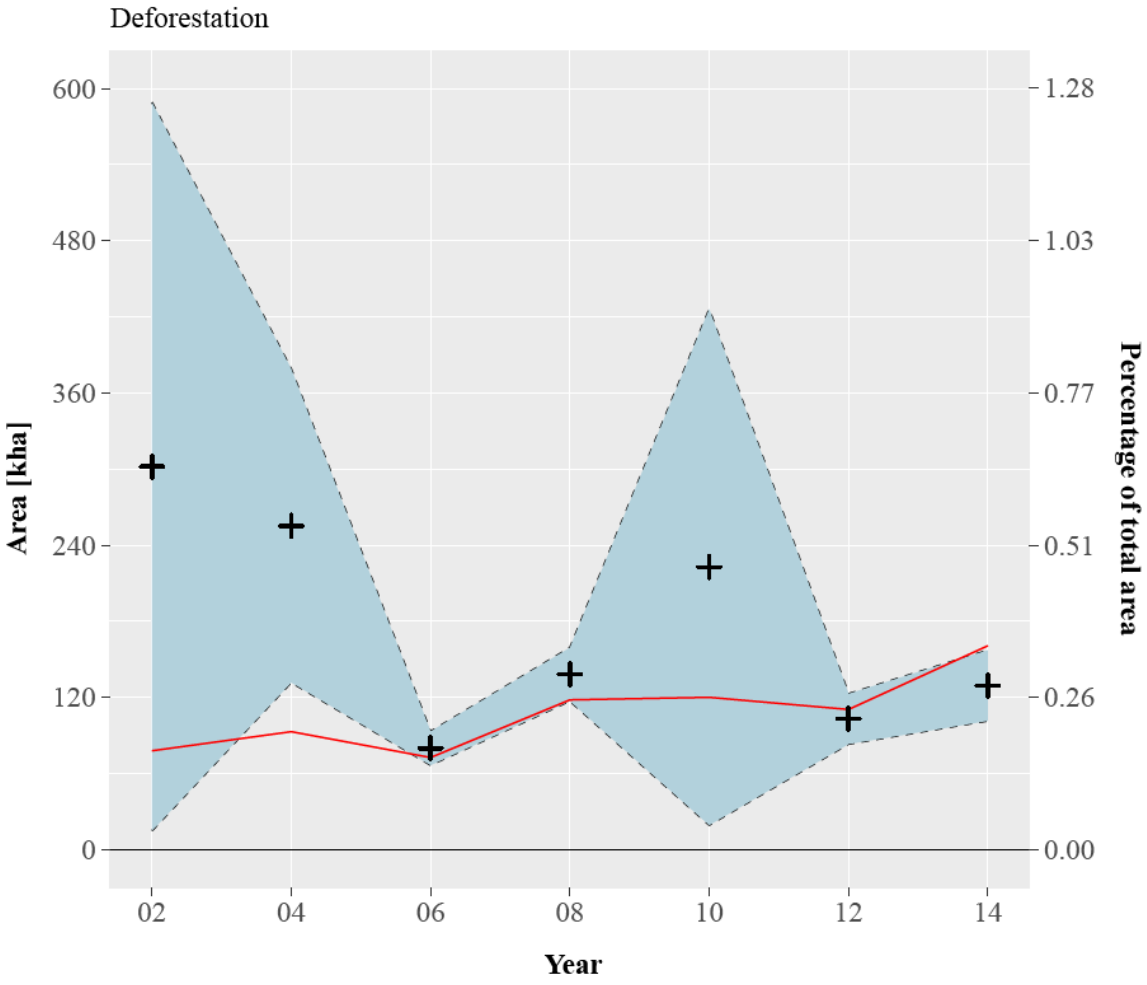

Figure 2-8. Biennial area estimates with 95% confidence intervals for the combined *Forest to pasture* and *Forest to secondary forest* classes (called *Deforestation* here), estimated from the reference data using the multiple-samples-approach. Cross markers represent values that are statistically different from zero (i.e. confidence interval does not include zero). Colored areas represent consecutive periods with confidence intervals that do not contain zero. The red continuous line represent areas obtained directly from the map by pixel-counting. The years on the x-axes represent the middle of each biennial period for visualization purposes (02 for 2002, 04 for 2004 and so on).

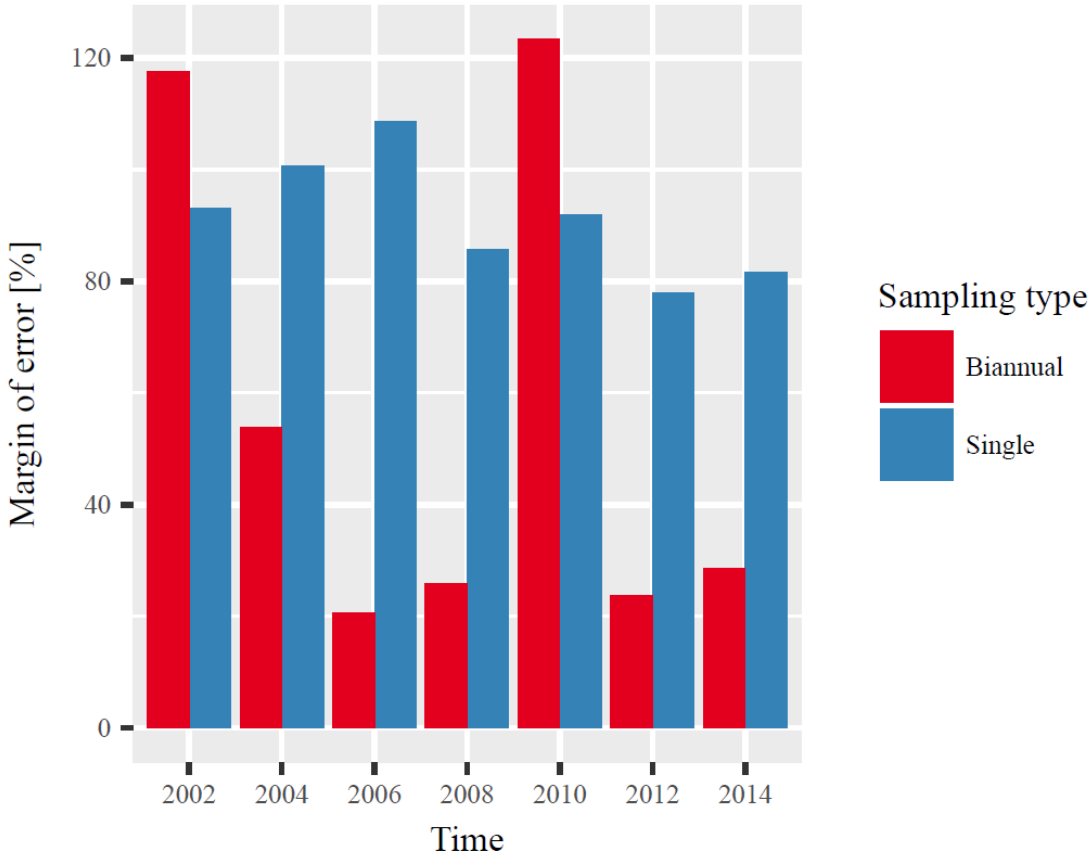

Figure 2-9. Comparison of margins of error of the biennial *Forest-to-Pasture* area estimates obtained by multiple-samples-approach (with the *Buffer* stratum) and single-sample-approach.

The overall accuracy of the map 2001-2016 was 94.1% (± 0.81%). Class-specific accuracies of biennial area estimates were highly variable (Table 2-3 and Table 2-4). Not surprisingly, higher accuracies were obtained for larger map classes including stable land categories and lower accuracies for the change classes.

	2001-2003	2003-2005	2005-2007	2007-2009	2009-2011	2011-2013	2013-2015
Other to other	4	0	0	4	0	4	4
Stable forest	99	98	98	99	98	98	99
Stable grassland	87	91	89	89	92	92	91
Stable Urban + Stable other	42	32	44	22	20	42	24
Stable pasture-cropland	81	89	84	92	81	95	85
Stable secondary forest	30	24	42	58	54	12	38
Stable water	86	78	72	68	92	76	56
Forest to pasture	62	64	58	38	38	48	40
Forest to secondary forest	50	28	34	52	58	24	22
Gain of secondary forest	4	4	2	10	6	2	2
Loss of secondary forest	8	6	22	28	20	8	18

Table 2-3. User's accuracy for each class and period, in percentage.

	2001-2003	2003-2005	2005-2007	2007-2009	2009-2011	2011-2013	2013-2015
Other to other	100	0	0	98		22	100
Stable forest	99	99	99	99	99	98	98
Stable grassland	90	72	76	89	83	85	88
Stable Urban + Stable other	85	95	87	99	86	91	60
Stable pasture-cropland	83	76	73	83	80	76	73
Stable secondary forest	45	46	48	64	53	29	51
Stable water	97	97	98	94	94	96	86
Forest to pasture	21	23	49	48	24	54	59
Forest to secondary forest	8	11	37	22	20	22	7
Gain of secondary forest	36	6	10	2	2	3	1
Loss of secondary forest	7	100	16	20	9	26	29

Table 2-4. Producer's accuracy for each class and period, in percentage.

2.4 Discussion

The analysis provided evidence of a small but steady decline in primary forest driven by conversion to pasture. Although subtle and low, the rate of this conversion was estimated to have increased during the period (excluding the very uncertain area estimate for 2003-2005). Overall, these results are consistent with the official national estimates of forest cover loss (Cabrera et al., 2011) and with the spatial patterns of land cover change reported in previous studies (Armenteras et al., 2006; Etter et al., 2006a, 2006b). To properly model the carbon emissions and removals, estimating the rate of primary forest to pasture is important but not sufficient – the fate of the post-disturbance landscape will determine if, when, and how the carbon emitted by the forest conversion activity is offset by secondary activities such abandonment and forest regeneration that remove atmospheric carbon. I found that the area of primary forest that was converted to pasture, but that reverted back to forest during the study period (i.e. *Forest-to-Secondary-Forest*), never reached above 60 kha per period -- in comparison, the area estimates of *Forest-to-Pasture* were never below 60 kha per period. If treating the conversion of forest to pastures as "forest loss" and not accounting for the post-disturbance dynamics involving pasture abandonment and secondary forest regeneration, the implications of land change activities on terrestrial carbon dynamics would be mischaracterized.

Along with the establishment of pasture, illicit cropland is an important driver of deforestation in the Colombian Amazon. According to Government statistics, coca plantations affect a much smaller area than forest to pasture conversion in the Colombian Amazon (UNODC, 2016) but our observations indicate that coca plantations are more

likely to be abandoned. Pasture and coca were not separated but the latter was included in the pasture category. The decision to not distinguish coca from pasture was driven by the focus of this study on the mapping and estimation of IPCC land categories -- both coca and pasture were considered as belonging to the IPCC *Cropland* category (GFOI, 2016) -- and because of the similarity in spectral signature between coca and pasture. However, because of the observed difference in the post-disturbance dynamics between coca and pasture, an article exploring the drivers and patterns of the land change dynamics in the region is currently in preparation in which separate area estimates are provided for coca and pasture.

In addition to the dynamics of conversion between forest and pasture, individual rates of gain and loss of *Secondary Forest* were monitored and estimated. These dynamics are typically a result of conversion from pastures to secondary forest, and vice versa. Except for a dip from 2010 to 2012, the combined effect of *Secondary Forest* dynamics resulted in a stable area of *Secondary Forest* without any obvious trend throughout the study period (Figure 2-7 h-j).

2.4.1 Comparison of sampling approaches

Of importance to this study and future potential applications of the presented methods is the estimation protocol. While maps are essential for stratifying the study area to guide the sampling, the results communicated to decision makers within frameworks and treaties such as REDD+ and UNFCCC are not obtained directly from maps but

estimated from sample data. As explained earlier, even the most sophisticated classification approach will not generate map products that are free of errors, which necessitates a sampling-based approach to area estimation. The importance of sampling-based estimation in a remote sensing context has been explained and illustrated in several articles (McRoberts, 2011; Olofsson et al., 2014; Stehman, 2013) and international guidance documents (GFOI, 2016, 2014), but few studies have explored methods for providing a time series of estimates. A notable exception is Cohen et al. (2016), who provided annual estimates of forest disturbance across the U.S. by two-stage cluster sampling with primary sampling units stratified by forest area. Also, Potapov et al. (2017) presented annual area estimates of forest cover loss in Bangladesh using a single sample with continuous reference observations. Because international treaties and climate negotiations require annual or biennial reporting (GFOI, 2016), the topic of estimating areas at high temporal frequency will need further exploration by the remote sensing community. The collection of sample data is often an arduous task and approaches that relieve practitioners of the burden of collecting such data are needed. Therefore, I tested a single-sample-approach similar to that of Cohen et al. (2016) and Potapov et al. (2017) in which only one sample is selected but reference conditions on the land surface are observed for the entire study period. Such an approach provides sample data for any point in time during the study period, which – in theory – allows for estimation of area for any time interval using a ratio estimator and indicator functions (Stehman, 2014). But as originally hypothesized, I found that only a few or no sample units at annual and biennial intervals were located in areas of the land change activities of interest, partly because of

their very small area. As a result, several biennial estimates of *Forest-to-Pasture* and *Forest-to-Secondary Forest* were not significantly different from zero (i.e. area estimates had negative lower confidence bounds) or displayed large levels of uncertainty. The approach of using sample data representing each time interval generated more precise estimates but required examination of 1,050 sample units in each of the seven samples selected (i.e. 1,050 × 7 sample units). Even with such a large amount of sample data, some biennial area estimates of land change activities were not significantly different from zero (Figure 2-7). This finding is different from that of Cohen et al. (2016) and Potapov et al. (2017) who were able to use a single sample for annual estimation. However, the former study used a very large sample of 7,200 units, and the latter used only sample units mapped as forest cover loss for estimation of annual change dynamics, thus not including omissions of forest loss in the forest and non-forest strata, which, as evident by this study, often has a detrimental impact on precision of estimates. Still, the results presented here should not be taken as evidence that the single-sample-approach will not work for providing a time series of estimates. Our result is just one example and others have already shown its utility (Potapov et al., 2017; Stehman 2014). As discussed further below, of importance to the lack of success of the single-sample-approach is the sheer size of the land categories of interest – even the most prevalent activity, Forest-to-Pasture, was just a tenth of a percent of the study area annually. In a situation where the area of the land change of interest is larger, as is often the case, I recommend an investigation into the feasibility of the single-sample-approach. Also, in a comparison of the margins of error between the approaches of single and multiple samples, the single-

sample-approach yielded smaller errors for two out of seven years (Tables C-6 and C-7 in Appendix C). With an increased focus on the reporting of activities at high temporal frequency, more research is needed to explore these types of approaches to inference of time series of area estimates.

Finally, a word about the issue of cost of sampling approaches discussed above. An underlying assumption of the discussion is that cost is synonymous with time and directly related to sample size. As a result, the single-sample-approach is assumed less costly simply because of the smaller sample size. But to use a single sample requires an assessment of land surface events over the entire estimation period (fifteen years in the case of the presented study). In rapidly changing landscapes, such an assessment would be time-consuming and could potentially eliminate the cost saving of the single-sample-approach.

2.4.2 Stratification and omission errors

An important difference between this study and Cohen et al. (2016) and Potapov et al. (2017) is the size of the land change activities of interest in relation to the study area. In the former studies, forest disturbance activities occupied 1.5-4.5% and 4-9% of the forest area per year respectively, whereas the corresponding numbers in this study are about a quarter of a percent. Inferring information about such a small part of a population by sampling is difficult in general and often associated with large uncertainty; the same statistical problem is encountered in many medical and public health studies concerned

with the prevalence of rare conditions, behaviors and diseases among large populations (Rahme & Joseph, 1998). In general, the problem is a consequence of the difficulty involved in achieving a sampling that results in sufficient precision in estimates of the phenomenon of interest (e.g. area of deforestation, prevalence of a disease, or votes in an election) across the entire population. In the context of using remote sensing to map and estimate areas of land change activities, a map depicting the spatial distribution of change is normally used to stratify the study area (i.e. the population) with the aim of ensuring sufficient sampling of activities. As witnessed in several countries, if very large strata are present, like *Forest* in this study, in which activities are observed (i.e. omission errors in the map used as stratification), the impact can be substantial (Espejo & Jonckheere 2017). From the formulas of the stratified estimator and the associated variance estimator (Cochran 1977, Eqs. 5.1 and 5.7), it can be deduced that the impact of omission errors is a result of the size of the stratum in which the errors occur in combination with the sampling intensity: the larger the stratum and the lower the sampling intensity, the higher the impact of omitted land change activity, especially if the activity data stratum is small. That is exactly the situation in this study: a land change activity stratum of less than a percent of the study area, and a forest stratum of 80% with low sampling intensity because of a relatively small sample size (less than 40%, or 400 out of 1,050, of the sampling units were allocated to the *Forest* stratum). By creating a buffer stratum around map classes of land change activity with a much smaller area but with higher sampling intensity that hopefully contains the activities omitted in the map, the impact of omission errors in the map is reduced. This approach has been successfully explored in other

studies of land change activities in support of REDD+ (Potapov et al., 2017), and our results further support the recommendation of using a buffer stratum to reduce the impact of omission errors. The number and area weight of omission errors "captured" by the buffer stratum are presented in the confusion matrices in Appendix B. The issue of the impact of omission errors further highlights the importance of sample allocation when designing a stratified sample; a larger sample size in large strata will reduce the impact of omission errors (i.e. a sample allocated proportionally to the strata area) when sampling for area estimation (Stehman, 2012). As more and more countries and studies are facing issues related to omission errors and precision in estimates of land change activity data, combined with an increasing number of studies highlighting the efficiency of buffer strata, more research is needed on how to define buffer strata. For example, a larger buffer would capture more errors but its stratum weight would increase with its size; this in turn could be balanced by increased sampling intensity, but that would raise cost. How to best define the buffer spatially for optimal efficiency? These relevant questions require better answers if remote sensing is to reach its full potential for greenhouse gas reporting.

Stratified random sampling was used to select the location of the sample units for the single-sample- and multiple-sample-approach. The main benefit of using a stratification when estimating land change is the ability to target the sampling to ensure a sample size in each category that is large enough to produce sufficiently precise area estimates (GFOI, 2016, p. 126). But for stratified sampling, achieving an allocation of sample units to strata that is proportional to the strata weights would require a very large sample size simply because some strata are very small. The result is often that fewer

sample units are allocated to large strata relative their weights. As discussed above, the impact of omission errors is a result of the size of the stratum in which the errors occur in combination with the sampling intensity. Hence, in a situation as in this study with a very large forest stratum (90%) and very small land change stratum (<1%), simple random sampling merits consideration. The standard errors of the area estimates that would have occurred for simple random sampling were approximated by using the variance estimator for simple random sampling (Cochran 1977, p. 26) and the area proportions estimated from the stratified random sample (Table C-5 in Appendix C). For the biennial area estimates of *Forest-to-Pasture*, the standard errors would have been two times larger on average if using simple random sampling instead of a stratified random sampling, and more than four times larger for certain intervals (although smaller than stratified random sampling for two out of the seven bi-annual estimates) -- hence, a substantial benefit was gained by the stratified design. The result supports the recommendations of Olofsson et al. (2014, p. 47) and GFOI (2016, p. 126) of employing a stratified design when aiming at estimating areas of land change activity.

Area estimates and the uncertainty in estimates are of primary importance to this study but because of the impact of omission errors on estimates, user's and producer's accuracy (Table 2-3 and Table 2-4) of map classes need mentioning. The complement of omission error is producer's accuracy and for some of the map classes, especially the ones involving land change activities, large omission errors were observed as illustrated by the error matrices in Appendix B. Look for example at the error matrices for 2001-2003 in Tables B-1 and B-2: even though 31 out of 50 sample units allocated to the

Forest-to-Pasture stratum were correct, the one single omission of *Forest-to-Pasture* in the *Forest* stratum represents an area of 114 Mha (or a 0.22 proportion of the study area)! In comparison, the 31 units correctly classified as *Forest-to-Pasture* represent an area of 40 Mha (0.077). The very large area proportion represented by this single omission error, in addition to a very low Producer's accuracy of 20.7% (Table 2-4), yields a large confidence interval that includes zero (because the 2001-2003 estimate was not significantly different from zero, it was not plotted in Figure 2-7h). Note that the buffer stratum in this case "captures" 11 sample units observed as *Forest-to-Pasture* that otherwise would have been present in the *Forest* stratum to further decrease the precision of the area of *Forest-to-Pasture*. The total area represented by these 11 units was 20 Mha (0.037).

2.5 Conclusions

The Colombian Amazon has experienced a continuous level of deforestation but at a small rate of less than 0.3% of the study area, or around 103 kha, for the 2013 – 2015 period. The deforestation, primarily driven by establishment of pasturelands, was estimated to have increased after 2005. Some of the post-deforestation landscapes did not stay deforested but were abandoned and reverted back to secondary forest. I estimated that around 29 kha per year of the pasturelands were quickly abandoned in the 2013 – 2015 period, -- hence, less than the equivalent of 30% of the post-deforestation landscapes was estimated to have begun to regenerate. These results show that the fate of post-disturbance landscapes can be monitored and estimated with the presented

methodology, but that more work is needed to further reduce the uncertainties. Increasing sample size, improving map accuracy and introducing buffer strata are all viable approaches to increase precision. The latter option was tested and it was found that the addition of a buffer stratum to capture omission errors had a marked effect on reducing the uncertainty on area estimates. Guidelines for how to design buffer strata in other situations with different distributions of strata weights, sample size, map accuracies etc. require more research. Finally, it was determined that the use of a single sample to estimate the area of land change activities at biennial frequency did not achieve acceptable levels of precision. Higher precision was achieved when sample data were collected for each time interval for which area estimates were desired.

CHAPTER 3: SPATIAL REPRESENTATION OF THE PROBABILITY OF ERRORS IN MAPS OF LAND CHANGE

3.1 Introduction

The topic of uncertainty in classifications of remote sensing data has been studied extensively, but approaches that provide information on pixel-level confidence in maps of *change* in land cover are scarce. Khatami et al. (2017a) provide a comprehensive review of the main approaches used to characterize the local quality of land cover maps. The authors indicate that a common approach is to use the probabilities of class membership as a metric of the classification confidence, including posterior probabilities from maximum likelihood classifiers (Brown et al., 2009; Foody, 1992), decision trees and random forest (Liu et al., 2004; Loosvelt et al., 2012), soft output of support vector machines (Giacco et al., 2010), relevance vector machine (Foody, 2008) and boosting methods (McIver and Friedl, 2001), among others. Besides using the probabilities of a single class, other approaches use the difference between the first and second largest class membership values (Prasad and Arora, 2014), or the membership values of all classes using entropy metrics (Dehghan and Ghassemian, 2006; Loosvelt et al., 2012; Shadman Roodposhti et al., 2019). The idea behind these approaches is that a higher probability of class membership, or the more dominant a single class membership is relative to those of other classes, the greater the certainty associated with that class. These methods have been applied to the global land cover MODIS product for assigning classification confidence and providing the second most likely class, as well as for map correction

based on ancillary data (Friedl et al., 2010, 2002). Despite their potential, examples of the use of classification confidence information analysis based on the underlying land cover maps are rare in the literature.

As noted by Khatami et al. (2017a), the kind of classification quality metrics mentioned above are different than accuracy metrics, even though they might be correlated in some cases. To fill this gap, researchers have investigated methods to spatialize classification accuracy using empirical methods that link accuracy with independent variables, often employing a logistic regression because the dependent variable is dichotomous (Burnicki, 2011; Carmel, 2004). Another approach used for this purpose is to spatially interpolate classification accuracy of test data (Comber et al., 2012; Comber, 2013; Foody, 2005). Khatami et al. (2017a, 2017b) presented an approach based on the interpolation of a sample of binary reference observations (i.e. correct or incorrect map label) using a surface fitting function applied to spatial and spectral domains. The methods proposed by Khatami et al. (2017a, 2017b) outperformed their own benchmark methods and successfully demonstrated a technique to predict accuracies at unsampled locations. What is missing from all these methods are approaches that inform the level of confidence in pixels mapped as *change*. It is the *change* in land use and land cover that is of primary importance in many remote sensing applications. Per-pixel accuracy or change confidence values could be used to account for the spatial accuracy of the input maps in applications such as carbon modelling (Quaife et al., 2008), urban land-use mapping (Cockx et al., 2014) and hydrological models (Miller et al., 2007), or used to propagate uncertainty in numerical models.

Maps that depict changes on the land surface are of importance for a range of applications, topics and studies. For example, tropical countries that participate in the REDD+ framework rely almost exclusively on remote sensing for monitoring land cover change and the carbon emissions associated with them (GFOI, 2016). Remote sensing has the advantage over surveys and inventories of providing wall-to-wall coverage of the study area at little or no cost, but translating spaceborne measurements of reflected sunlight into complex land-surface processes is inherently difficult and results are bound to be imperfect. Errors in maps of land change limit the potential of remote sensing science to contribute to policy and decision-making. To advance the utility of remote sensing-based maps, several articles published in remote sensing journals since 2010 have described the importance of area and map accuracy estimation (McRoberts and Walters, 2012; Olofsson et al., 2014; Stehman, 2013) but estimates of area bias and map accuracy do not provide information about whether an individual pixel in the map was correctly classified as change or not. The lack of pixel-level information is an issue when the spatial representation of mapped features is of interest -- which is often the case and maybe the reason for why a map was made in the first place!

The repositories of satellite data with a spatial resolution that readily captures human activities on the land surface are growing and becoming increasingly accessible (e.g. Landsat and Sentinel-2). Data availability in combination with powerful computing platforms (e.g. Google Earth Engine) and open source software (e.g. GDAL, QGIS) allow users to process large quantities of data and creating a wide array of spatial products. Thus, a move towards spatially explicit products is natural. Examples are

plentiful in the literature of applications for which spatial patterns of land change are essential input: assessments of the edge effects of fragmented forests in studies of biogeochemical cycles (Smith et al., 2018); studies of the effect of land change on biodiversity (O'Connor et al., 2015); and impact assessments of forest damage on protected areas (Gillespie et al., 2015) to mention a few. Another area of importance in this context is national carbon accounting. For monitoring of terrestrial carbon emissions within the REDD+ framework, the highest tier of methodological approaches is typically spatially explicit, such that the land cover and associated carbon dynamics are tracked at the level of individual pixels (or segments or stands) (GFOI, 2016; IPCC, 2006). Pixel-based methods for REDD+ reporting are being explored or used in Indonesia, Kenya and Mexico (GFOI, 2016). In support of REDD+ in Mexico, a spatially-explicit version of the CBM-CFS3 model (Kurz et al., 2009) was used to quantify emission and removals associated with pixel-level forest change (Mascorro et al., 2015). Pixel-level change in forest cover was provided as input to the model in the form of three sets of maps for which population-level accuracy was estimated from sample data; the omission error of forest change in the maps ranged from 77% to 85% and the commission error from 38% to 63%. If the sample data reflect true conditions, the estimated accuracy reported in Mascorro et al. (2015) entails that up to 85% of the actual forest change in the study area was missing in the map, and up to 63% of the forest change depicted in the maps was not observed in the sample data. This example is not unique and is not included to criticize Mascorro et al. (2015), but rather to highlight a problematic situation. If land change maps – more or less accurate – are to be used directly in subsequent pixel-level analysis

of the impact of change on carbon dynamics, biodiversity, ecosystem services, socioeconomics, etc., attention to errors and uncertainty is required. Otherwise, the result is an analysis that is – more or less – driven by classification errors.

In this chapter I present a method that provides pixel-level probabilities of omission and commission of change. The method is based on an analysis of the residuals of the time segments generated in Chapter 2, and is applied over the entire study area.

3.2 Methods

3.2.1 Estimating the probabilities of errors of omission and commission

Recently, methods have been implemented to test all time segments for missing breaks (an omission test) and to remove spurious breaks (a commission test) over time series of Landsat data (Bullock et al., 2019). The omission test is based on the cumulative sum (CUSUM) of ordinary least square regression (OLS) residuals –originally introduced by Brown et al. (1975) and further extended for use with OLS residuals by Ploberger and Krämer (1992)– returns the probability of observing the data under the null hypothesis of no structural change (Seabold and Perktold, 2010). The Chow test of equality between sets of coefficients in two linear regressions (Chow, 1960) is used to test for commission errors, and retrieves the probability associated with the test statistic, which follows the F distribution. The Chow test is used to determine the presence of structural break in a period known *a priori,* such as the break in the time series detected by a change detection algorithm. Common omission and commission errors in the study area are exemplified in

Figure 3-1 and Figure 3-2, respectively. Similar approaches have been used in other change detection algorithms that operate on Landsat time series. For example, LandTrendr (Kennedy et al., 2010) identifies potential vertices that indicate changes in the time series, and then creates a set of segments connecting them, thus describing the broad temporal trajectory of the data. These segments are subsequently merged into simpler models by removing vertices that result in the least increase on the mean standard error of the regression model, resembling the commission test mentioned above. On the other hand, the BFAST algorithm (Verbesselt et al., 2010a) decomposes the time series into trend, seasonal and noise components. Prior to the fitting of piecewise linear model and estimation of break points using the Bai and Perron method (2003), this algorithm test whether one or more points are occurring using an OLS residuals-based Moving SUM (MOSUM) test. This test is functionally similar to the omission test mentioned previously. These type of algorithms rely on the use of a fixed probability to determine the occurrence of an omission or commission error. In contrast, the methods I present here calculate the probability associated with a potential omission or commission event before a decision to split or merging segments is made.

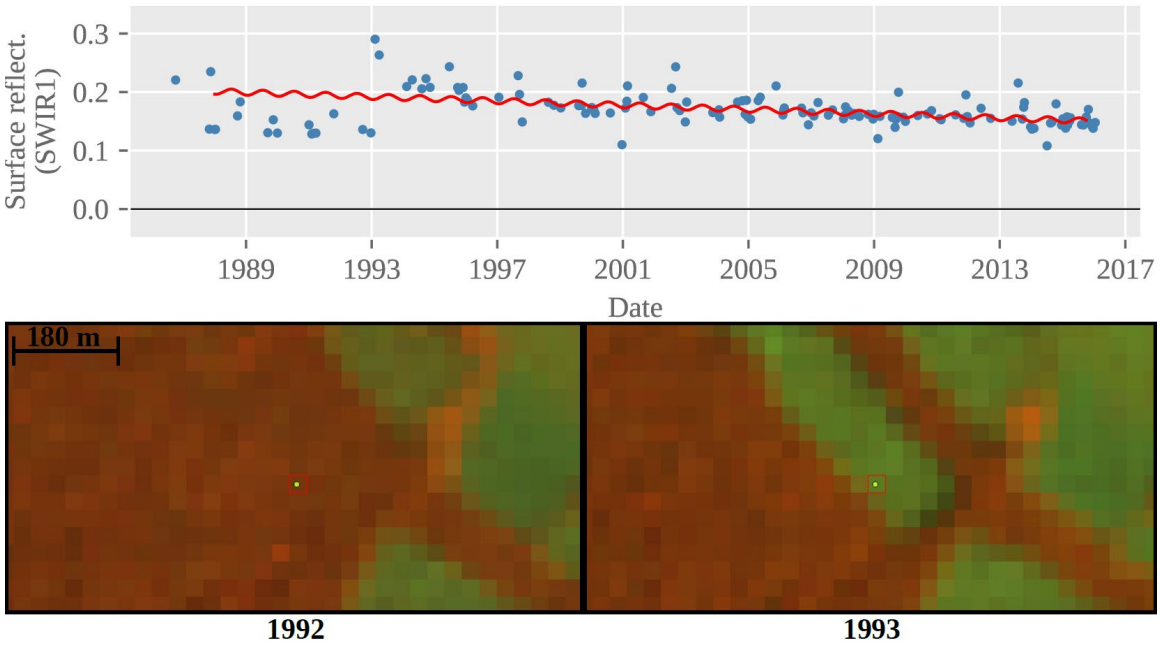

Figure 3-1. Landsat time series (SWIR1) and model results showing the omission of change around 1993. The darker color represents forest, the green color represents pastures. Images correspond to 1992-359 (left) and 1993-041 (right). Latitude: 1.44972, Longitude: -71.93989. RGB: NIR, SWIR1, RED.

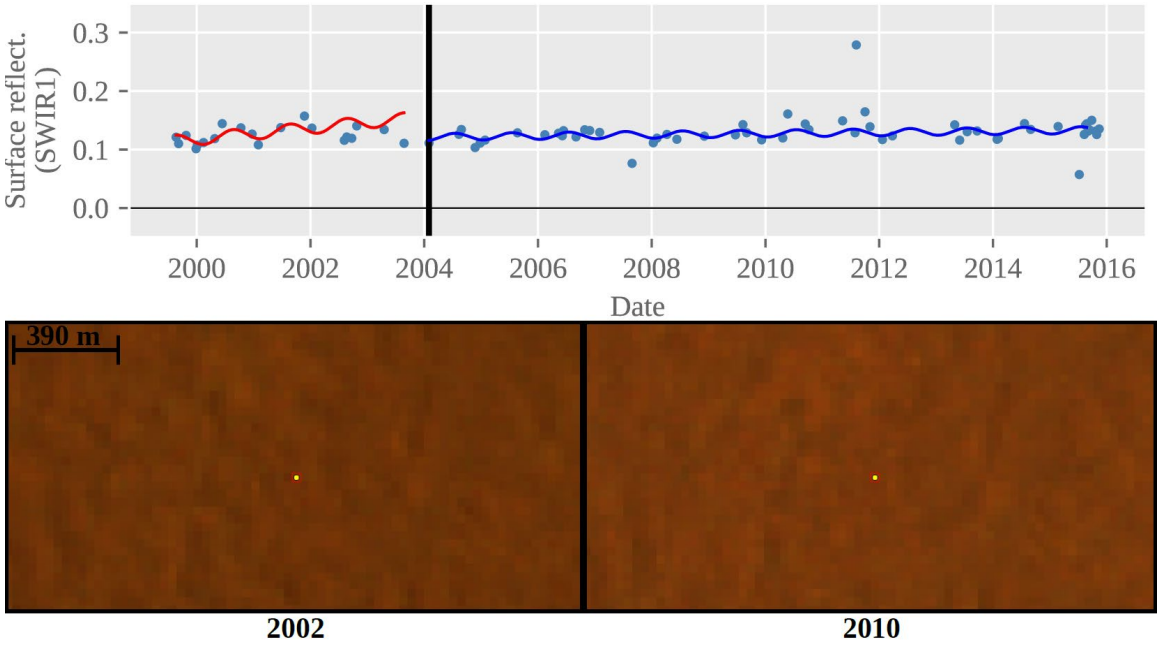

Figure 3-2. Landsat time series (SWIR1) and model results showing the commission of change around 2004. The area shows stable, continuous forest. Images correspond to 2002-234 (left) and 2010-280 (right). Latitude: -0.85516, Longitude: -72.82126, RGB: NIR, SWIR1, RED.

The omission test was applied to every time segment fit by the original run of CCDC (Chapter 2), but only the first short wave infrared (SWIR1) observations were used for the test. This choice was made because the omission errors of primary interest are related to the conversion of primary forest to pastures, which should be easily detectable in the SWIR1 Band. The commission test was applied to every pair of subsequent temporal segments for the entire time range. For example, a pixel for which three time segments were fit by the CCDC algorithm would have three omission and two commission probability values. Unlike the omission test, I used a multivariate version of the commission test that calculates the F-statistic per band and then computes a weighted mean that is used to derive the probability, as described in Bullock et al. (2019). I applied the test over the Red, NIR, SWIR1 and SWIR2 observations. I use this modified version as a more robust way to test for the presence of commission errors, given that the CCDC algorithm was run specifying a minimum of nine observations to fit a segment (instead of the default of 16), making commission errors more likely.

3.2.2 Relationship between probabilities of omission and commission errors

Once the probabilities were calculated, I tested if they were related to the presence of actual omission or commission errors using two approaches. In the first approach, I obtained the probabilities for segments intercepting the year 2010 because I expect both types of errors to be easier to detect towards the second half of the study period, when the changes or lack thereof should be easily identifiable in the time series. The probabilities

were obtained for all pixels and reclassified into six bins as shown in Table 3-1 in the next section. In the case where more than one break occurs for a single pixel, only the first break was considered. The bins were assigned to focus attention on probabilities closer to one as an attempt to determine the point at which most true omission or commission events are detected. Omission probabilities were masked to sample only those pixels that were located in the *Stable Forest* stratum in 2010, while commission probabilities were masked to sample pixels that had undergone change in the 2001-2016 period. One sample for each type of error was selected under stratified random sampling using the bins as strata; 20 sampling units were allocated per bin. For each unit in the samples, the fitted temporal segments were manually inspected along with the time series of Landsat data to determine the presence or absence of the respective omission or commission errors. I expected to see a higher incidence of omission and commission errors in the bins that represent the highest probabilities for each type.

The second approach leveraged the biennial maps and reference data of stable and change land cover classes collected for the analysis described in Chapter 2 to explore the relationship between omission and commission events as recorded in the reference data and the calculated omission and commission probabilities. For each biennial period between 2001 and 2015, map and reference labels were compared to determine the presence of omission and commission errors and relabeled as follows:

- Sample units that displayed stable map labels and change reference labels were considered *Omission* examples.

- Sample units that displayed change map labels and stable reference labels were considered *Commission* examples.
- Sample units that displayed both change map and reference labels (independent from whether the map and reference labels matched or not) were considered *Change*.
- Sample units that displayed both stable map and reference labels (independent from whether the map and reference labels matched or not) were considered *Stable*.

Omission probabilities for sample units labeled as *Omission* and *Stable* were filtered to include only those that were not flagged as change by the change detection algorithm. In turn, commission probabilities for sample units labeled as *Commission*, *Change* and *Stable* were filtered to include only those that were flagged as change by the algorithm. For this reason, the *Stable* units were considered as *Commission* for this case only, as the presence of an actual change flag indicates that the algorithm assigned a change when there was none, according to the map and reference labels. Box-plots and mean values with 95% confidence intervals were calculated from the values obtained in this procedure.

Finally, data on the first and second most likely classes as well as their predicted class probabilities were calculated from each of the time segments. Classification of time segments was performed using the Scikit-learn implementation of random forest (Pedregosa et al., 2011). Class probabilities were computed as the mean predicted class probability of the trees in the forest. Class probabilities from the second most likely class

were subtracted from those of the most likely class as a way to represent the confidence in the assigned label. Therefore, values closer to one are indicative of higher confidence of the classifier in the assigned label, and values closer to zero represent lower confidence in the assigned label. I will refer to this measure as *class membership confidence*. A map of class membership confidence for 2010, as well as a map of the number of clear observations per pixel were created to aid in the interpretation of the results.

Class probabilities and class membership confidence values, either calculated as explained previously (using a random forest classifier) or using other classification methods (e.g. posterior probabilities of a Maximum-Likelihood classifier) are fundamentally different from the omission and commission probabilities calculated in this chapter. Omission and commission probabilities pertain to the *change event* (detected or not) in the time series, while class probabilities represent the confidence in the label assigned by the classifier to a given temporal segment, not the change. Furthermore, the two types of probabilities are not necessarily related. For example, in Figure 3-1, a random forest classifier could assign a label of *Pasture* with a class probability of 0.4 to the temporal segment, but this number alone is not useful to determine if a *change* was omitted and what was the probability of such omission. Similarly, in Figure 3-2, the classifier could assign a label of *Forest* with a class probability of 1 to both temporal segments, but it is not possible to determine the probability of an error of commission of change from these numbers alone.

3.3 Results

The maps of omission and first commission probabilities for the year 2010 are shown in Figure 3-3 and Figure 3-4, respectively. Figure 3-5 shows the map of the number of clear observations per pixel after removing cloudy and shadowed observations as flagged by Fmask. The map of class membership confidence in 2010 is shown in Figure 3-6. Figure 3-7 and Figure 3-8 show the aggregated distribution of the omission and commission probability values for all the biennial periods analyzed. The results of the interpretation of the omission and commission samples are shown in Table 3-1 and Table 3-2, respectively. The tables indicate a clear positive relationship between probabilities and the actual presence of omission and commission errors; the errors of omission and commission are concentrated in the bins with the highest probabilities of omission and commission.

Bin	Omission probability	Omission NO	Omission YES
1	0 - 0.3	20	
2	0.3 - 0.6	20	
3	0.6 - 0.8	19	1
4	0.8 - 0.9	16	3
5	0.9 - 0.95	6	10
6	0.95 – 1	6	13

Table 3-1. Count of absence (NO) or presence (YES) of break omission per probability bin. Showing only the units that were labelled as high confidence.

Bin	Commission probability	Commission NO	Commission YES
1	0 - 0.3	15	
2	0.3 - 0.6	9	4
3	0.6 - 0.8	1	4
4	0.8 - 0.9	5	6
5	0.9 - 0.95	2	10
6	0.95 - 1	2	9

Table 3-2. Count of absence (NO) or presence (YES) of commission error per probability bin. Showing only the units that were labelled as high confidence.

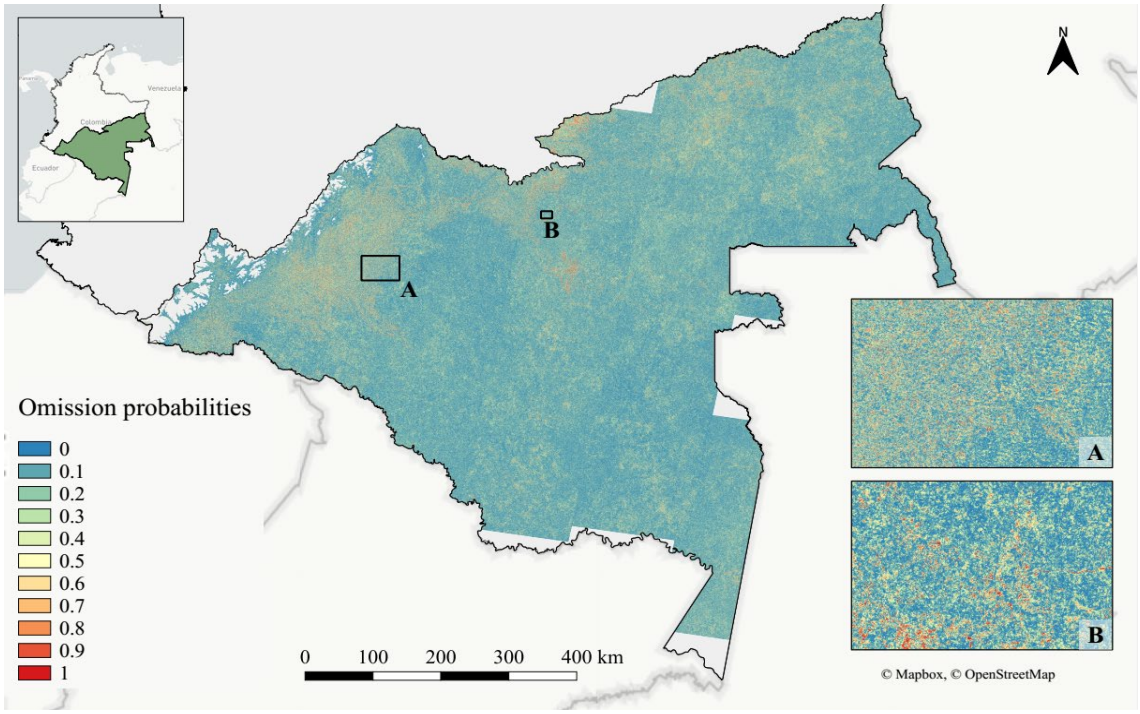

Figure 3-3. Map of omission of change probabilities for temporal segments intersecting 2010. Insets are retained to match those in Figure 2-5, where more detailed the land categories and their conversions are presented.

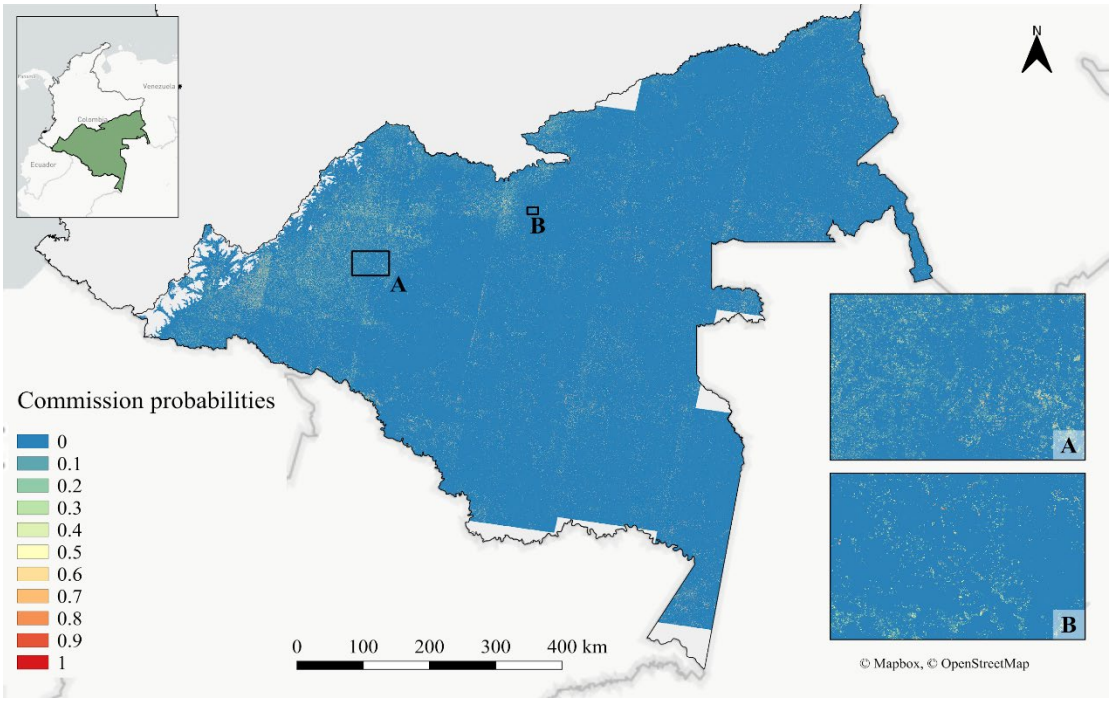

Figure 3-4. Map of the commission of change probabilities for breaks in the 2009 - 2011 period. Insets are retained to match those in Figure 2-5, where more detailed the land categories and their conversions are presented.

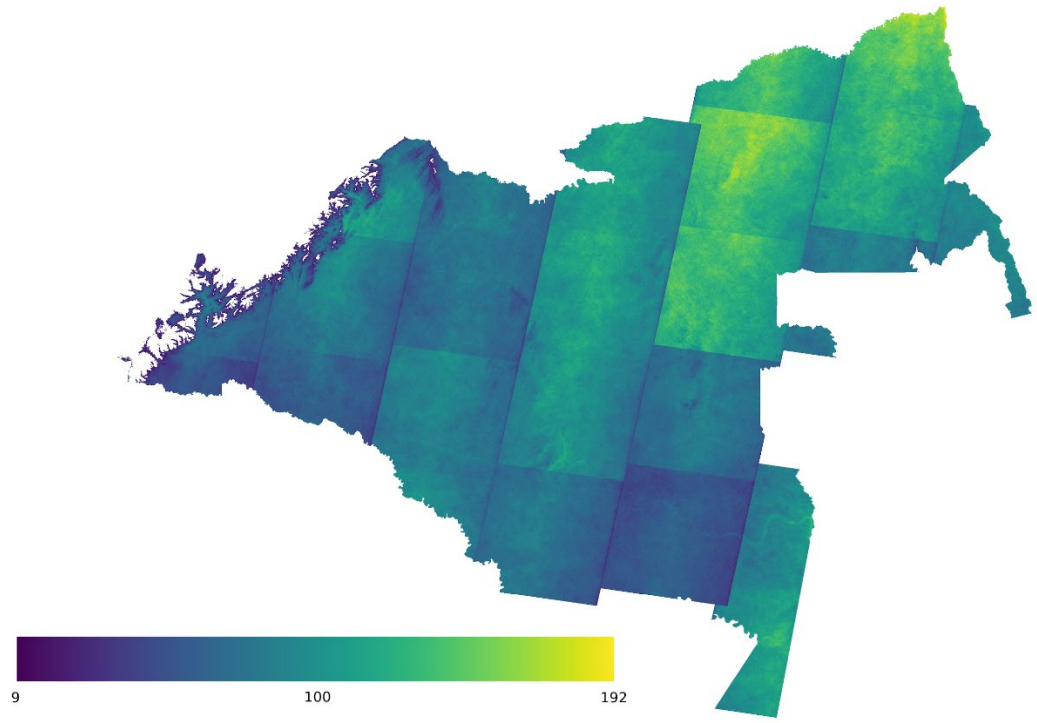

Figure 3-5. Number of cloud-free observations per pixel calculated per scene, without taking into account the overlap across them. The time series of most of the scenes in the Northeast area start in 1980's, while for the rest of the scenes they start between 1997 to 2000, explaining the large difference in the number of clear observations.

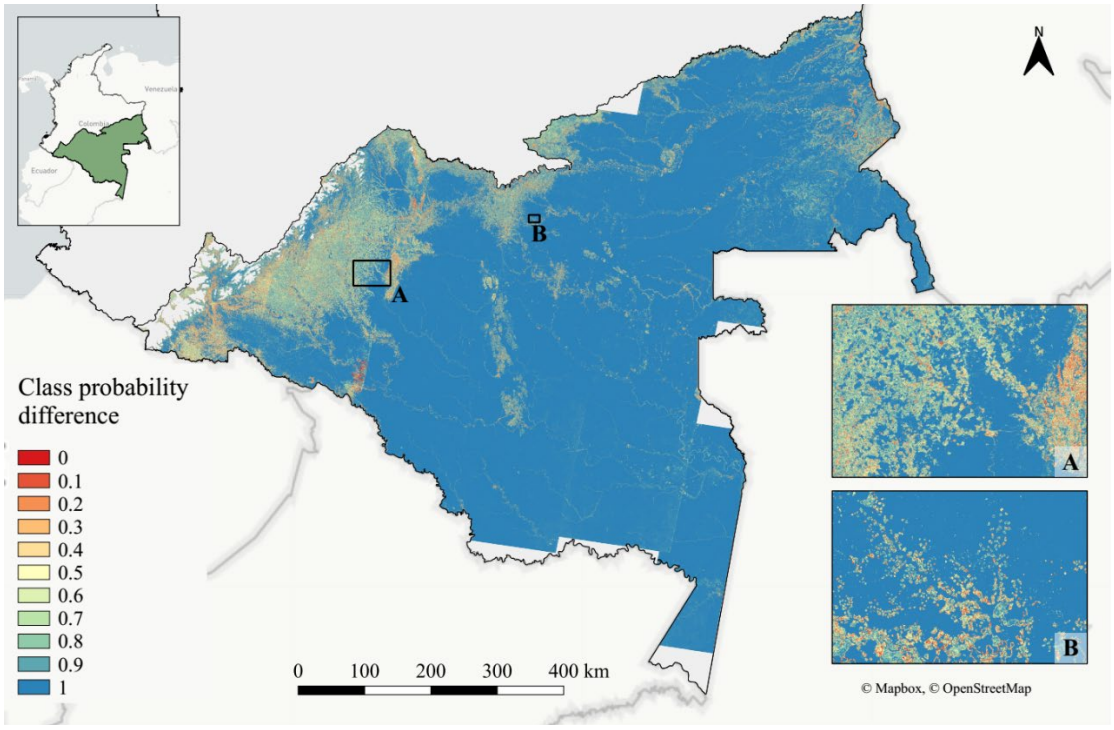

Figure 3-6. Map of class membership confidence in 2010. Insets are retained to match those in Figure 2-5, where more detailed the land categories and their conversions are presented.

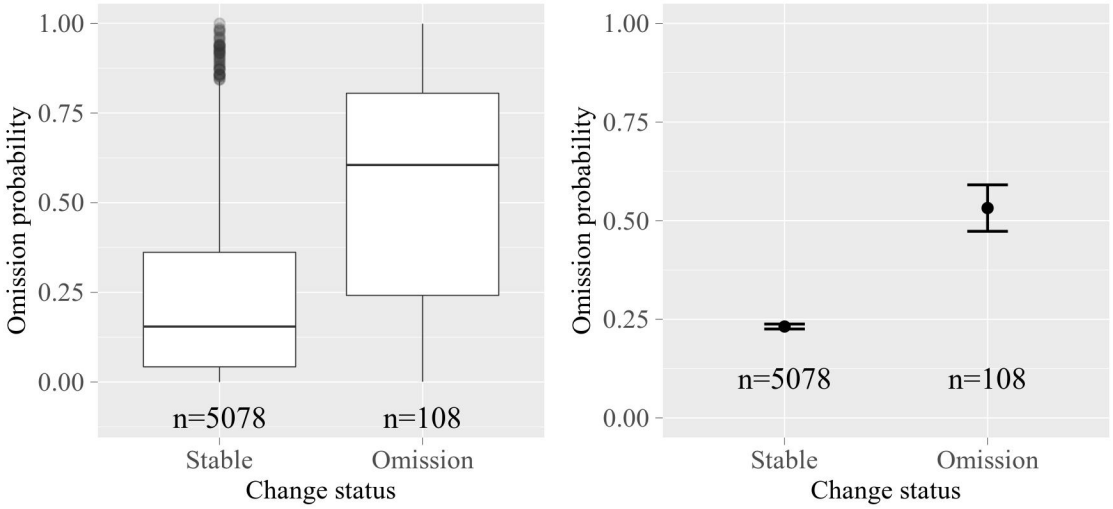

Figure 3-7. Distribution of omission probabilities per change status class, shown as a boxplot (left) and as the mean with 95% confidence intervals (right).

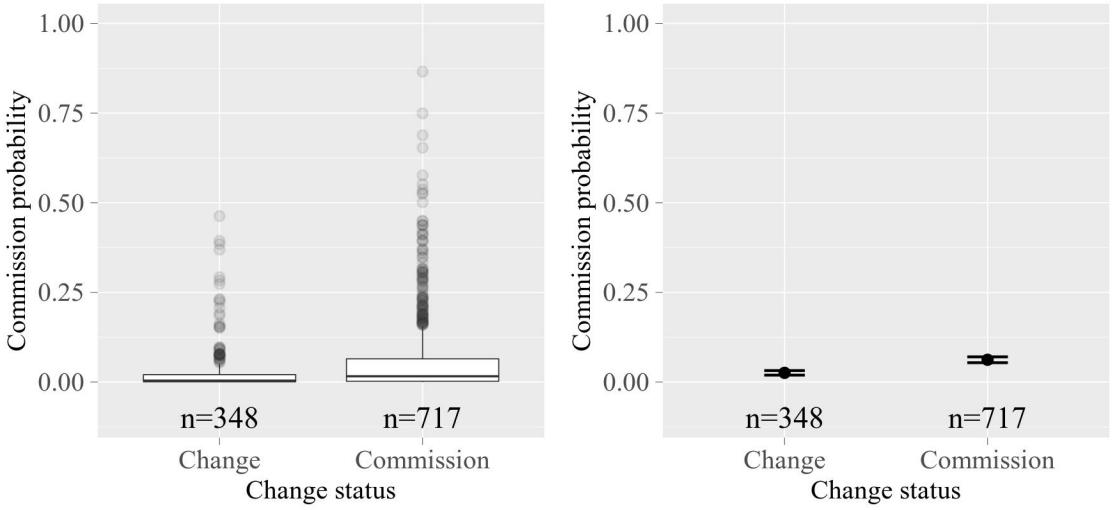

Figure 3-8. Distribution of commission probabilities per change status class, shown as a boxplot (left) and as the mean with 95% confidence intervals (right).

3.4 Discussion

3.4.1 Omission and commission probability maps and samples

The map of omission probabilities (Figure 3-3) reflects the expected distribution pattern of higher incidence of omitted changes near the deforestation frontier (Insets A and B). The map of commission probability (Figure 3-4) shows lower overall values than the omission map. This pattern is also expected, considering that most of the study area corresponds to the *Stable Forest* class, in which commission errors of change cannot occur. Both the commission and omission map have seams along the edges of certain Landsat footprints with varying degrees of intensity. The seams occur because the number of clear observations per footprint for the study period vary dramatically, as seen

in Figure 3-5. The seams are also influenced by the clipping of the footprints along the WRS-2 boundaries, which results in the inclusion of the far edges of the footprints where fewer observations are available.

The sample data show an overall positive relationship between the presence of omission or commission errors and their corresponding probability values, although the relationship is stronger for the omission probabilities. The absence of omission errors in the higher probability bins and the presence of errors in low bins are caused by unfiltered clouds and shadows, or by edges between very distinct classes. Commission probabilities show a slightly weaker relationship with the actual incidence of commission errors. In many cases, the presence or absence of commission errors in unexpected probability bins is caused by noise in time series and differences in temporal data density that trigger false detection of change. These results do not represent the inability of the test to capture the commission of changes but rather highlight the issue of noise in the time series and its negative effect on change detection. For example, pixels in *Stable Forest* with a relatively high density of observations early in the time series, combined with unfiltered noise, exhibit a higher degree of detection of a spurious change and misclassification of time segments due to a changing slope, which is uncharacteristic of time segments in forests (Figure 3-9). In addition, a comparison of the sample data for both types of errors revealed a higher proportion of sample units for the commission probabilities that were removed because of low confidence in the reference label. The removed sample units corresponded to cases where the occurrence of change (or lack thereof) could not be determined accurately. This included agricultural fields and pastures that cannot be

characterized in full detail given the low temporal density of the Landsat series in this region (Figure 3-10). Detected changes in river sandbanks that experience seasonal flooding were also excluded from the sample results. Overall, assessing the presence of commission errors was a more challenging task than assessing the occurrence of omission errors, which tend to be more conspicuous.

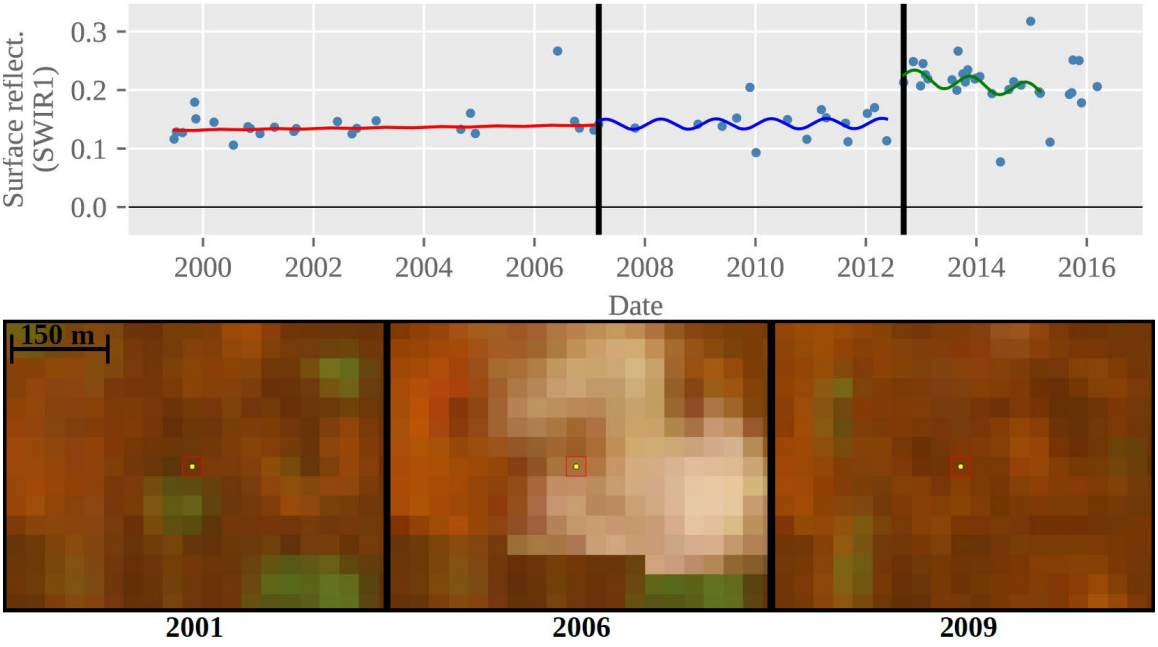

Figure 3-9. Time series (SWIR1) showing a commission of change in 2007 caused by an unscreened cloud and lower data density. Dark, orange and brown pixels correspond to forest, green and bright orange pixels represent pastures or croplands, and white pixels represent clouds. The commission probability for that change is 0.41 and 0.02 for the next one in 2012. Images show three points in time for the stable forest period: 2001-236 (left), 2006-154 (center) and 2009-146 (right). Latitude:-0.85516, Longitude: -72.82126. RGB: NIR, SWIR1, RED.

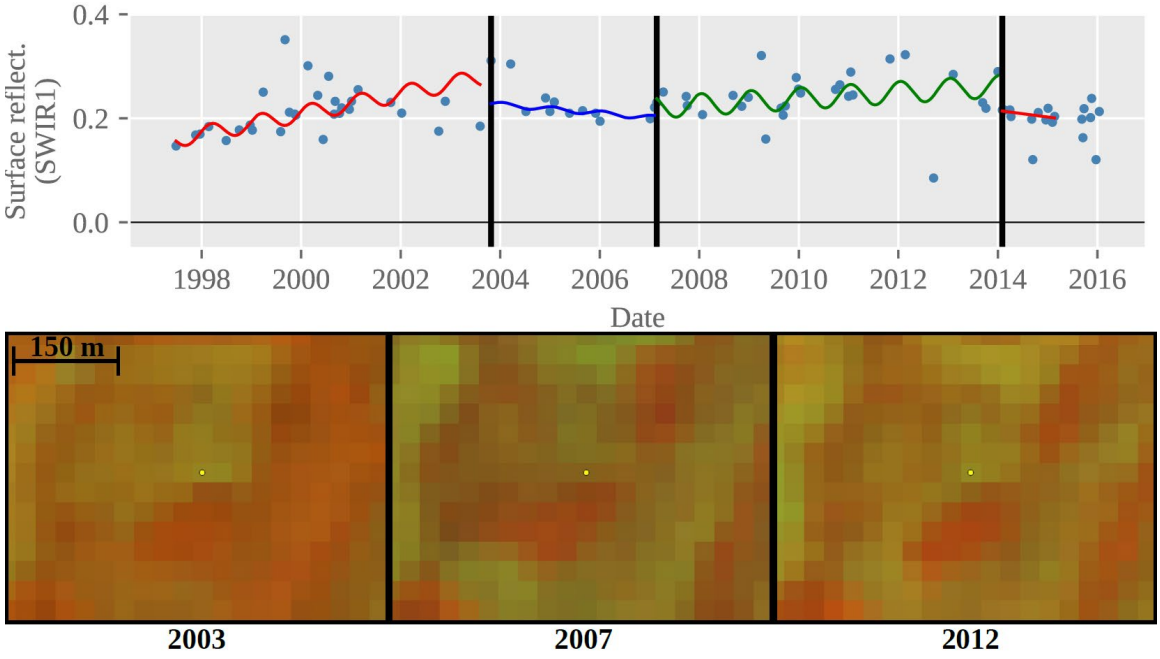

Figure 3-10. Time series (SWIR1) showing a sample unit with medium low confidence in the interpretation of occurrence of commission of the change in 2007. The segments and reflectance values are clearly different but the time series and the images show agricultural cycles (lighter colors) that are difficult to characterize given the low data density. Darker orange pixels represent denser vegetation. The commission probability for that change is 0.28. Images correspond to 2003-299 (left), 2007-054 (center) and 2012-052 (right). Latitude: 1.23088, Longitude: -75.30760. RGB: NIR, SWIR1, RED.

Landsat time series in the tropics have a large number of cloudy or shadowed observations, and their removal is essential for the change detection algorithm to behave properly. I applied two masking procedures, Fmask (Zhu and Woodcock, 2012) and Tmask (Zhu and Woodcock, 2014b), and while they removed a significant proportion of the noise, they did not mask all the unwanted observations. The issue is compounded by the fact that some of the cloudiest spots in the study area are those that have the largest historical land cover changes (Northwest area, Figure 3-5). This phenomenon translates into areas of change with a lower number of available observations, resulting in higher frequency of omission errors, and higher numbers of available observations in areas with

little or no change, that along with unfiltered noise result in commission errors. A common example of this behavior for the omission errors include relatively sparse time series in the northwestern region of the Colombian Amazon, where clearly visible changes from forest to pastures are obscured by the presence of a few noisy points near the dates of change, and therefore appear as gradual transitions to the algorithm. In the case of commission errors, a common occurrence is the presence of noise in early time series of stable forest in the Northeast section of the Colombian Amazon, prompting the incorrect detection of change. An example of an omission error due to a transition that appears gradual to the change detection algorithm can be seen in Figure 3-9. The first observation in this example corresponds to a cloud shadow that was not masked by any of the noise filtering mechanisms. The model fit for the training period, shown in the first panel, has a slope that is artificially higher due to that initial point with low (but not unusual) value. This model is used to predict the next consecutive observations and test for change, but the test is rejected and a new model is fitted including new observations. This processed is repeated (second to fourth panel) but subtle increases in slope for each iteration results in smaller residuals when the prediction passes the date of true change (1993) and consequently, in an error of omission in the change detection. The last panel shows the definitive segments fitted by the CCDC algorithm, with a break being detected only until the year 2000.

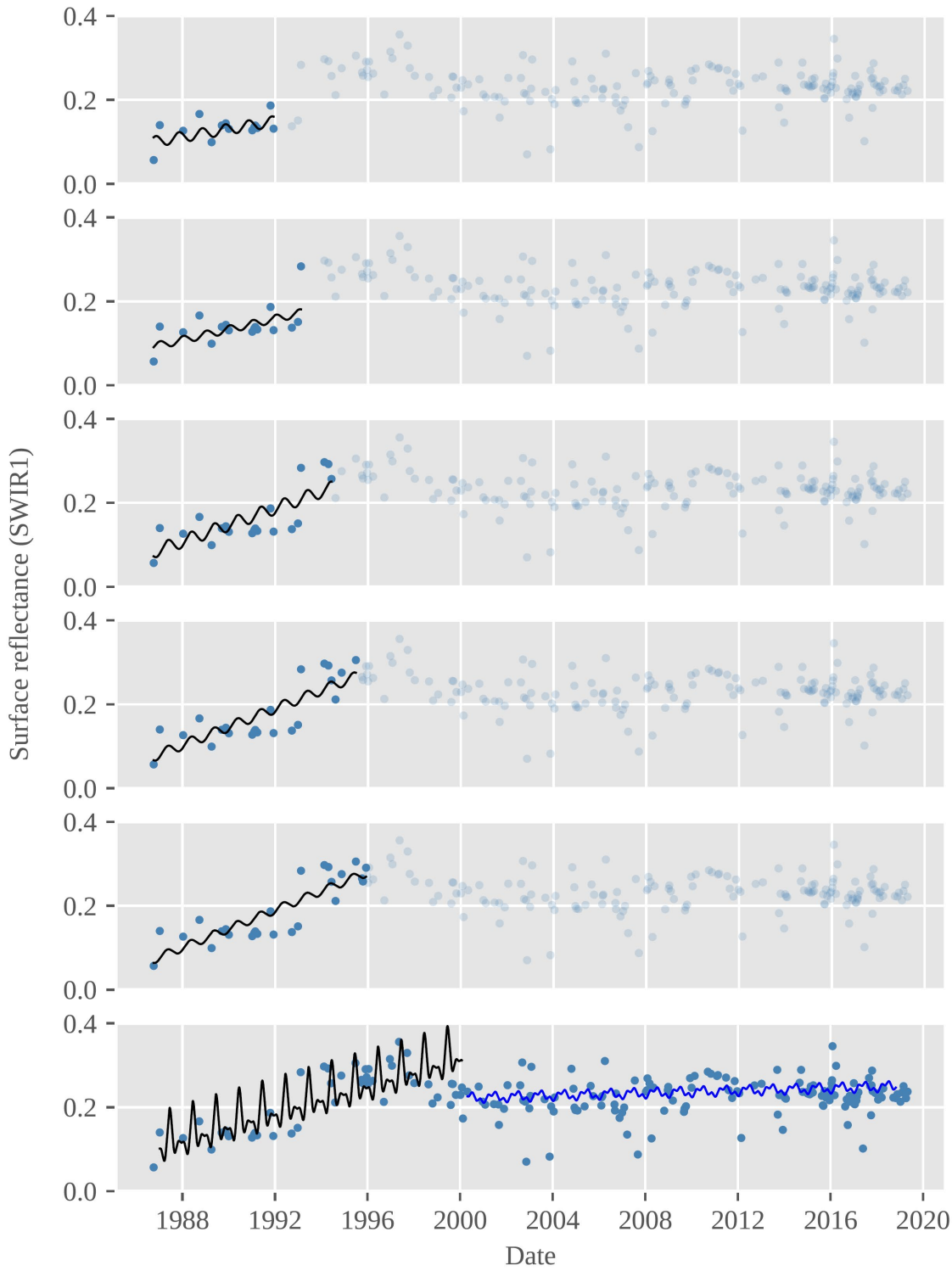

Figure 3-11. Time series (SWIR1) showing an omission of change that should have been detected in 1993. The error is caused by the gradual increase in surface reflectance as seen by the change detection algorithm with each new observation included in each consecutive model**.** Longitude-71.9849, Latitude 1.482737.

3.4.2 Analysis of biennial reference labels

The analyses of omission and commission probabilities using the previously created biennial maps and reference labels of stable and change land cover classes show a similar pattern as the samples interpreted in this study. Omission probabilities have significantly (at a 95% confidence level) higher values for sample units with confirmed omission events compared to those that are stable (Figure 3-7). The outliers in the *Stable* class with high probability values in Figure 3-7 are almost exclusively sample units with a single time segment during the study period that omit change outside of the biennial period analyzed, and thus appear as stable both in the map and the reference data. The phenomenon occurs because the omission probabilities are calculated per time segment and not per biennial period, resulting in high probability values that extend beyond the time when the error actually occurred.

The analysis of commission probabilities presents a less clear distinction between classes as shown by the box-plots in Figure 3-8. The commission class overlaps with the change class, but the former displays a broader distribution of values and outliers with higher probabilities compared to the latter. The confidence intervals around the mean show a clear separation between the classes, but both plots show evidence of a majority of values concentrated in the very low ranges of probability. The results suggest that it is challenging to characterize commission errors in a continuous probability scale. However, a closer inspection at the time series of multiple units with very low commission probabilities but labeled as stable in the reference data and change by the

maps, show time segments that are very different from each other due to unfiltered noise. The effect of this noise can result in at least two outcomes. The first is to generate an actual commission error, caused by a dramatic change in the slope of one of the resulting segments, therefore resulting in a low commission probability when the segments before and after the break are compared by the Chow test (A similar behavior is seen in Figure 3-10). The second potential outcome is to modify the timing of a break when it actually occurs, causing the map to show change while the reference data does not, and therefore appearing as a commission error (Figure 3-12). Both cases seem to indicate that commission errors are more likely to occur as a result of unfiltered noise in the time series compared to omission errors; therefore, the commission probability distribution will be more skewed toward smaller values than in the case of omission probabilities. Ultimately, comparing the coefficients of two time segments might provide suboptimal results if one of the time segments represents the wrong trend or incorrect timing of change. This contrasts with the simplicity of the omission test, which operates over a single segment.

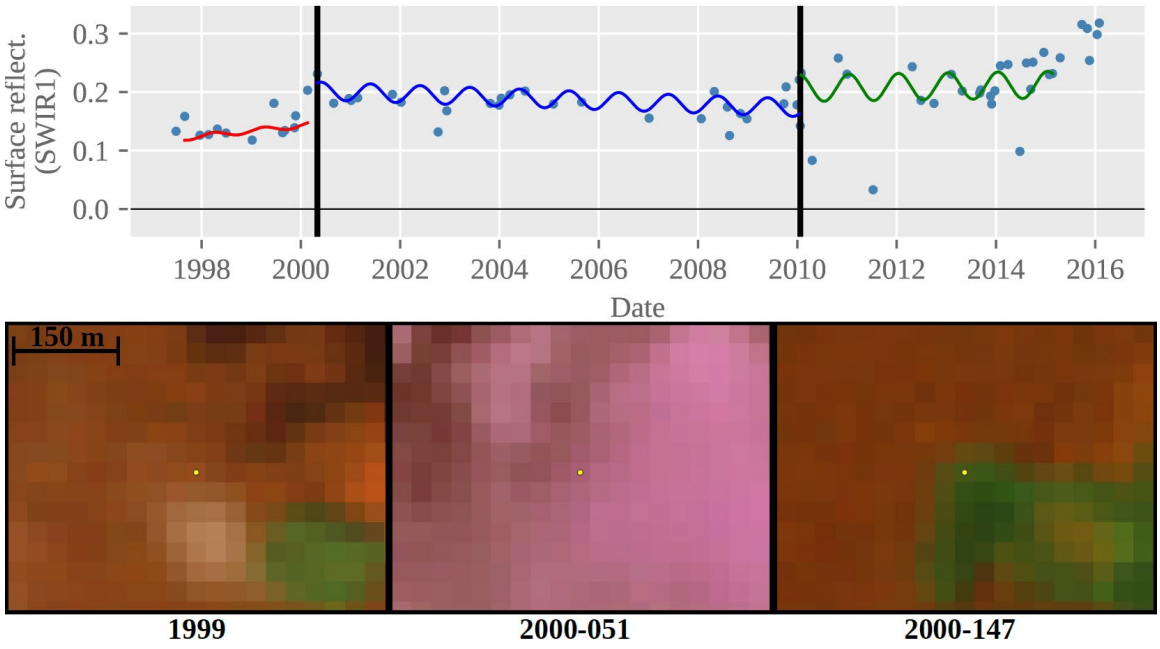

Figure 3-12. Time series of the SWIR1 band for one of the biennial sample units. A change is incorrectly detected in 2002 and therefore mapped as change for the 2001 – 2003 period, while the reference labels for that period indicate a stable class. Orange and brown pixels represent stable vegetation, green represents pastures and white and pink represent clouds. The commission probability for that change is 0.03. Images correspond to 1999-168 (left), 2000-051 (center) and 2000-147 (right). The first two images show unfiltered noise that contributed to fitting a time segment with a positive slope, also preventing the correct detection of change. Latitude: 1.35867, Longitude: -74.48269. RGB: NIR, SWIR1, RED.

3.4.3 Applications of omission and commission probability maps

The first logical use of maps of omission and commission probabilities is to simply determine which pixels in a change map are omission and commission errors. Omission probabilities can be regarded as a property of the stable periods in the time series while commission probabilities are a property of the detected changes, and therefore both are of interest to users of land cover and land cover change maps.

Omission probabilities can also be used to aid in the stratification of change maps for area estimation, because they provide an independent source of information to

construct buffer zones around areas of change that "capture" omission errors in the largest map classes (e.g. omission errors in the change from forest to pastures in the Colombian Amazon). These buffer zones are demonstrated to diminish the negative effects of omission errors in the standard errors of area estimates (Arévalo et al., 2019; Potapov et al., 2017). The construction of such buffer zones could be done by selecting the omission probabilities that exceed a certain threshold around areas of change. The delimitation of these areas could be further refined by filtering the selected pixels to those that present class membership probabilities below a given threshold. This targeted approach would result in buffer zones with a small area proportion compared to other classes in the map, particularly the largest one (such as forest in this study), maximizing their effectiveness. The determination of thresholds for that purpose could be done through a similar sampling exercise to the one conducted in this study.

Finding the optimal probability value at which most omission and commission errors are represented can also be used to break a time segment or merge two of them into a single one, respectively. Previous research on the use of the omission and commission tests in dense time series of Landsat observations (Bullock et al. 2019) has shown the utility of these tests for finding missed or incorrect breaks during post-processing. However, this approach used a fixed high-probability value as the threshold for assigning or removing breaks, and the authors advocate for a less conservative selection of those parameters. It is possible that the optimal probability value to determine the existence or lack of breaks varies across different circumstances, for example, in places with different temporal data densities. Modifying the time segments this way has the potential to

improve classification results because the new segments would represent the land cover dynamics more accurately. Furthermore, new omission and commission probabilities can be calculated for the modified segments, still providing valuable information about the uncertainty in the detection of change events. The order in which these tests are applied and its consequences on correct detection of change (or lack thereof) is still an issue that needs to be addressed, but our results and the approach used by Bullock et al. (2019) seems to indicate a greater benefit to applying the omission test first followed by the commission test.

Omission and commission probabilities, as well as class membership confidence values can also be used to represent errors in spatially explicit carbon models. For example, a system that tracks emissions and sequestration of carbon associated with land conversions at the pixel-level require omission and commission error probabilities to ensure that modeled carbon emissions are not the results of classification errors. In that system, a pixel mapped as stable forest that exhibits a high probability of being an omission error and low confidence in the class label should probably be treated as a forest loss event. Conversely, the emissions associated with a pixel mapped as forest loss should be weighted down or assumed to be zero if the commission probabilities are high and the class membership confidence is low for one or two of the segments. Alternatively, using a similar approach to the delimitation of buffer zones to contain the effect of omission errors, the probabilities could be used to stratify the study area into homogeneous zones where changes (or lack thereof) are believed to be highly likely (or unlikely). Areas estimated for these zones and their uncertainty could be used in a

traditional carbon bookkeeping model, where zones with higher probabilities of change errors receive a special treatment different from the zones with lower probabilities. For instance, more conservative emission rates could be used for zones believed to have higher probabilities of commission errors, because the changes that would release carbon to the atmosphere would not be as prevalent as the maps indicate.

3.5 Conclusions

An approach to characterize the probability of omission or commission of change in pixels of maps of land cover and land change was presented. It was found that the omission probabilities represent the probability the change detection algorithm having omitted the detection of a change on the land surface, whereas the commission probabilities represent the probability of the change detection algorithm having detected false change. The relationship between commission probabilities and actual commission errors in the maps was weaker than that of the omission errors. The techniques used to calculate omission and commission probabilities are sensitive to noise in the time series and extra measures must be taken to remove noise beforehand. Error probability maps would be useful in a range of applications in which the uncertainty in the presence and timing of change detection is important.

CHAPTER 4: CARBON EMISSIONS ASSOCIATED WITH LAND CONVERSIONS AND RECOVERY OF DISTURBED LANDSCAPES

4.1 Introduction

Emissions associated with land use and land cover change account for around a tenth of the annual CO_2 emissions released into the atmosphere by human activities (Achard et al., 2014; Harris et al., 2012; Houghton et al., 2012). But the net carbon fluxes of tropical ecosystems remain poorly quantified, with different approaches indicating either an overall sink or a modest net source (Arneth et al., 2017; Baccini et al., 2017; Houghton et al., 2012). Reducing the uncertainty in these fluxes and their attribution is an essential but challenging task given the magnitude and complexity of the problem. While tropical deforestation and the carbon emissions resulting from it have been extensively studied during the last few decades (Achard et al., 2002; Baccini et al., 2012a; Brown, 1997b; DeFries et al., 2002; Hansen et al., 2013; Tyukavina et al., 2015), carbon dynamics associated with more subtle land transitions have been less explored, contributing to the uncertainty in the fluxes. An abandoned landscape following a disturbance is a good example of a transition that is hard to study with more traditional methods because of the gradual change in the spectral signal associated with recovery of the disturbed landscape. Monitoring the fate of the disturbed landscape requires frequent observations over a long period, a situation unattainable in the tropics until recently. In traditional approaches to carbon accounting, disturbed forests are usually assumed to either regrow or stay in the disturbed state (Kuemmerle et al., 2011; Tyukavina et al.,

2015); little attention has been paid to characterizing the post disturbance landscape in more detail, thus leading to an incomplete representation of the carbon dynamics. Recent work has attempted to address this issue by focusing on the role of secondary forest and regrowing vegetation in carbon sequestration (Chazdon et al., 2016; Schwartz et al., 2017) and its effect on global carbon sink dynamics (Pugh et al., 2019).

A range of methods exist to estimate the carbon stocks in land ecosystem and quantify the emissions associated with land change, including process-based models, comparison of wall-to-wall biomass maps and bookkeeping models. Process-based models rely on the understanding of biophysical and ecological processes (Fisher et al., 2014; Friedlingstein et al., 2006; Houghton et al., 2012; Piao et al., 2009; Pongratz et al., 2009). These models are typically global in scope, essential for improving our understanding of global carbon cycle feedbacks and necessary to generate climate projections. Wall-to-wall biomass maps are generated by empirically relating in-situ measurements of biomass (or rather, estimates by allometry) to data acquired through active-sensors, such as Lidar metrics or radar imagery and, in turn, to coarse-resolution optical satellite imagery (Baccini et al., 2012a, 2017, 2018; Mitchard et al., 2013; Saatchi et al., 2011). While valuable to estimate carbon stocks and emission benchmarks, most biomass maps only cover short periods because consistent and repeated Lidar or radar measurements in the required spectral frequency are not available at a global scale, therefore restricting the possibility to track carbon pools directly and periodically over large areas. Upcoming missions such as GEDI and BIOMASS (Dubayah, 2018; Le Toan et al., 2011; Stysley et al., 2016) will contribute to this issue, but their temporal coverage

will be limited and therefore will not enable a continuous monitoring of tropical aboveground biomass that can be sustained in the future.

An alternative approach to study the effects of land change on carbon dynamics is through carbon accounting or bookkeeping models. A bookkeeping model can estimate carbon emissions and sequestration at multiple temporal and spatial scales, effectively enabling the calculation of change in terrestrial carbon storage associated with a particular land cover class, or as a result of land change. Models like those proposed by Houghton et al. (1983, 1999, 2001) and Moore et al. (1981) rely on the availability of rates of land change in combination with information on terrestrial carbon accumulation and emissions. Bookkeeping models track the fluxes between multiple carbon pools using empirical data. They have been used to quantify carbon dynamics at the global (Baccini et al., 2012a; Houghton and Nassikas, 2017; Quéré et al., 2018), regional (Baumann et al., 2017; Houghton and Hackler, 2006; Loarie et al., 2009; Toomey et al., 2013), and national and subnational level (Andersen et al., 2016; Carlson et al., 2012; Kuemmerle et al., 2011; Numata et al., 2010; Olofsson et al., 2011, 2010). Operational carbon bookkeeping models suggested as compliant with IPCC Tier 3 (i.e. spatially explicit) include the Carbon Budget Model of the Canadian Forest Sector (CBM-CFS3; (Kurz et al., 2009) and the Australian Full Carbon Accounting Model (Australian Government, 2017). CBM-CFS3 is a stand-based model that estimates emissions and removals by integrating forest inventory data and growth curves with spatial data on forest management and disturbances. The FullCAM model requires pixel-based activity data and relies on an integrated suite of process-based models.

Having to choose between process-based models, comparison of wall-to-wall biomass maps and various bookkeeping models present challenges for estimation of carbon fluxes for REDD+ and MRV purposes. For example, process-based methods often require detailed parameterization rarely attainable at the scale of the national or regional remote sensing studies. Single wall-to-wall biomass mapping can be used to derive emission factors, but with the exception of the moderate resolution maps of AGB created by Baccini et al. (2012b), their sporadic availability restricts their use for detailed continuous carbon monitoring and reporting. Spatially explicit carbon bookkeeping models have been successfully applied in Canada and Australia, but they can be difficult to implement in the tropics because of demanding input data that are not readily available in many countries. Furthermore, meeting the IPCC reporting criteria related to uncertainty and bias in a pixel-based approach is inherently difficult, as estimates of area bias and uncertainty pertain to whole populations (i.e. study areas) and are not directly related to pixel-level information, as explained in Chapter 3. For these reasons, two methods of lesser complexity are typically employed by countries to estimate their FREL and subsequent emissions for REDD+ reporting: the *stock change* and the *gain/loss* approach. As detailed in Section 1.3, the stock change approach allows the direct estimation of changes in wood carbon stocks and is typically conducted in non-tropical countries with an operational forest inventory program. The gain/loss approach requires information on activity data (areas that experience land change) and emission factors (carbon contents per area unit per land class), and it is typically used in tropical countries. This method may not properly account for gradual and non-linear carbon fluxes, such as

the carbon emitted due to forest degradation, or the carbon sequestration caused by forest regrowth, because it usually relies on average values that may result in over or under estimation of the carbon that is emitted to or removed from the atmosphere.

Given the availability of methods and input data available for the estimation of carbon fluxes, an aspect that deserves more attention is the effect of methodological choices on the estimated values of those fluxes. Previous research has indicated that choices related to the temporal evolution, state of carbon stocks at the beginning of the period, the temporal attribution of fluxes, and the treatment of fluxes prior to the study period may significantly affect the estimation of carbon fluxes (Hansis et al., 2015). Research to evaluate the effects of different scenarios of temporal attribution of carbon emissions resulting from land change (Davis et al., 2014) suggests that the choice of attribution depends on the purpose of the emission accounting. An approach to monitoring land cover and conversions based on Landsat time series, combined with sample-based estimates of area bias and uncertainty, provides us with an array of data that can be used in multiple ways to estimate carbon emissions associated with land change. For example, a carbon accounting model could use areas of land cover and change calculated directly from maps by "pixel counting" (not recommended), or ideally estimated using an unbiased estimator applied to sample data, as shown in Chapter 2. Furthermore, maps of change could be used in spatially explicit bookkeeping approaches, as previous attempts have shown (Gebhardt et al., 2014; Kurz et al., 2009), but application in tropical ecosystems using remote sensing-based maps as inputs has

resulted in large classification errors biasing the estimation of carbon emissions (Mascorro et al., 2015).

Previous research on carbon stocks and fluxes in Colombia have assessed the Aboveground Biomass (AGB) at the national (Anaya et al., 2009; Rodríguez-Veiga et al., 2019) and regional levels in the Chocó and Amazon region (Asner et al., 2012; Meyer et al., 2019) using remote sensing data from optical, radar and Lidar sensors. There is little research on the AGB values for secondary and regrowing forest, but Saldarriaga et al. (1988) found AGB values ranging from 44 Mg ha^{-1} for ten-year-old stands to 326 Mg ha^{-1} for mature forests. The country presented its official emission factor for deforestation activities in their national FREL (MADS and IDEAM, 2014), calculated using country-specific allometric models and accounting for national and regional circumstances (Alvarez et al., 2012; Phillips et al., 2016, 2011a, 2011b). Carbon emissions at the national level were estimated for the period 2005-2010 by Yepes et al. (2011), and along with other periods of variable length in Ramírez-Delgado et al. (2018). These reports are valuable and constitute a milestone in terms of the national reporting of deforestation and associated emissions. However, they do not provide any measures of uncertainty on the estimates, and the results for earlier periods are not comparable with each other due to significant methodological differences. Therefore, estimating the carbon fluxes associated with multiple land conversions at different levels of temporal aggregation and providing uncertainty on the estimates would contribute to fill these gaps and provide a set of future recommendations to further reduce uncertainty. The objectives of this chapter are: i) to estimate the gross and net carbon emissions and removals in the Colombian Amazon for

the period 2001 -2015 at different levels of temporal aggregation, and ii) to analyze the differences in the carbon emissions and removals resulting from applying a gain/loss approach and a simple carbon bookkeeping model over biased and bias-adjusted areas of land change.

4.2 Methods

Carbon emissions and removals were calculated for each biennial period using two different approaches. The first method is the gain/loss approach, multiplying the emissions factors per land change class presented in Table 4-1 by two different sets of activity data. The first set corresponded to change areas calculated directly from each biennial map through “pixel-counting”, also referred to as “biased areas”. The second set corresponded to the biennial bias-adjusted areas and 95% confidence intervals, as described in Chapter 2. These data were also aggregated into longer periods (three, two and one period) using error propagation techniques (IPCC, 2006, vol. 1, Chapter 3). The data were aggregated to study the effect on overall uncertainty in emissions and removals relative to various study periods. Net emission values with 95% confidence intervals per biennial and aggregated periods were calculated by a Monte Carlo simulation, using the mean and confidence intervals of the areas of land change to parametrize a normal distribution per change class and period. From each probability distribution, a sample of 10,000 random numbers was drawn, and then multiplied by the emission factors. The resulting values for all change classes per period were added together to obtain a

distribution of net emission values, from which the mean and standard error were calculated. The standard error was calculated as the square root of the variance of the resulting distribution. A Monte Carlo approach was used instead of a simpler propagation technique because the areas and confidence intervals for each biennial period are not independent.

The emission factor used for deforestation activities was the one reported by the Colombian Government for their FREL submitted to the UNFCC (MADS and IDEAM, 2014), corresponding to an AGB of 273.15 ± 9.8 Mg ha^{-1} (SE= 1,8%) for Tropical Rain Forest. Emission factors for the classes *Secondary Forest* and *Gain of secondary forest* were derived from the values reported in Poorter et al. (2016), who estimated an average AGB of 122 Mg ha^{-1} after twenty years of forest recovery for the Neotropics, corresponding to 6.1 Mg ha^{-1} yr^{-1}. Based on this information, an AGB gain value of 12.2 Mg ha^{-1} was used for each biennial period. For the *Loss of Secondary forest* class, it was assumed that the secondary forest would have a biomass of half that of a mature forest. Therefore, a value of 136.57 Mg ha^{-1} was used. AGB values were multiplied by 0.47 to calculate the carbon emitted or sequestered (MADS and IDEAM, 2014). For the gain/loss approach it was assumed that all carbon was instantaneously released to the atmosphere as a result of conversion from *Forest to Pasture, Forest to Secondary Forest* and *Loss of Secondary Forest.* While it is known that some of the carbon may be emitted at a later time after a land cover conversion, instantaneous release of carbon was assumed in order to associate the emissions with the activities during a given period. This is helpful to understand the immediate effect of land change dynamics on the carbon budget, as it

allows us to associate any emissions due to land change to the time when the land change occurs.

The second approach is a simplified carbon bookkeeping method adapted from Reinmann et al. (2016), which employs commonly used carbon bookkeeping approaches (Houghton et al., 1983; Moore et al., 1981) and freely available online at https://github.com/xjtang/CBookie/. The two sets of biennial change areas used for the gain/loss approach were also used as inputs for this model. However, in contrast to that approach, carbon emissions were disaggregated into different fractions allocated as *burned,* deadwood left as *slash*, *durable* products*,* and converted to *elemental* carbon through burning, plus an *unreleased* category representing delayed carbon emissions. This disaggregation was done as a way to evaluate the potential contributions of these pools to immediate and delayed emissions over time, compared to the instantaneous emissions assumed in the gain/loss approach. Values for these fractions and their rates of decay were taken from Houghton et al. (2000). Fractions were assigned as follows: 0.2 for burned , 0.7 for slash, 0.08 for durable and 0.02 for elemental (Carvalho et al., 1998; Fearnside et al., 1993). Rates of decay were assigned as follows: Durable products decayed with a constant rate of 0.1 $year^{-1}$, elemental carbon decayed at 0.001 $year^{-1}$ and dead wood left on site (*slash*) decayed exponentially at a rate of 0.1 $year^{-1}$, following those used in Houghton et al. (2000). The model requires initial AGB values for each period to determine the carbon emissions associated to forest cover loss during that period, or to determine the total forest regrowth at the end of the period. AGB values for the deforestation activities were the same used in the gain/loss approach, but AGB values

of *Secondary forest* were calculated as follows. Carbon sequestration for the *Secondary forest* and *Gain of secondary forest* classes followed a log growth curve presented in Poorter et al. (2016). The initial AGB value for the *Secondary forest* class was the same as in the first approach (136.57 Mg ha^{-1}) for each biennial period, while the initial AGB value per period for the *Gain of secondary forest* class was assumed to be zero. Therefore, the biomass value for the *Secondary Forest* class at the time of loss was determined by the log function mentioned previously after regrowing during each individual biennial period. This effectively assumes the *Secondary Forest* at the beginning of each period to be approximately 20 years old, as the true age of secondary forest in the study area is currently unknown. A summary of the values used in the two approaches is presented in Table 4-1. An additional run of the bookkeeping model without the disaggregation into emission fractions was performed, replacing the AGB value for the *Secondary forest* class for 68 Mg ha^{-1} (half of the value of 136 Mg ha^{-1} used initially), to determine the contribution of this class to the carbon removals if I assumed younger tree stands in this class.

Land cover change class	Type	Gain/loss approach	Accounting approach
Forest to pasture	Emission	273.15 Mg ha^{-1}	273.15 Mg ha^{-1}
Forest to secondary forest	Emission	273.15 Mg ha^{-1}	273.15 Mg ha^{-1}
Secondary forest	Removal	6 Mg ha^{-1} yr^{-1} based on annual rates from Poorter et al. (2016)	Based on log function from Poorter et al. (2016), starts at 136.6 Mg ha^{-1}
Gain of secondary forest	Removal	6 Mg ha^{-1} yr^{-1} based on annual rates from Poorter et al. (2016)	Based on log function from Poorter et al. (2016), starts at 0 Mg ha^{-1}
Loss of secondary forest	Emission	136.6 Mg ha^{-1} yr^{-1}	Based on log function from Poorter et al. (2016)

Table 4-1. Total AGB values used to calculate carbon emissions and removals for each land cover change class and approach.

4.3 Results

The carbon emissions and removals calculated using the different approaches are presented below. All the fluxes are expressed as total Tg C per time period (left axis) and Mg C ha^{-1}per biennial period (right axis), obtained by dividing the total flux by the area

of the study region (46,821,572 ha). ‘Single year’ labels in the x-axis represent the middle of each biennial period.

4.3.1 Gain / loss approach

Emissions and removals calculated from bias-adjusted areas with 95% confidence intervals are shown in Figure 4-1. In addition, the estimated *Deforestation* area (Figure 2-7), which considers *Forest to Pasture* and *Forest to Secondary Forest* as a single class, was used to calculate the emissions as shown in Figure 4-2. A comparison of the mean carbon emissions and removals calculated from areas of change obtained from bias-adjusted areas, as well as mapped areas through “pixel-counting” are shown in Figure 4-3. Confidence intervals are shown –even when they contain zero– in order to illustrate their effect on the estimated net emissions. Finally, margins of error for the estimated net emissions per original and aggregated period are shown in Table 4-2.

Because there were seven biennial periods, the aggregation into three and two periods was done using only six biennial periods at a time, to avoid a misleading comparison of periods with different lengths. For this reason, two sets of estimates were created for each set of longer periods: one starting in 2001 and ending in 2013, and another starting in 2003 and ending in 2015. The results of the aggregation into three periods are shown in Figure 4-4 and Figure 4-5. Figure 4-6 and Figure 4-7 show the results of the aggregation into two periods. The aggregation using all of the biennial periods is shown in Figure 4-8.

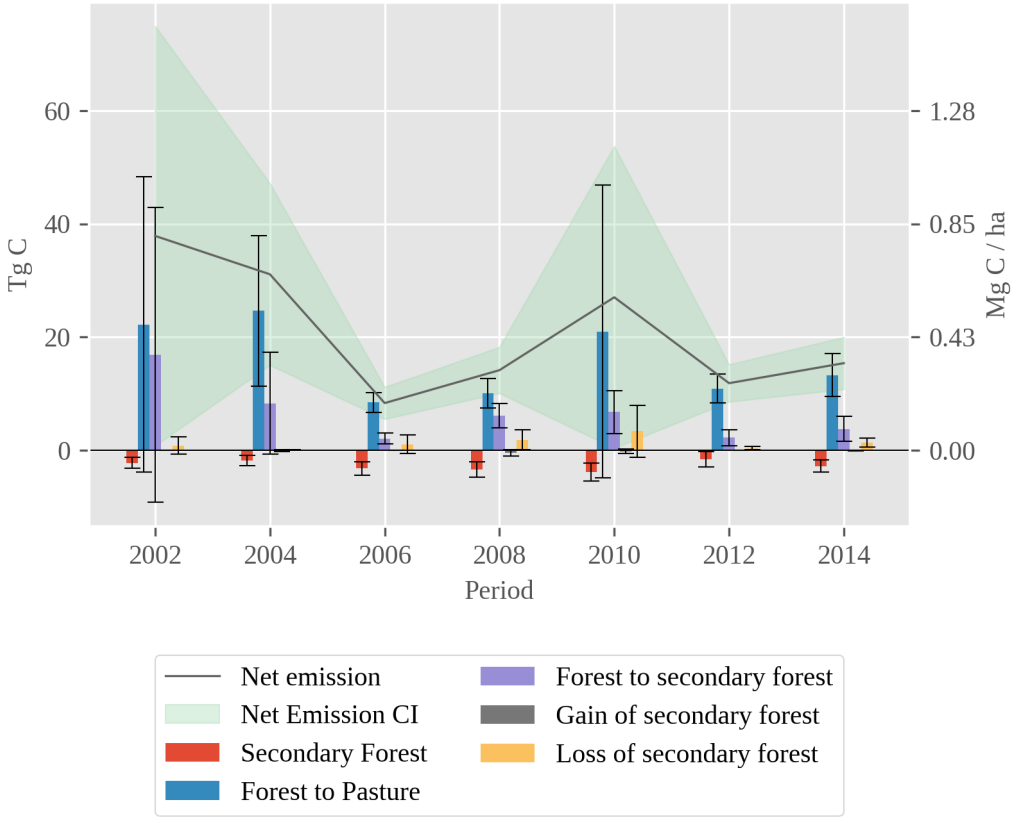

Figure 4-1. Carbon emissions and removals calculated using the gain/loss approach, obtained from bias-adjusted areas with 95% confidence intervals. The continuous line represents net mean emissions per period calculated using a Monte Carlo sampling approach, and the green fill represents its 95% confidence interval.

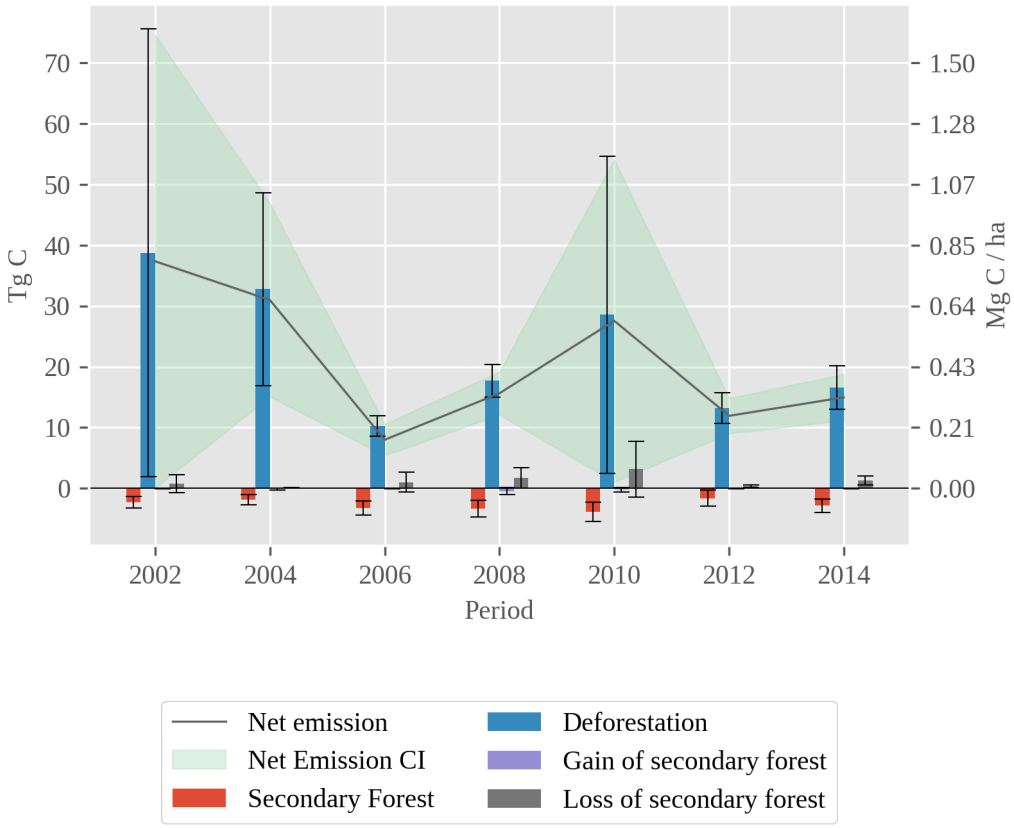

Figure 4-2. Carbon emissions and removals calculated with the gain/loss approach using bias-adjusted areas with 95% confidence intervals. The *Forest to pasture* and *Forest to secondary forest* have been merged into a single class called *Deforestation*. The continuous line represents net mean emissions per period calculated using a Monte Carlo sampling approach, and the green fill represents its 95% confidence interval.

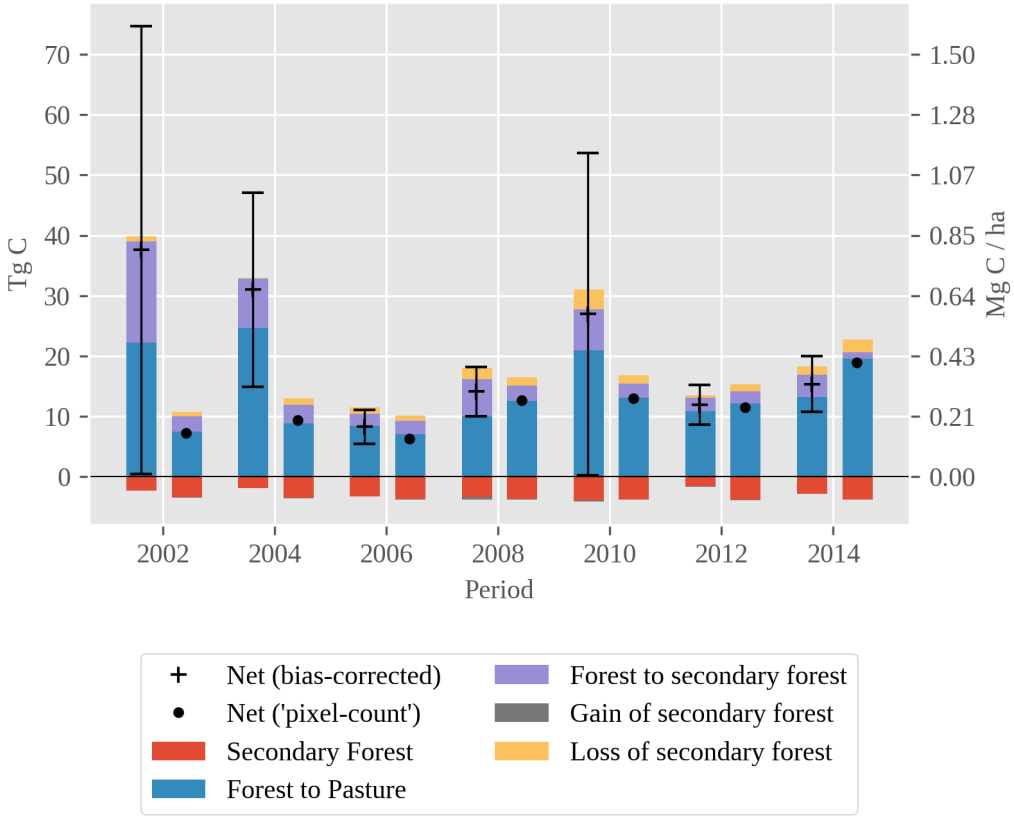

Figure 4-3. Carbon emissions and removals calculated using the gain/loss approach, with activity data from bias-adjusted areas (left bar per period) and with mapped areas through "pixel-counting" (right bar per period). 95% confidence intervals are shown for the net estimates of the bias-adjusted values.

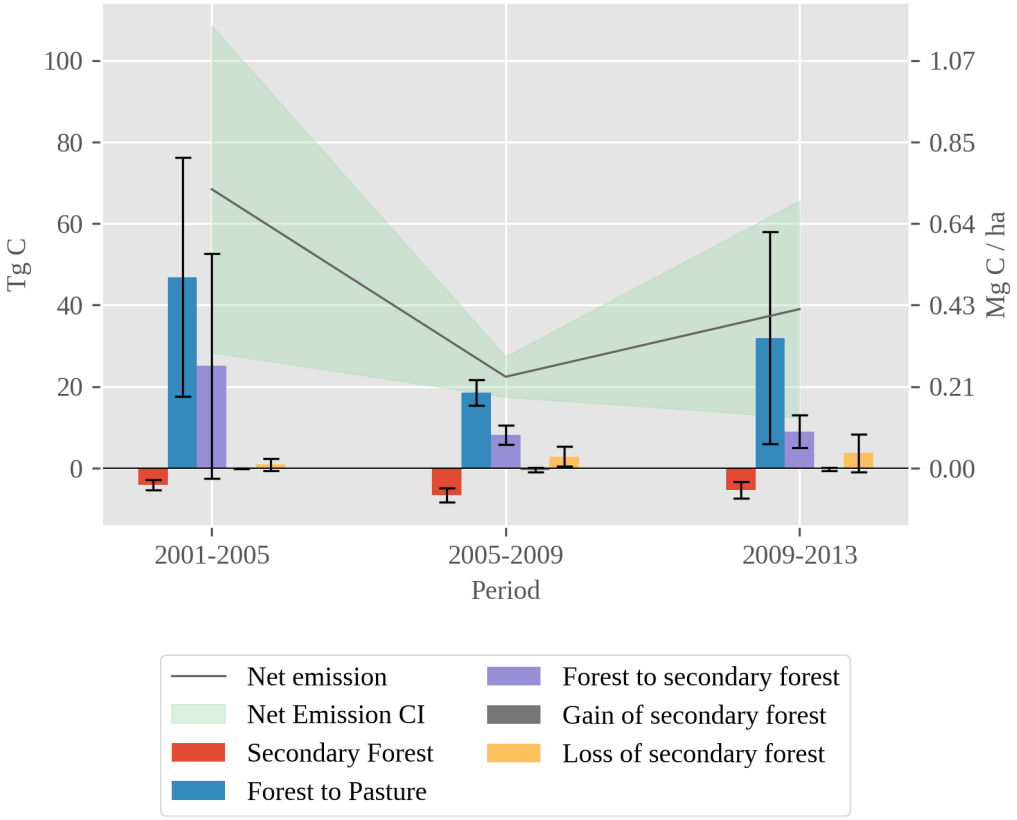

Figure 4-4. Carbon emissions and removals calculated with the gain/loss approach using bias-adjusted areas with 95% confidence intervals. The six biennial periods starting in 2001 and ending in 2013 have been merged into three periods. The continuous line represents net mean emissions per period calculated using a Monte Carlo sampling approach, and the green fill represents its 95% confidence interval.

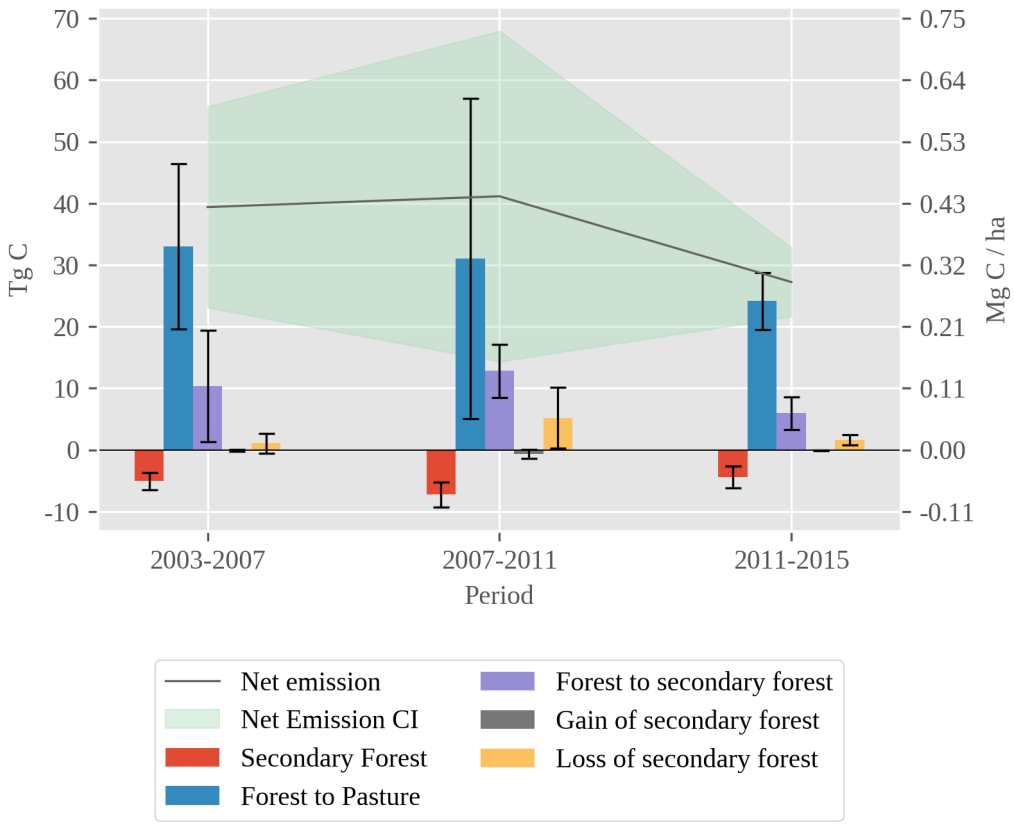

Figure 4-5. Carbon emissions and removals calculated with the gain/loss approach using bias-adjusted areas and their 95% confidence intervals. The six biennial periods starting in 2003 and ending in 2015 have been merged into three periods. The continuous line represents net mean emissions per period calculated using a Monte Carlo sampling approach, and the green fill represents its 95% confidence interval.

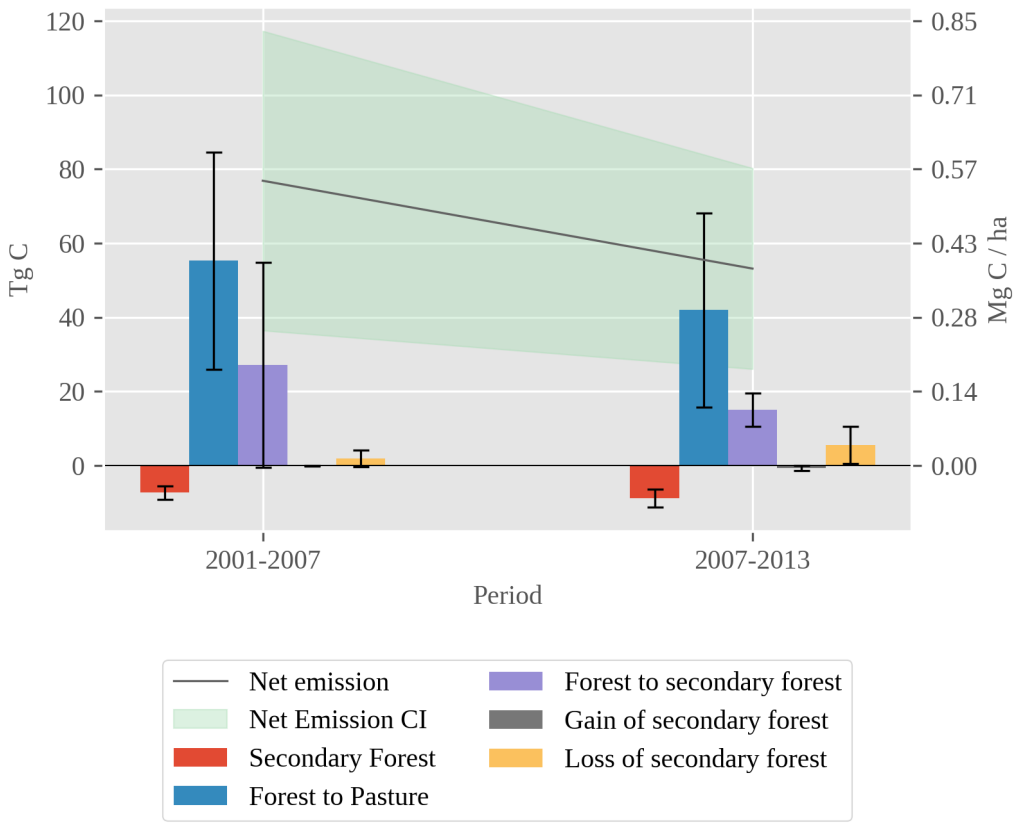

Figure 4-6. Carbon emissions and removals calculated with the gain/loss approach using bias-adjusted areas and their 95% confidence intervals. The six biennial periods starting in 2001 and ending in 2013 have been merged into two periods. The continuous line represents net mean emissions per period calculated using a Monte Carlo sampling approach, and the green fill represents its 95% confidence interval.

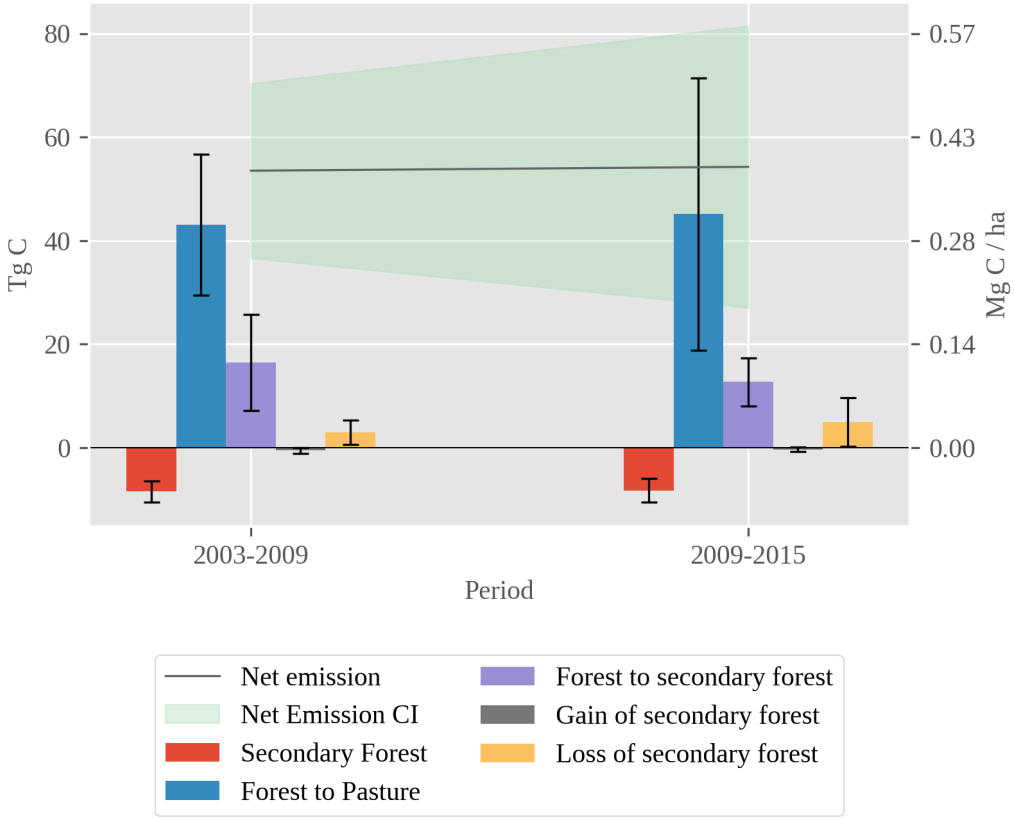

Figure 4-7. Carbon emissions and removals calculated with the gain/loss approach using bias-adjusted areas with 95% confidence intervals. The six biennial periods starting in 2003 and ending in 2015 have been merged into two periods. The continuous line represents net mean emissions per period calculated using a Monte Carlo sampling approach, and the green fill represents its 95% confidence interval.

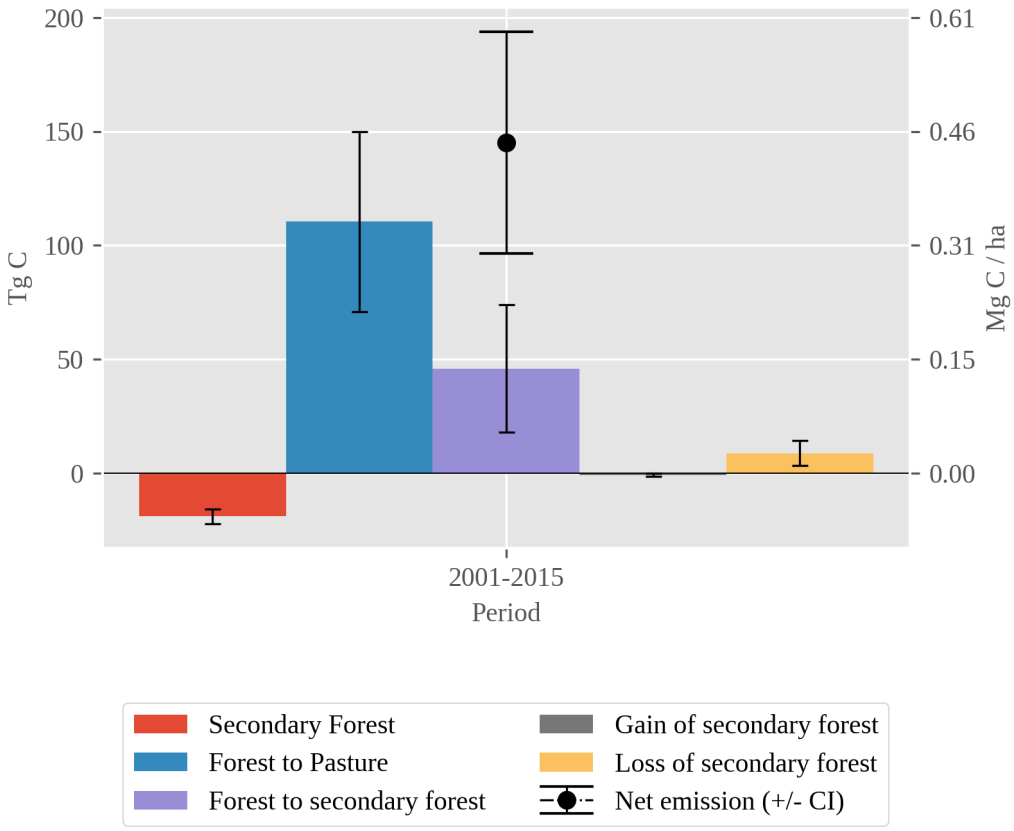

Figure 4-8. Carbon emissions and removals calculated with the gain/loss approach using bias-adjusted areas with 95% confidence intervals. The seven biennial periods have been merged into one. The marker represents net mean emissions for the entire aggregated period, calculated using a Monte Carlo sampling approach, and the error bar represents its 95% confidence interval.

Starting period	Biennial periods	Three periods	Two periods	One period
2001		0.50	0.52	
	0.53			0.34
2003		0.43	0.41	

Table 4-2. Mean margin of error of the net emission estimate for each original and aggregated period. (Margin of error = half width of confidence interval / area estimate).

4.3.2 Carbon bookkeeping

Carbon emissions and removals calculated with the carbon bookkeeping model, using the bias-adjusted areas of land change, as well as the areas obtained from the maps through "pixel-counting" are shown in Figure 4-9, disaggregated based on their source pool. Emissions are shown in darker colors while unreleased emissions are shown in lighter colors. Figure 4-10 shows the aggregated emissions and removals under the scenario of the *Secondary forest* class regrowing from an initial AGB of 68 Mg ha^{-1}.

In these two figures, the unreleased values per period represent the contribution of that period to the unreleased pool, because the values for the unreleased and other fractions were calculated as the difference between cumulative values reported by the bookkeeping model. Showing the contribution to the unreleased fraction per period facilitates the comparison with the *gain/loss* approach results, because the sum of the released and unreleased emissions per period in the bookkeeping results should be almost identical to those from the *gain/loss* approach, because the same emission factors for deforestation activities were used in both cases. The calculation of emitted and

unreleased carbon per period from cumulative values caused two periods (2005-2007 and 2011-2013) to present unreleased carbon values that are negative (bias-adjusted areas, Figure 4-9 and Figure 4-10). For example, the cumulative unreleased emissions for the *slash* fraction up to the 2011-2013 period were slightly larger than the cumulative emissions up to 2013-2015, resulting in a negative 'contribution' of the 2011-2013 to the *unreleased slash* pool when the difference was calculated.

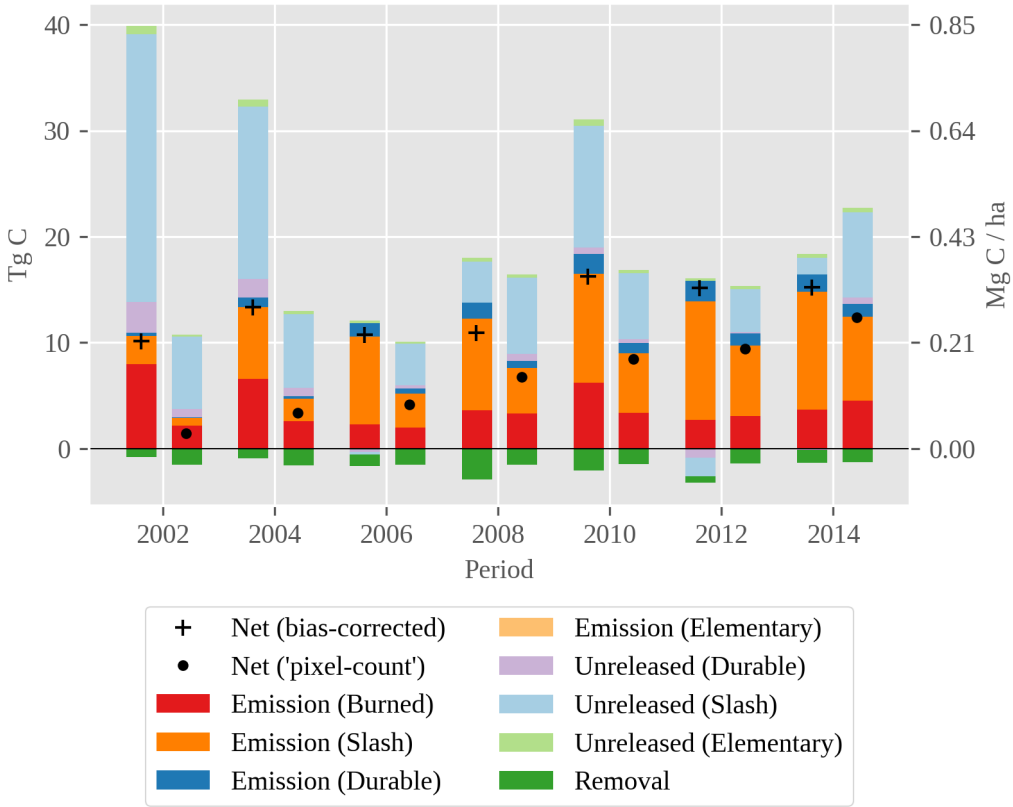

Figure 4-9. Carbon emissions and removals disaggregated by product, calculated with a carbon accounting model applied to change areas obtained from bias corrected areas (left bar per period) and "pixel-counting" (right bar per period).

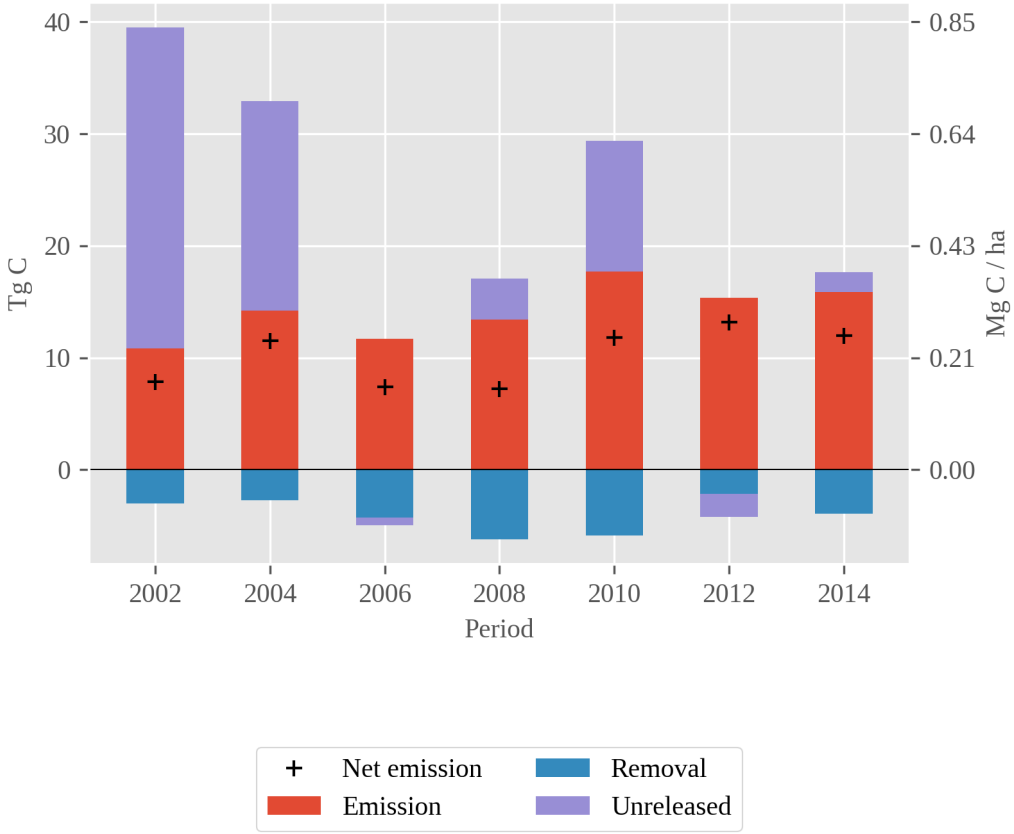

Figure 4-10. Carbon emissions and removals per biennial period calculated with a carbon accounting model applied to bias corrected change areas, assuming that all secondary forest regrows from an initial AGB of 68 Mg ha^{-1}.

4.4 Discussion

The effect of the uncertainty of land change area on the estimation of carbon emissions and removals calculated using the *gain/loss* approach is illustrated in Figure 4-1; the estimated carbon emissions vary greatly because of the substantial uncertainty in the estimated areas of forest loss. The first and fifth periods (2001-2003, 2009-2011)

exhibit the largest uncertainty simply because the area estimate of the main carbon-emitting activity*, Forest to pastures,* is associated with very large uncertainty, with the 95% confidence intervals of the area estimates 2001-2003 and 2009-2011 including zero (i.e. I cannot infer that the areas are significantly different from zero). An alternative version of this figure showing emissions from *Deforestation* reveals a decrease in net emissions between the 2003-2005 period and the 2005-2007 period, followed by an increase in the period 2007- 2009, and stable emissions until 2015, excluding the highly uncertain 2009-2011 period (Figure 4-2). For both figures, small removals of atmospheric carbon by regrowing *Secondary Forest* are usually followed by emissions of similar magnitude from *Loss of secondary forest*, although only three of those losses have confidence intervals that do not include zero. Other removals associated with the *Gain of secondary forest* are negligible. While the aggregation of area estimates of deforestation activities into a *Deforestation* class results in estimates that are different from zero for all periods, it has an imperceptible effect on the calculation of the net emissions and 95% confidence intervals. Both original and *Deforestation* net estimates are different from zero and display equivalent levels of precision, suggesting that the estimation of the *Deforestation* class might be unnecessary for the estimation of net emissions. In addition, a comparison of the mean carbon emissions calculated from these bias-adjusted areas with those obtained from "pixel counting" (Figure 4-3) shows visible differences in the trend of emissions. Even if the two highly uncertain estimates are ignored, net emissions from bias-adjusted areas are higher than those obtained from "pixel-counting" areas except for the last period. On average, 20.9 Tg C (0.45 Mg C ha^{-1}) are emitted per

biennial period according to the bias-adjusted area results, contrasting with 11.3 Tg C (0.24 Mg C ha^{-1}) for the emissions derived from mapped areas. These results are a direct reflection of the area trends shown in Chapter 2, and highlight the importance of using bias-adjusted area estimates to get a more accurate depiction of the land change dynamics and their related carbon emissions.

The aggregation of emissions into longer periods was effective at reducing the uncertainty around most gross and net estimates of carbon emissions and removals (Figure 4-4 to Figure 4-8, Table 4-2). In the three-period aggregation, the bounds of the confidence intervals on the net emissions were driven by the large uncertainty in the *Forest to Pasture* estimate for the first and fifth periods. As seen in Figure 4-4, when the aggregation starts in 2001, the area estimates representing 2001-2003 and 2009-2011 have the largest confidence intervals. A similar situation is observed in the period 2007-2011 of Figure 4-5, with the aggregation starting in 2003. Even with the reduction in uncertainty in both cases, it is not possible to assess the direction of the trend in the net and most of the gross estimates. This also holds true for the aggregation into two periods, where the overall uncertainty is reduced when the aggregation starts in 2003 (Figure 4-7) but the trend in emissions cannot be established.

The net emission between the years 2001 and 2015 in the study area was 145.3 Tg C, corresponding to an average of 10.38 Tg C $year^{-1}$ (0.22 Mg C ha^{-1} $year^{-1}$) according to the aggregated results for the entire study period (Figure 4-8). In comparison, the average annual emission based on the national FREL, calculated for the Colombian Amazon Biome for the period 2000-2012, was 10.64 Tg C $year^{-1}$ (0.23 Mg C ha^{-1} $year^{-1}$) (MADS

and IDEAM, 2014). The analysis provides evidence of average annual carbon emissions highly consistent with those reported by the Colombian government for the FREL and in their national reports (Ramírez-Delgado et al., 2018). However, the results presented here include estimates of the uncertainty in the emissions associated with the land change classes for each biennial and aggregated interval, as well as for the net emissions, while the official estimates do not. The small differences between the total emissions can be attributed to multiple factors. First, the total mapped area was slightly larger in this study (46,821,572 ha vs 45,896,100 in the FREL) because a different boundary definition for the Amazon Region was used. Second, the FREL uses a smaller value of mean annual forest loss area than the results presented in this chapter (82,863 ha vs 87,016 ha). Finally, the net emissions shown in this chapter include the carbon removals from the atmosphere due to forest regrowth, while the value reported in the FREL does not.

The results of running the bookkeeping models with biased ("pixel-counted") and bias-adjusted areas of change offer an insight into the carbon dynamics when emissions are not assumed to be instantaneous. As expected, lower emissions per period, compared to the *gain/loss* approach, can be seen in Figure 4-9, as emissions go into the *unreleased* pool for delayed release. Emissions calculated from bias-adjusted areas present a less clear temporal pattern of immediate and delayed emission from *slash* than those calculated from "pixel-counting", which show a steady increase in emissions from this pool. In both the bias and bias-adjusted cases, the emissions associated with durable products can be seen increasing over time, while the emissions from *elementary* carbon are not even visible at the scale of the figure. In turn, removals due to the *Secondary*

forest and *Gain of secondary forest* classes are mostly uniform for the biased areas, while they peak in the 2007-2009 period for the biased-adjusted, simply following the pattern in the magnitude of the areas. Overall, the net emissions per period are higher for the results from bias-adjusted areas than for the areas calculated from "pixel-counting". As mentioned previously, the clear differences between the estimates from these two types of change areas are due to the different magnitude of the areas that go into the bookkeeping model, but also caused by the very large emissions associated with deforestation in earlier periods for the bias-adjusted case, because their delayed emissions carry through the entire study period. For example, the biased and bias-adjusted areas are similar in the period 2005-2007, but the large unreleased emissions from earlier periods result in higher emissions associated with *slash* for the bias-adjusted areas compared with the biased areas. This situation contrasts with the *gain/loss* approach, for which the total emissions in that period are roughly similar in both cases (Figure 4-3).

While the use of biased areas based on "pixel-counting" goes against established recommendations (Olofsson et al., 2014), they were included in this study to illustrate the potential difficulties involved in the estimation and reporting of carbon emissions for REDD+. Using biased areas may result in over or under estimation of carbon emissions, as shown in Figure 4-3 and Figure 4-9, where net emissions from bias-adjusted areas are higher. However, using sample-based estimates of area can be challenging because it is difficult to obtain precise estimates, particularly when the change areas are small. The complexity of achieving a higher precision in the area estimates is compounded by the requirement to report at annual or biennial time intervals. Alternatives to increase the

precision of area estimates include the increase in sample size, the increase in the accuracy of the maps used for stratification of the sample, and the inclusion of a buffer stratum around areas of change that minimizes the impact of omission errors on the estimates, as explained in Chapter 2. Those buffers can be obtained from maps of omission probability, using the methodology detailed in Chapter 3. With these and other tools, efforts to increase the precision of carbon emissions should focus on the reduction of the uncertainties in the estimates of change areas.

Other sources of uncertainty in the estimation of carbon emissions result from the choice of land cover classes and changes included in the analysis, as well as the parameters used to calculate their emission factors. To illustrate this situation, the bookkeeping model was run with a lower starting biomass (68 Mg ha^{-1}) for the *Secondary forest* class, which assumes younger forest stands (Figure 4-10). The increased carbon removals –on average three times higher than those using the higher starting biomass- highlight the importance of parameter selection for the function chosen to simulate forest regrowth, and the importance of including a *Secondary forest* class, as it has the potential to offset part of the emissions in the study area. For the bookkeeping model I assumed a starting AGB value of 136.57 Mg ha^{-1} for the *Secondary Forest* class –representing tree stands twenty years old– that was used for every biennial period to simplify the analyses. This assumption was made because the age of the oldest secondary forests in the study area is unknown and the time series for most of the Landsat scenes covering the study area start only until the year 1997. Other potential initial mean AGB values were calculated for the pixels labelled as *Secondary forest* in the year 2001 and 2016 using the

AGB datasets for the year 2001 from Baccini et al. (2018) and for the year 2016 from Rodríguez-Veiga (2019), respectively. For 2001, the mean AGB value was 211.7 Mg ha^{-1}, but it was only 38 Mg ha^{-1} for the year 2016. For reference, the mean AGB for stable forest calculated from Baccini et al. (2018) was 283.7 Mg ha^{-1}. The large disparity in the results could be attributed to different techniques employed to estimate the AGB values in the two maps, as well as the low accuracy of the mapped *Secondary Forest* areas for these two periods (Table 2-3 and Table 2-4). These low accuracies could result in forests being misclassified as *Secondary Forest* early in the time series, explaining the higher mean AGB value when compared to 2016, when pastures could have been misclassified as *Secondary Forest*. None of these values were used in the bookkeeping model, as they would result in drastically different removals of carbon from the atmosphere, but this situation highlights the importance of accounting for the age and estimating the growth rates of secondary forests in the study region.

In contrast to the non-spatial model presented above, a spatially explicit carbon bookkeeping model operating on the time segments would not depend on manually setting the initial AGB for the *Secondary Forest* class. Initial values for the biomass in each land cover class can be taken from an AGB map like the one created by Baccini et al. (2018). *Secondary Forest* is assumed to start growing from a biomass of zero, and the AGB for any point in time is calculated using a regrowth function and the length of the time segment. In addition, a spatial model would make it possible to accommodate the spatial variability in the emission fractions, incorporating the knowledge on the locations in the study area where wood extraction (Southwest) or fires (Northeast) are more

common. A drawback of this method is that it relies exclusively on the land cover class labels recorded in the time segments or maps used as inputs, and the low accuracies for certain land cover classes would produce biased emission estimates. An example of this situation is observed in the model used in Mascorro et al. (2015), where pixel-level change was provided as an input to the model, but up to 85% of the actual forest change was missing from the map, according to their sample data. Such issues need to be resolved before these type of spatial approaches can be used widely. Developing methods to adjust the input areas or emissions obtained from spatial models to match the emissions obtained from bias-adjusted areas is a future research avenue.

4.4.1 Future directions

A main limitation of this study is the uncertainty around biennial estimates of land change, which drives the uncertainty in the emissions estimated from them. These uncertainties are reduced when periods are aggregated, but they are still large enough that their temporal trend cannot be determined confidently. While having area and emissions estimates with high uncertainty is better than not knowing the uncertainty at all, an increase in the precision of the area estimates is desirable, particularly if the goal is to prove a reduction in emissions over time. Another limitation stems from the assumptions regarding the spatial distribution and the initial values of AGB for some of the land cover classes considered, particularly the *Secondary forest* class. More attention should be paid to determining the approximate age of tree stands, particularly prior to and at the

beginning of the time series. The creation of a forest baseline map using imagery obtained between 1970 – 1990 would contribute to this goal. With this information on stand age, the model could be modified to keep track of different secondary forest fractions with varying ages, instead of assuming *Secondary Forest* regrowth from the same starting conditions in each biennial period. Regarding the forest class, AGB values disaggregated by forest type are available (Yepes et al., 2011) and may contribute to a more accurate depiction of carbon fluxes, particularly in areas closer to the Andes where the plant communities are different than in the lower lands. Upcoming results from the National Forest Inventory program should provide updated information on AGB contents for some of these different forest types in the study area, as well as rates of regrowth.

Single values of AGB per class were used for the analyses presented in this chapter, but if more data from other sources can be collected, probability distributions could be constructed and used for sampling in a Monte Carlo approach, allowing the propagation of uncertainty in the AGB values. The standard error of the AGB of forest for the Colombian Amazon was reported in the national FREL, but it was not included in any of the calculations, as the effect of the AGB variability in the final emissions would be negligible compared to the effect of the uncertainty in the area estimates. However, if the uncertainties in the estimated areas were reduced, the propagation of uncertainty in the AGB values would be necessary.

Similarly, uncertainty was not accounted for in the bookkeeping model. One of the objectives of this study was to calculate and analyze the instantaneous and potential delayed emissions due to land conversion, which to my knowledge has not been done in

the study region. This analysis would be greatly enriched by running the bookkeeping model in a Monte Carlo simulation, sampling from distributions representing the land change areas, as well as the different parameters such as emission factors and regrowth rates. This type of simulation could contribute to determine the uncertainty in the carbon emissions calculated through the bookkeeping method, as well as the potential of *Secondary Forest* for carbon removals.

Finally, the analysis presented in this chapter focused on the carbon dynamics associated with land change, but other stable land cover classes may also contribute to total emissions. For example, natural fires are common in the natural grasslands present in the study area and nearby, but while their magnitude and frequency have been studied, their contribution to carbon emissions have not (Armenteras et al., 2017). Fire is also known to be more frequent and intense in fragmented landscape forests, where its occurrence results in a higher degree of biomass combustion (Armenteras et al., 2013). I assumed the emission fraction due to fire to have a value of 0.2 in the bookkeeping model based on the literature, but more attention is needed to determine if this and the other fraction values are truly representative of the study area. It may be possible to determine and assign these values in a spatially explicit way. Other information that could be used in the bookkeeping model corresponds to soil organic carbon from primary forest, degraded and improved pasture systems (Mosquera et al., 2012a, 2012b), as well as coarse woody debris dynamics after forest to pasture conversion (Navarrete et al., 2016).

4.5 Conclusions

Net carbon emissions in the Colombian Amazon average 10.38 Tg $year^{-1}$ (0.22 Mg C ha^{-1} $year^{-1}$), with a total of 145.3 (± 48.47) Tg C emitted between 2001 and 2015. These results are consistent with official national estimates, but provide a measure of uncertainty around the estimated net and gross values per land change class. The conversion from forest to pasture contributes most of the emissions and the regrowth of secondary forest accounts for most of the removals from the atmosphere. The aggregation of biennial periods into longer periods contributes to a reduction in the uncertainty around the net and gross emissions, particularly for the classes that represent the smallest areas of change. However, even after the period aggregation it is not possible to determine the direction of the emission trends. The regrowth of secondary forest has the potential to offset a considerable fraction of the gross emissions, but more research is needed to parametrize the regrowth curve with more accurate values of AGB based on the true age of the secondary forest stands. A reduction in the uncertainty of estimates of area is needed to increase the precision in the estimated carbon fluxes.

.

CHAPTER 5: CONCLUSION

Accurate reporting of greenhouse gas emissions and removals due to land cover change depends on the proper quantification of land change areas and their uncertainty. The opening of the Landsat archive has enabled the continuous monitoring of the land surface through algorithms that detect temporal trends, as well as gradual and sudden changes over time. At the same time, a set of best practices and guidance has become available to estimate areas of change and their resulting emissions in a transparent and statistically robust way. Combining the vast information contained in the Landsat archive and this set of good practices, this dissertation presents the results of the continuous estimation of areas of change and carbon emissions and removals in the Colombian Amazon, as well as the estimation of errors in the detection of changes.

5.1 Key findings

This dissertation presents a methodology for the continuous estimation of areas of land cover change and their uncertainties using time series of Landsat data, unbiased estimators of area and biennial reference data (Chapter 2). Building upon the time series, methods to estimate the probability of errors of omission and commission of change are presented (Chapter 3). Finally, making use of the land change areas estimated in Chapter 2, carbon emissions and removals resulting from these land conversions are estimated (Chapter 4). The key findings of this work are summarized as follows:

- The Colombian Amazon has experienced low deforestation rates in the last decade compared to neighboring countries, driven by the establishment of pastures that sometimes are abandoned and left to regrow. It is possible to estimate very small areas of change at biennial intervals, including the gain and loss of secondary forest, but uncertainties need to be addressed.
- Probabilities of omission and commission of change in time series of Landsat data can be calculated using statistical approaches. Omission probabilities represent the probability of a time segment having omitted the detection of a change in the time series, while commission probabilities represent the probability of the change detection allocating a false change.
- Net carbon emissions average 10.38 Tg $year^{-1}$ (0.22 Mg ha^{-1} $year^{-1}$) in the study area, with conversion from forest to pastures contributing to most of the carbon emissions, and regrowth of secondary forest contributing to most of the removals from the atmosphere. Secondary forest has the potential for offsetting a considerable fraction of the emissions.

Overall, this dissertation contributes to the understanding of land cover changes in the Colombian Amazon and their resulting carbon emissions and removals. In addition, it provides methods and valuable lessons to quantify and reduce the uncertainty in the detection of changes in time series of Landsat data, and the land change area estimated from them. Furthermore, the results from Chapter 2 and 4 illustrate the inherent difficulties of reporting at the annual or biennial intervals required by the REDD+

mechanism, particularly for countries with a high forest coverage and low forest conversion areas. The high uncertainty in the estimated carbon emissions was a direct result of the uncertainty in the area of changes. This uncertainty can be reduced by: 1) increasing the accuracy of the maps used as strata for the sample selection, improving its efficiency; 2) increasing the sample size and the allocation to the largest class, in this case *Forest,* and 3) creating multiple forest strata with different area weights to minimize the effects of omission errors. A better stratification can be attained by using the omission and commission probabilities developed in Chapter 3 to determine the areas where omission errors are more likely to occur, and isolate them into a separate forest stratum with a small map proportion that reduces the negative effect of the 'captured' omission errors.

The long-term viability of the REDD+ program as a mechanism to effectively decrease emissions from deforestation and degradation will depend on the reduction of the uncertainties in areas of change and the carbon emissions resulting from them. However, the results presented here indicate that even if a moderate reduction in uncertainty is achieved, annual reporting of emissions resulting from multiple land cover changes beyond forest gain and loss seems implausible, especially for countries with low deforestation and low technical capabilities. The challenge to report at such small time intervals is further illustrated by the reduced number of countries that have reported within the REDD+ mechanism, and by the lack of examples of countries receiving payments in exchange for proving a reduction in emissions. Continuous monitoring of land change activities is possible but more challenging than previously thought, and if

uncertainties cannot be further reduced through the practical recommendations provided above, reporting requirements might need to be modified to permit the estimation of carbon emissions over longer periods. Donor agencies and governments will also need to be aware of the challenges associated with the estimation of carbon emissions at such short intervals if they want their contributions to end in useful and opportune results.

A reduction of the uncertainty in emissions from land cover change is also essential for constraining the global carbon budget. Unlike individual countries, the continuous estimation of areas of forest gain and loss at the global scale in shorter periods is a more plausible task because the combined areas of change are larger and easier to estimate with higher certainty, although the mapping and sample interpretation efforts required to accomplish that task are not small. However, the uncertainty in carbon stocks for the areas undergoing change is likely to be the largest source of uncertainty in the emission estimates, and needs to be addressed with a combination of data from optical, lidar and radar sensors, field plot data and robust statistical or machine-learning techniques. Additionally, the location of land changes and biomass stocks are of great interest. Spatial measures of uncertainty are needed to maximize the utility of maps of change and biomass stocks while accounting for their errors. A first attempt to generate such spatial measures of uncertainty was presented in Chapter 3, but further research is required.

5.2 Recommendations for future work

5.2.1 Continuous monitoring of land change activities and post-disturbance dynamics from Landsat time series

In Chapter 2 I estimated the areas of land cover and their changes with quantified uncertainty, but for some biennial periods and classes the uncertainty was very high and sometimes included zero. While this behavior is unsurprising given the small fractional areas that I attempted to map and estimate, higher efficiency in the estimation would be achieved with more accurate maps of land change, as mentioned previously. In this study, undesired clouds and noise were persistent even after multiple steps aimed at filtering them, both prior and during the execution of the change detection algorithm. Considering the relatively low number of historical cloud-free images in the area, it is important to preserve as many images as possible without discarding valuable information. However, this goal is at odds with the need to filter unwanted noise, as more aggressive filtering algorithms will almost inevitably discard usable data. Future analysis of similar characteristics will require the application of other algorithms that can successfully filter additional clouds and shadows, or the use of a change detection algorithm that is more robust to noise. Time series with more cloud-free and shadow-free observations, and with well distributed values across time will result in a better detection of changes, which in turn will benefit the classification of the temporal segments. Another step that can improve the accuracy of the final maps is the establishment of labelling rules that enforce expected land cover transitions while discarding improbable ones. For example,

conversions from forest to pastures are the most likely change to occur, but the inverse is very unlikely in the span of fifteen years. The accuracy of the secondary forest class could be improved by a similar rule-enforcing system, given that the classification of this class is mostly dependent on the slope of the time segment. A metric derived from the relationship between the length and the slope of the temporal segment could be used to enforce that time segments labelled as *Secondary Forest* meet certain desired characteristics. In addition, other improvements could be made to the classification process itself, such as the inclusion of the amplitude of the harmonic terms or texture information as additional training features to the classifier. Once these steps have been conducted and more accurate maps are generated after additional cloud and shadow screening, recommendations such as the use of a buffer stratum to capture omission errors and increase in the sample size of the largest class will contribute to a more efficient estimation of areas of change.

5.2.2 Spatial representation of the probability of errors in maps of land change

Chapter 3 demonstrated the use of two methods to determine the probability of time segments presenting errors of omission of change, or the probability of commission of change between two adjacent segments. Similar to the findings in Chapter 2, more effective techniques are needed to filter clouds and shadows, in order to obtain probabilities of omission or commission of change that truly represent the conditions in the time series, instead of reflecting the unpredictable spikes and changes in temporal

data density caused by noise. Another related aspect that deserves attention is the relationship between temporal data density and the probabilities of omission and commission of change. The number of total and clear observations are known vary as a function of time (less or no observations between 1993-1997 and more after 2013) and season (less clear observations in rainy vs dry season), but the cloud and shadow removal of data points results in time series with varying temporal data density for any point in time. The effect of the data density variability caused by these factors on the accurate and timely detection of changes is unknown.

The methods presented in Chapter 3 are currently used as the basis for some change detection algorithms (such as BFAST), or as post-processing steps to combine or split temporal segments (CCDC). The time segments used in this study had undergone a post-processing step to remove unwanted breaks, resulting in a smaller probabilities of commission for the newly created segments. The effect of splitting or merging temporal segments prior to the calculation of omission and commission probabilities on these new segments was not analyzed here, but needs to be addressed. In addition, the distribution of omission and commission probabilities over time needs to be tested and analyzed with a set of multiple samples distributed across time, because previous research indicates that breaks detected by the omission test occur more often in the middle of the time series (Bullock et al., 2019; Robbins et al., 2011). Finally, the application of the methods presented in Chapter 3 is closely tied to the CCDC algorithm, but additional research is needed to determine if and how it can be extended to other algorithms, particularly if they do not use all available Landsat observations, or use anniversary images or composites.

5.2.3 Carbon emissions associated with land cover change

A major motivation for this dissertation is to advance the monitoring of carbon dynamics associated with land change activities. The research presented in Chapter 4 is the first step towards implementing a carbon bookkeeping model "on top" of the monitoring system presented in Chapter 2, such that carbon dynamics are computed at the pixel level following land activities as informed by the CCDC/YATSM algorithm. A complicated but important component of such a framework will be estimation of bias and uncertainty. Most carbon bookkeeping models suitable for a gain/loss approach to estimating carbon emissions operate on estimates pertaining to large areas and large time spans (Houghton et al., 2012; Kuemmerle et al., 2011; Olofsson et al., 2011). For the modeling of carbon emissions to be spatially explicit, estimates of area bias and uncertainty at the population scale need to be spatialized. For example, a conversion of primary forest to pasture followed by regeneration of forest would trigger a release of carbon from the logged primary forest and soil according to the emissions curves used in the model, followed by sequestration of carbon by the recovering forest according to a pre-defined growth curve. The methods and results presented in Chapter 3 could provide information on omission and commission of change that could be used to propagate bias and uncertainty information to estimates of carbon emission and removals at the pixel level. However, more research is needed to determine how that propagation would work, and how to accommodate the effect of misclassification in the time segments that go into

the bookkeeping model. Another issue that requires attention is the carbon content (emissions factors) of landscapes experiencing recovery or degradation. While recent studies in the Amazon have started to provide such important data (Longo et al., 2016; Poorter et al., 2016), more measurements are needed to better understand the carbon dynamics of post-disturbance landscapes. Finally, the inclusion of forest degradation in future analyses would enhance our understanding of the changes in the landscape and their effects on carbon emissions. Forest degradation is defined by the IPCC as the process leading to long-term loss of carbon but without a change in land cover (GFOI, 2014). Forest degradation was not accounted for in this dissertation, but recent research has been conducted in the Amazon Basin to characterize forest degradation using time series of degradation indices (Bullock et al., 2018).

ACKNOWLEDGEMENTS

Chapter 2 was funded by NASA CMS grant NNX16AP26G (PI: Olofsson), SilvaCarbon Research grant 14-DG-11132762-347 (PI: Olofsson) and USGS/NASA Landsat Science Team grant (PI: Woodcock). I thank Chongyang Zhu, Katelyn Tarrio and Yihao Liu for assisting with the sample data collection. Their hard work and dedication are greatly appreciated.

Chapter 2 and 3 were funded by NASA Carbon Monitoring System (CMS) grant NNX16AP26G (PI: Pontus Olofsson). Special thanks to Xiaojing Tang for the implementation of the spatial model used in Chapter 3 and his general help, greatly facilitating the research.

APPENDIX A. Biennial area estimates calculated from reference data obtained for a single stratified random sample, using indicator functions

Biennial area estimates and 95% confidence intervals (dotted lines) for stable and change classes defined in the stratification, calculated from reference data obtained for a single stratified random sample, using indicator functions as explained in (Stehman, 2014). This sample was drawn from the strata map calculated between 2001 and 2016. Cross markers represent values that are statistically different from zero (i.e. confidence interval does not include zero). The red continuous line represents mapped areas (i.e. pixel-counting). Time represents the middle year of each biennial period for visualization purposes (e.g. 02 = 2002). The y-axes were set independently to aid in the visualization of the areas given the large differences in magnitude, and may be different from those in Figure 2-6. The panel for the "Other to other" class was removed, as it did not contain any relevant information.

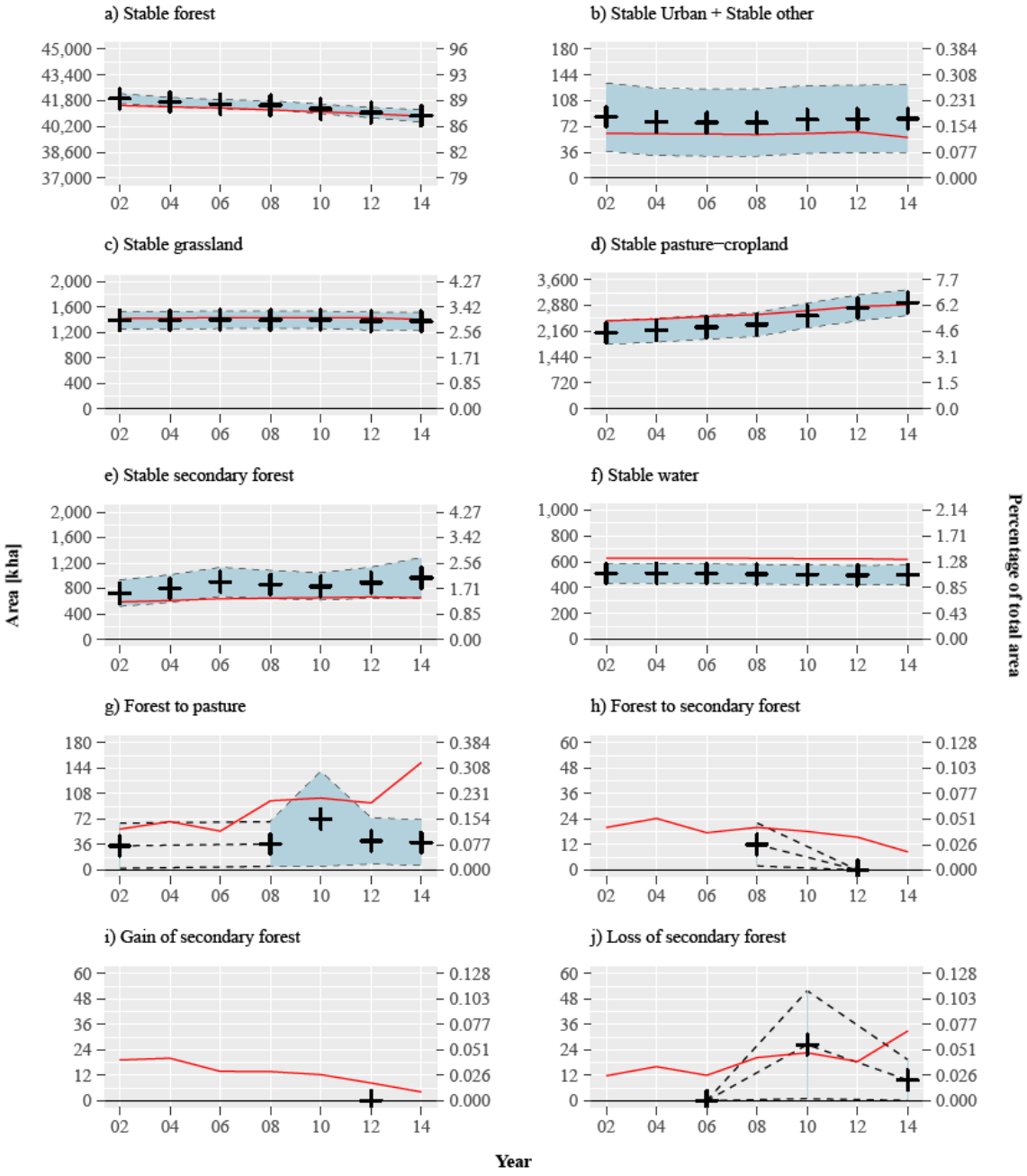

Figure A-1. Biennial area estimates and 95% confidence intervals (dotted lines) for stable and change classes defined in the stratification, calculated from reference data obtained for a single stratified random sample

APPENDIX B. Confusion matrices for each of the periods, in sample counts and area proportion.

	Oth. to Oth.	For.	Grass.	Urban	Past.	Sec. For.	Wat	For. to Past.	For. to Sec. For	Sec. For. Gain	Sec. For. Loss	(n_h)	(W_h)
Oth. to Oth.	2	3	13	4	12	7	2	7	0	0	0	50	0.12
For.	0	397	0	0	1	0	0	1	1	0	0	400	88.47
Grass.	0	5	65	0	5	0	0	0	0	0	0	75	3.03
Urban	0	4	10	21	3	1	11	0	0	0	0	50	0.13
Past.	0	5	3	0	61	6	0	0	0	0	0	75	5.23
Sec. For.	0	18	1	0	15	15	0	0	0	0	1	50	1.26
Wat	0	7	0	0	0	0	43	0	0	0	0	50	1.35
For. to Past.	0	3	0	0	6	0	0	31	10	0	0	50	0.12
For. to Sec. For	0	2	0	0	8	4	0	10	25	1	0	50	0.04
Sec. For. Gain	0	2	0	0	21	24	0	1	0	2	0	50	0.04
To Uncl.	0	5	1	0	30	2	10	0	1	1	0	50	0.00
Sec. For. Loss	0	1	0	0	13	6	1	16	5	4	4	50	0.03
Buff	0	32	0	0	4	0	0	11	3	0	0	50	0.17

Table B-1. Confusion matrix in sample counts for period 2001-2003.

	Oth. to Oth.	For.	Grass.	Urban	Past.	Sec. For.	Wat	For. to Past.	For. to Sec. For	Sec. For. Gain	Sec. For. Loss	(n_h)	(W_h)
Ot. Ot	0.0049	0.0073	0.0318	0.0098	0.0293	0.0171	0.0049	0.0171	0.0000	0.0000	0.0000	50	0.12
For.	0.0000	87.808	0.0000	0.0000	0.2212	0.0000	0.0000	0.2212	0.2212	0.0000	0.0000	400	88.47
Grass.	0.0000	0.2020	2.6264	0.0000	0.2020	0.0000	0.0000	0.0000	0.0000	0.0000	0.0000	75	3.03
Urban	0.0000	0.0107	0.0267	0.0561	0.0080	0.0027	0.0294	0.0000	0.0000	0.0000	0.0000	50	0.13
Past.	0.0000	0.3489	0.2093	0.0000	4.2561	0.4186	0.0000	0.0000	0.0000	0.0000	0.0000	75	5.23
Sec. For	0.0000	0.4538	0.0252	0.0000	0.3782	0.3782	0.0000	0.0000	0.0000	0.0000	0.0252	50	1.26
Wat	0.0000	0.1883	0.0000	0.0000	0.0000	0.0000	1.1569	0.0000	0.0000	0.0000	0.0000	50	1.35
For.Past.	0.0000	0.0074	0.0000	0.0000	0.0148	0.0000	0.0000	0.0766	0.0247	0.0000	0.0000	50	0.12
For. Sec	0.0000	0.0017	0.0000	0.0000	0.0069	0.0034	0.0000	0.0086	0.0214	0.0009	0.0000	50	0.04
Sec.Gain	0.0000	0.0016	0.0000	0.0000	0.0172	0.0197	0.0000	0.0008	0.0000	0.0016	0.0000	50	0.04
To Uncl.	0.0000	0.0000	0.0000	0.0000	0.0000	0.0000	0.0000	0.0000	0.0000	0.0000	0.0000	50	0.00
Sec.Loss	0.0000	0.0005	0.0000	0.0000	0.0065	0.0030	0.0005	0.0080	0.0025	0.0020	0.0020	50	0.03
Buff	0.0000	0.1088	0.0000	0.0000	0.0136	0.0000	0.0000	0.0374	0.0102	0.0000	0.0000	50	0.17

Table B-2. Confusion matrix in area proportions for period 2001-2003.

	Oth. to Oth.	For.	Grass.	Urban	Past.	Sec. For.	Wat	For. to Past.	For. to Sec. For	Sec. For. Gain	Sec. For. Loss	(n_h)	(W_h)
Oth. to Oth.	0	1	11	1	20	8	4	4	1	0	0	50	0.11
For.	0	394	4	0	2	0	0	0	0	0	0	400	88.23
Grass.	0	0	68	0	5	1	0	1	0	0	0	75	3.04
Urban	0	6	14	16	4	1	9	0	0	0	0	50	0.13
Past.	0	0	1	0	67	4	0	2	1	0	0	75	5.34
Sec. For.	0	6	2	0	27	12	0	1	1	1	0	50	1.30
Wat	0	10	1	0	0	0	39	0	0	0	0	50	1.34
For. to Past.	0	3	0	0	8	0	0	32	7	0	0	50	0.15
For. to Sec. For	0	2	1	0	5	3	0	23	14	2	0	50	0.05
Sec. For. Gain	0	0	2	0	21	23	0	1	1	2	0	50	0.04
To Uncl.	1	0	0	8	16	1	21	1	0	2	0	50	0.00
Sec. For. Loss	3	0	2	0	23	2	0	13	3	1	3	50	0.03
Buff	0	31	0	0	4	0	0	15	0	0	0	50	0.21

Table B-3. Confusion matrix in sample counts for period 2003-2005.

	Oth. to Oth.	For.	Grass.	Urban	Past.	Sec. For.	Wat	For. to Past.	For. to Sec. For	Sec. For. Gain	Sec. For. Loss	(n_h)	(W_h)
Ot. Ot	0.0000	0.0022	0.0242	0.0022	0.0440	0.0176	0.0088	0.0088	0.0022	0.0000	0.0000	50	0.11
For.	0.0000	86.909	0.8823	0.0000	0.4412	0.0000	0.0000	0.0000	0.0000	0.0000	0.0000	400	88.23
Grass.	0.0000	0.0000	2.7588	0.0000	0.2029	0.0406	0.0000	0.0406	0.0000	0.0000	0.0000	75	3.04
Urban	0.0000	0.0158	0.0369	0.0422	0.0105	0.0026	0.0237	0.0000	0.0000	0.0000	0.0000	50	0.13
Past.	0.0000	0.0000	0.0713	0.0000	4.7741	0.2850	0.0000	0.1425	0.0713	0.0000	0.0000	75	5.34
Sec. For	0.0000	0.1566	0.0522	0.0000	0.7045	0.3131	0.0000	0.0261	0.0261	0.0261	0.0000	50	1.30
Wat	0.0000	0.2688	0.0269	0.0000	0.0000	0.0000	1.0483	0.0000	0.0000	0.0000	0.0000	50	1.34
For.Past.	0.0000	0.0088	0.0000	0.0000	0.0234	0.0000	0.0000	0.0938	0.0205	0.0000	0.0000	50	0.15
For. Sec	0.0000	0.0021	0.0010	0.0000	0.0052	0.0031	0.0000	0.0239	0.0146	0.0021	0.0000	50	0.05
Sec.Gain	0.0000	0.0000	0.0017	0.0000	0.0180	0.0197	0.0000	0.0009	0.0009	0.0017	0.0000	50	0.04
To Uncl.	0.0000	0.0000	0.0000	0.0001	0.0001	0.0000	0.0001	0.0000	0.0000	0.0000	0.0000	50	0.00
Sec.Loss	0.0021	0.0000	0.0014	0.0000	0.0158	0.0014	0.0000	0.0089	0.0021	0.0007	0.0021	50	0.03
Buff	0.0000	0.1325	0.0000	0.0000	0.0171	0.0000	0.0000	0.0641	0.0000	0.0000	0.0000	50	0.21

Table B-4. Confusion matrix in area proportions for period 2003-2005.

	Oth. to Oth.	For.	Grass.	Urban	Past.	Sec. For.	Wat	For. to Past.	For. to Sec. For	Sec. For. Gain	Sec. For. Loss	(n_h)	(W_h)
Oth. to Oth.	0	2	5	3	23	8	0	8	0	0	1	50	0.08
For.	0	393	3	0	4	0	0	0	0	0	0	400	88.13
Grass.	0	2	67	0	6	0	0	0	0	0	0	75	3.06
Urban	0	1	15	22	2	1	9	0	0	0	0	50	0.13
Past.	0	2	2	0	63	8	0	0	0	0	0	75	5.50
Sec. For.	0	12	0	0	16	21	0	0	0	0	1	50	1.37
Wat	0	13	1	0	0	0	36	0	0	0	0	50	1.35
For. to Past.	0	0	0	0	14	0	0	29	6	1	0	50	0.12
For. to Sec. For	0	2	0	0	6	9	0	13	17	3	0	50	0.04
Sec. For. Gain	0	1	0	0	14	34	0	0	0	1	0	50	0.03
To Uncl.	2	4	0	1	30	5	7	0	0	0	1	50	0.00
Sec. For. Loss	0	4	0	0	19	7	0	7	1	1	11	50	0.03
Buff	0	29	0	1	5	0	0	13	2	0	0	50	0.18

Table B-5. Confusion matrix in sample counts for period 2005-2007.

	Oth. to Oth.	For.	Grass.	Urban	Past.	Sec. For.	Wat	For. to Past.	For. to Sec. For	Sec. For. Gain	Sec. For. Loss	(n_h)	(W_h)
Ot. Ot	0.0000	0.0032	0.0080	0.0048	0.0367	0.0128	0.0000	0.0128	0.0000	0.0000	0.0016	50	0.08
For.	0.0000	86.586	0.6610	0.0000	0.8813	0.0000	0.0000	0.0000	0.0000	0.0000	0.0000	400	88.13
Grass.	0.0000	0.0816	2.7350	0.0000	0.2449	0.0000	0.0000	0.0000	0.0000	0.0000	0.0000	75	3.06
Urban	0.0000	0.0026	0.0394	0.0577	0.0052	0.0026	0.0236	0.0000	0.0000	0.0000	0.0000	50	0.13
Past.	0.0000	0.1467	0.1467	0.0000	4.6198	0.5866	0.0000	0.0000	0.0000	0.0000	0.0000	75	5.50
Sec. For	0.0000	0.3278	0.0000	0.0000	0.4371	0.5737	0.0000	0.0000	0.0000	0.0000	0.0273	50	1.37
Wat	0.0000	0.3497	0.0269	0.0000	0.0000	0.0000	0.9685	0.0000	0.0000	0.0000	0.0000	50	1.35
For.Past.	0.0000	0.0000	0.0000	0.0000	0.0329	0.0000	0.0000	0.0681	0.0141	0.0023	0.0000	50	0.12
For. Sec	0.0000	0.0015	0.0000	0.0000	0.0045	0.0068	0.0000	0.0098	0.0128	0.0023	0.0000	50	0.04
Sec.Gain	0.0000	0.0006	0.0000	0.0000	0.0083	0.0201	0.0000	0.0000	0.0000	0.0006	0.0000	50	0.03
To Uncl.	0.0000	0.0001	0.0000	0.0000	0.0006	0.0001	0.0001	0.0000	0.0000	0.0000	0.0000	50	0.00
Sec.Loss	0.0000	0.0020	0.0000	0.0000	0.0097	0.0036	0.0000	0.0036	0.0005	0.0005	0.0056	50	0.03
Buff	0.0000	0.1023	0.0000	0.0035	0.0176	0.0000	0.0000	0.0459	0.0071	0.0000	0.0000	50	0.18

Table B-6. Confusion matrix in area proportions for period 2005-2007.

	Oth. to Oth.	For.	Grass.	Urban	Past.	Sec. For.	Wat	For. to Past.	For. to Sec. For	Sec. For. Gain	Sec. For. Loss	(n_h)	(W_h)
Oth. to Oth.	2	2	5	0	14	9	3	8	1	5	1	50	0.10
For.	0	396	1	0	2	1	0	0	0	0	0	400	87.77
Grass.	0	1	67	0	7	0	0	0	0	0	0	75	3.06
Urban	0	1	15	1 1	0	2	21	0	0	0	0	50	0.13
Past.	0	1	1	0	69	2	0	0	0	2	0	75	5.61
Sec. For.	0	13	0	0	7	29	0	0	0	0	1	50	1.39
Wat	0	16	0	0	0	0	34	0	0	0	0	50	1.34
For. to Past.	0	2	0	0	10	8	0	19	8	0	3	50	0.21
For. to Sec. For	0	0	1	0	1	3	0	17	26	1	1	50	0.04
Sec. For. Gain	0	0	0	0	6	38	0	0	1	5	0	50	0.03
To Uncl.	1	2	1	2	21	10	4	0	0	9	0	50	0.00
Sec. For. Loss	0	1	0	0	15	9	0	7	4	0	14	50	0.04
Buff	0	28	0	0	5	0	0	9	7	0	1	50	0.28

Table B-7. Confusion matrix in sample counts for period 2007-2009.

	Oth. to Oth.	For.	Grass.	Urban	Past.	Sec. For.	Wat	For. to Past.	For. to Sec. For	Sec. For. Gain	Sec. For. Loss	(n_h)	(W_h)
Ot. Ot	0.0042	0.0042	0.0105	0.0000	0.0294	0.0189	0.0063	0.0168	0.0021	0.0105	0.0021	50	0.10
For.	0.0000	86.887	0.2194	0.0000	0.4388	0.2194	0.0000	0.0000	0.0000	0.0000	0.0000	400	87.77
Grass.	0.0000	0.0408	2.7322	0.0000	0.2855	0.0000	0.0000	0.0000	0.0000	0.0000	0.0000	75	3.06
Urban	0.0000	0.0026	0.0389	0.0285	0.0000	0.0052	0.0544	0.0000	0.0000	0.0000	0.0000	50	0.13
Past.	0.0000	0.0748	0.0748	0.0000	5.1586	0.1495	0.0000	0.0000	0.0000	0.1495	0.0000	75	5.61
Sec. For	0.0000	0.3601	0.0000	0.0000	0.1939	0.8034	0.0000	0.0000	0.0000	0.0000	0.0277	50	1.39
Wat	0.0000	0.4291	0.0000	0.0000	0.0000	0.0000	0.9119	0.0000	0.0000	0.0000	0.0000	50	1.34
For.Past.	0.0000	0.0084	0.0000	0.0000	0.0418	0.0335	0.0000	0.0795	0.0335	0.0000	0.0126	50	0.21
For. Sec	0.0000	0.0000	0.0009	0.0000	0.0009	0.0026	0.0000	0.0146	0.0223	0.0009	0.0009	50	0.04
Sec.Gain	0.0000	0.0000	0.0000	0.0000	0.0035	0.0223	0.0000	0.0000	0.0006	0.0029	0.0000	50	0.03
To Uncl.	0.0001	0.0002	0.0001	0.0002	0.0016	0.0008	0.0003	0.0000	0.0000	0.0007	0.0000	50	0.00
Sec.Loss	0.0000	0.0009	0.0000	0.0000	0.0130	0.0078	0.0000	0.0061	0.0035	0.0000	0.0121	50	0.04
Buff	0.0000	0.1567	0.0000	0.0000	0.0280	0.0000	0.0000	0.0504	0.0392	0.0000	0.0056	50	0.28

Table B-8. Confusion matrix in area proportions for period 2007-2009.

	Oth. to Oth.	For.	Grass.	Urban	Past.	Sec. For.	Wat	For. to Past.	For. to Sec. For	Sec. For. Gain	Sec. For. Loss	(n_h)	(W_h)
Oth. to Oth.	0	4	6	2	14	6	8	5	3	0	2	50	0.10
For.	0	394	1	0	3	1	0	1	0	0	0	400	87.51
Grass.	0	2	69	0	4	0	0	0	0	0	0	75	3.06
Urban	0	2	13	10	2	2	21	0	0	0	0	50	0.13
Past.	0	3	4	0	61	5	0	0	0	1	1	75	5.84
Sec. For.	0	15	0	0	7	27	0	0	1	0	0	50	1.40
Wat	0	4	0	0	0	0	46	0	0	0	0	50	1.34
For. to Past.	0	1	0	0	18	1	0	19	8	0	3	50	0.22
For. to Sec. For	0	4	0	0	6	5	0	6	29	0	0	50	0.04
Sec. For. Gain	0	0	0	0	10	37	0	0	0	3	0	50	0.03
To Uncl.	0	0	5	1	20	6	11	0	0	3	4	50	0.01
Sec. For. Loss	0	1	0	0	20	10	0	5	4	0	10	50	0.05
Buff	0	35	0	0	3	3	0	5	3	0	1	50	0.28

Table B-9. Confusion matrix in sample counts for period 2009-2011.

	Oth. to Oth.	For.	Grass.	Urban	Past.	Sec. For.	Wat	For. to Past.	For. to Sec. For	Sec. For. Gain	Sec. For. Loss	(n_h)	(W_h)
Ot. Ot	0.0000	0.0080	0.0120	0.0040	0.0279	0.0120	0.0160	0.0100	0.0060	0.0000	0.0040	50	0.10
For.	0.0000	86.194	0.2188	0.0000	0.6563	0.2188	0.0000	0.2188	0.0000	0.0000	0.0000	400	87.51
Grass.	0.0000	0.0817	2.8173	0.0000	0.1633	0.0000	0.0000	0.0000	0.0000	0.0000	0.0000	75	3.06
Urban	0.0000	0.0053	0.0345	0.0265	0.0053	0.0053	0.0557	0.0000	0.0000	0.0000	0.0000	50	0.13
Past.	0.0000	0.2335	0.3113	0.0000	4.7469	0.3891	0.0000	0.0000	0.0000	0.0778	0.0778	75	5.84
Sec. For	0.0000	0.4208	0.0000	0.0000	0.1964	0.7574	0.0000	0.0000	0.0281	0.0000	0.0000	50	1.40
Wat	0.0000	0.1068	0.0000	0.0000	0.0000	0.0000	1.2283	0.0000	0.0000	0.0000	0.0000	50	1.34
For.Past.	0.0000	0.0044	0.0000	0.0000	0.0783	0.0044	0.0000	0.0827	0.0348	0.0000	0.0131	50	0.22
For. Sec	0.0000	0.0031	0.0000	0.0000	0.0047	0.0039	0.0000	0.0047	0.0225	0.0000	0.0000	50	0.04
Sec.Gain	0.0000	0.0000	0.0000	0.0000	0.0053	0.0194	0.0000	0.0000	0.0000	0.0016	0.0000	50	0.03
To Uncl.	0.0000	0.0000	0.0011	0.0002	0.0045	0.0014	0.0025	0.0000	0.0000	0.0007	0.0009	50	0.01
Sec.Loss	0.0000	0.0010	0.0000	0.0000	0.0193	0.0097	0.0000	0.0048	0.0039	0.0000	0.0097	50	0.05
Buff	0.0000	0.1973	0.0000	0.0000	0.0169	0.0169	0.0000	0.0282	0.0169	0.0000	0.0056	50	0.28

Table B-10. Confusion matrix in area proportions for period 2009-2011.

	Oth. to Oth.	For.	Grass.	Urban	Past.	Sec. For.	Wat	For. to Past.	For. to Sec. For	Sec. For. Gain	Sec. For. Loss	(n_h)	(W_h)
Oth. to Oth.	2	3	11	3	17	3	3	6	0	0	2	50	0.07
For.	0	393	2	0	4	1	0	0	0	0	0	400	87.27
Grass.	0	2	69	0	4	0	0	0	0	0	0	75	3.06
Urban	1	0	10	21	3	1	14	0	0	0	0	50	0.14
Past.	0	2	0	0	71	2	0	0	0	0	0	75	6.09
Sec. For.	0	22	0	0	22	6	0	0	0	0	0	50	1.42
Wat	0	12	0	0	0	0	38	0	0	0	0	50	1.33
For. to Past.	0	9	1	0	9	1	0	24	3	2	1	50	0.20
For. to Sec. For	0	10	0	0	6	6	0	16	12	0	0	50	0.03
Sec. For. Gain	0	2	0	0	9	36	0	0	0	1	2	50	0.02
To Uncl.	1	0	9	2	27	3	4	1	0	1	2	50	0.04
Sec. For. Loss	0	1	0	0	22	10	0	11	0	2	4	50	0.04
Buff	1	23	0	0	13	0	0	10	3	0	0	50	0.28

Table B-11. Confusion matrix in sample counts for period 2011-2013.

	Oth. to Oth.	For.	Grass.	Urban	Past.	Sec. For.	Wat	For. to Past.	For. to Sec. For	Sec. For. Gain	Sec. For. Loss	(n_h)	(W_h)
Ot. Ot	0.0026	0.0040	0.0145	0.0040	0.0224	0.0040	0.0040	0.0079	0.0000	0.0000	0.0026	50	0.07
For.	0.0000	85.743	0.4364	0.0000	0.8727	0.2182	0.0000	0.0000	0.0000	0.0000	0.0000	400	87.27
Grass.	0.0000	0.0816	2.8145	0.0000	0.1632	0.0000	0.0000	0.0000	0.0000	0.0000	0.0000	75	3.06
Urban	0.0027	0.0000	0.0275	0.0577	0.0082	0.0027	0.0384	0.0000	0.0000	0.0000	0.0000	50	0.14
Past.	0.0000	0.1625	0.0000	0.0000	5.7678	0.1625	0.0000	0.0000	0.0000	0.0000	0.0000	75	6.09
Sec. For	0.0000	0.6267	0.0000	0.0000	0.6267	0.1709	0.0000	0.0000	0.0000	0.0000	0.0000	50	1.42
Wat	0.0000	0.3204	0.0000	0.0000	0.0000	0.0000	1.0145	0.0000	0.0000	0.0000	0.0000	50	1.33
For.Past.	0.0000	0.0365	0.0041	0.0000	0.0365	0.0041	0.0000	0.0974	0.0122	0.0081	0.0041	50	0.20
For. Sec	0.0000	0.0066	0.0000	0.0000	0.0040	0.0040	0.0000	0.0106	0.0079	0.0000	0.0000	50	0.03
Sec.Gain	0.0000	0.0007	0.0000	0.0000	0.0032	0.0128	0.0000	0.0000	0.0000	0.0004	0.0007	50	0.02
To Uncl.	0.0008	0.0000	0.0075	0.0017	0.0224	0.0025	0.0033	0.0008	0.0000	0.0008	0.0017	50	0.04
Sec.Loss	0.0000	0.0008	0.0000	0.0000	0.0173	0.0079	0.0000	0.0087	0.0000	0.0016	0.0032	50	0.04
Buff	0.0056	0.1289	0.0000	0.0000	0.0729	0.0000	0.0000	0.0561	0.0168	0.0000	0.0000	50	0.28

Table B-12. Confusion matrix in area proportions for period 2011-2013.

	Oth. to Oth.	For.	Grass.	Urban	Past.	Sec. For.	Wat	For. to Past.	For. to Sec. For	Sec. For. Gain	Sec. For. Loss	(n_h)	(W_h)
Oth. to Oth.	2	1	22	2	14	2	0	7	0	0	0	50	0.05
For.	0	396	0	0	4	0	0	0	0	0	0	400	86.78
Grass.	0	0	68	0	7	0	0	0	0	0	0	75	3.00
Urban	0	4	18	12	2	4	9	0	0	1	0	50	0.12
Past.	0	2	3	0	64	5	1	0	0	0	0	75	6.19
Sec. For.	0	16	0	0	15	19	0	0	0	0	0	50	1.40
Wat	0	21	1	0	0	0	28	0	0	0	0	50	1.32
For. to Past.	0	5	0	0	17	1	0	20	5	1	1	50	0.32
For. to Sec. For	0	8	1	0	10	7	0	12	11	0	1	50	0.02
Sec. For. Gain	0	2	0	0	16	29	0	0	0	1	2	50	0.01
To Uncl.	0	0	4	3	30	4	2	0	0	3	4	50	0.29
Sec. For. Loss	0	0	0	0	20	7	0	8	6	0	9	50	0.07
Buff	0	30	0	0	5	5	0	8	2	0	0	50	0.43

Table B-13. Confusion matrix in sample counts for period 2013-2015.

	Oth. to Oth.	For.	Grass.	Urban	Past.	Sec. For.	Wat	For. to Past.	For. to Sec. For	Sec. For. Gain	Sec. For. Loss	(n_h)	(W_h)
Ot. Ot	0.0018	0.0009	0.0200	0.0018	0.0127	0.0018	0.0000	0.0064	0.0000	0.0000	0.0000	50	0.05
For.	0.0000	85.915	0.0000	0.0000	0.8678	0.0000	0.0000	0.0000	0.0000	0.0000	0.0000	400	86.78
Grass.	0.0000	0.0000	2.7208	0.0000	0.2801	0.0000	0.0000	0.0000	0.0000	0.0000	0.0000	75	3.00
Urban	0.0000	0.0097	0.0436	0.0291	0.0048	0.0097	0.0218	0.0000	0.0000	0.0024	0.0000	50	0.12
Past.	0.0000	0.1650	0.2475	0.0000	5.2798	0.4125	0.0825	0.0000	0.0000	0.0000	0.0000	75	6.19
Sec. For	0.0000	0.4487	0.0000	0.0000	0.4206	0.5328	0.0000	0.0000	0.0000	0.0000	0.0000	50	1.40
Wat	0.0000	0.5556	0.0265	0.0000	0.0000	0.0000	0.7408	0.0000	0.0000	0.0000	0.0000	50	1.32
For.Past.	0.0000	0.0325	0.0000	0.0000	0.1104	0.0065	0.0000	0.1299	0.0325	0.0065	0.0065	50	0.32
For. Sec	0.0000	0.0029	0.0004	0.0000	0.0037	0.0026	0.0000	0.0044	0.0040	0.0000	0.0004	50	0.02
Sec.Gain	0.0000	0.0004	0.0000	0.0000	0.0028	0.0051	0.0000	0.0000	0.0000	0.0002	0.0004	50	0.01
To Uncl.	0.0000	0.0000	0.0230	0.0173	0.1726	0.0230	0.0115	0.0000	0.0000	0.0173	0.0230	50	0.29
Sec.Loss	0.0000	0.0000	0.0000	0.0000	0.0281	0.0098	0.0000	0.0112	0.0084	0.0000	0.0126	50	0.07
Buff	0.0000	0.2564	0.0000	0.0000	0.0427	0.0427	0.0000	0.0684	0.0171	0.0000	0.0000	50	0.43

Table B-14. Confusion matrix in area proportions for period 2013-2015.

APPENDIX C. Area estimates, standard errors and margin of errors calculated from biennial samples and single sample using indicator functions.

	2001-2003	2003-2005	2005-2007	2007-2009	2009-2011	2011-2013	2013-2015
Other to other	2.3	1.0	0.0	2.0	0.0	5.5	0.9
Stable forest	41736.8	40967.1	41017.9	41186.8	40854.7	40787.2	40916.1
Stable grassland	1366.9	1805.8	1693.5	1440.6	1589.6	1547.2	1442.9
Stable Urban + Stable other	30.8	20.8	30.9	13.4	14.4	29.6	22.5
Stable pasture-cropland	2413.1	2929.5	2949.2	2900.6	2774.2	3566.5	3383.5
Stable secondary forest	394.6	319.8	564.8	591.5	673.4	276.0	490.0
Stable water	558.0	506.1	464.6	455.5	609.8	496.4	401.1
Forest to pasture	173.1	191.8	65.6	78.3	163.4	85.0	103.2
Forest to secondary forest	131.1	64.4	16.1	47.3	52.5	17.3	29.0
Gain of secondary forest	2.1	14.3	2.7	77.0	37.5	5.1	12.3
Loss of secondary forest	12.7	1.0	16.2	28.5	52.0	5.7	20.1

Table C-1. Areas in kha estimated from biennial samples.

	2001-2003	2003-2005	2005-2007	2007-2009	2009-2011	2011-2013	2013-2015
Other to other	0.0	3.4	0.8	5.0	4.0	25.1	0.0
Stable forest	41930.6	41715.7	41582.4	41518.0	41285.5	41058.3	40854.8
Stable grassland	1391.8	1395.2	1398.6	1398.6	1399.4	1378.3	1378.3
Stable Urban + Stable other	85.1	78.3	77.5	77.5	81.7	82.5	83.1
Stable pasture-cropland	2124.9	2189.5	2274.5	2349.9	2600.8	2809.9	2960.5
Stable secondary forest	727.8	799.9	905.5	862.9	834.6	892.2	967.8
Stable water	509.2	512.7	509.2	505.0	501.0	497.0	500.6
Forest to pasture	34.4	25.4	61.2	36.9	72.4	41.2	39.0
Forest to secondary forest	12.2	47.5	9.8	12.1	14.6	0.0	17.2
Gain of secondary forest	3.4	46.2	2.1	11.1	1.0	0.0	10.6
Loss of secondary forest	2.1	7.7	0.0	44.6	26.4	37.1	9.7

Table C-2. Areas in kha estimated from a single sample.

	2001-2003	2003-2005	2005-2007	2007-2009	2009-2011	2011-2013	2013-2015
Other to other	1.6	0.5	0.0	1.4	0.0	3.1	0.6
Stable forest	203.5	255.7	282.0	216.8	263.2	281.7	219.0
Stable grassland	80.2	215.1	192.1	120.2	132.9	151.3	82.5
Stable Urban + Stable other	4.9	4.2	4.8	3.6	3.8	4.7	5.8
Stable pasture-cropland	162.1	181.6	241.2	177.1	221.8	225.2	244.0
Stable secondary forest	86.5	77.7	102.9	122.9	137.8	119.4	96.2
Stable water	31.5	37.4	40.5	42.1	24.7	38.4	58.7
Forest to pasture	103.8	52.7	6.9	10.4	102.9	10.3	15.1
Forest to secondary forest	103.7	35.7	3.7	8.5	15.0	5.6	8.7
Gain of secondary forest	0.8	12.3	1.3	49.2	36.4	2.7	5.6
Loss of secondary forest	11.8	0.5	12.8	13.7	36.7	2.3	6.3

Table C-3. Standard error of area in kha estimated from biennial samples.

	2001-2003	2003-2005	2005-2007	2007-2009	2009-2011	2011-2013	2013-2015
Other to other	0.0	3.4	0.8	3.6	3.4	18.2	0.0
Stable forest	141.2	132.2	129.7	130.0	135.6	151.7	182.5
Stable grassland	66.2	66.2	66.3	66.3	66.3	68.2	68.2
Stable Urban + Stable other	24.0	23.6	23.6	23.6	23.8	23.8	23.8
Stable pasture-cropland	162.0	163.1	164.3	163.4	169.8	178.0	177.2
Stable secondary forest	103.3	107.0	112.5	110.0	106.4	121.4	159.3
Stable water	37.1	37.2	37.1	36.9	36.8	36.7	36.8
Forest to pasture	16.3	13.0	33.9	16.1	33.9	16.4	16.2
Forest to secondary forest	8.1	31.2	7.8	5.2	8.4	0.0	10.6
Gain of secondary forest	3.4	32.5	1.5	10.1	1.0	0.0	8.1
Loss of secondary forest	2.1	4.6	0.0	31.0	13.0	30.8	4.9

Table C-4. Standard error of area in kha estimated from a single sample.

	2001-2003	2003-2005	2005-2007	2007-2009	2009-2011	2011-2013	2013-2015
Other to other	10.1	6.6	0.9	9.4	0.0	15.7	6.2
Stable forest	449.6	477.9	476.1	470.1	481.8	484.2	479.7
Stable grassland	243.3	278.2	269.8	249.5	261.7	258.3	249.7
Stable Urban + Stable other	37.1	30.5	37.1	24.5	25.3	36.3	31.7
Stable pasture-cropland	319.5	349.9	351.0	348.3	341.1	383.3	374.1
Stable secondary forest	132.1	119.0	157.7	161.4	172.0	110.6	147.0
Stable water	156.8	149.4	143.2	141.8	163.8	148.0	133.2
Forest to pasture	87.7	92.3	54.1	59.1	85.2	61.5	67.7
Forest to secondary forest	76.4	53.6	26.8	45.9	48.4	27.8	36.0
Gain of secondary forest	9.7	25.3	10.9	58.6	40.9	15.1	23.5
Loss of secondary forest	23.8	6.6	26.9	35.7	48.1	16.0	29.9

Table C-5. Approximate standard error of area in kha from simple random sampling for each biennial period.

	2001-2003	2003-2005	2005-2007	2007-2009	2009-2011	2011-2013	2013-2015
Other to other	137.2	110.4	136.6	134.8		108.8	137.2
Stable forest	1.0	1.2	1.3	1.0	1.3	1.4	1.0
Stable grassland	11.5	23.3	22.2	16.3	16.4	19.2	11.2
Stable Urban + Stable other	31.4	39.9	30.6	52.4	51.5	31.0	50.1
Stable pasture-cropland	13.2	12.2	16.0	12.0	15.7	12.4	14.1
Stable secondary forest	43.0	47.6	35.7	40.7	40.1	84.8	38.5
Stable water	11.1	14.5	17.1	18.1	8.0	15.2	28.7
Forest to pasture	117.5	53.9	20.5	25.9	123.3	23.8	28.7
Forest to secondary forest	155.0	108.8	44.4	35.2	56.1	63.2	59.0
Gain of secondary forest	75.3	167.7	95.7	125.3	190.5	105.5	89.0
Loss of secondary forest	181.7	110.8	155.4	94.4	138.5	78.2	61.6

Table C-6. Margin of error estimated from biennial samples. (Margin of error = half width of confidence interval / area estimate).

	2001-2003	2003-2005	2005-2007	2007-2009	2009-2011	2011-2013	2013-2015
Other to other		196.0	196.0	141.8	163.0	141.7	
Stable forest	0.7	0.6	0.6	0.6	0.6	0.7	0.9
Stable grassland	9.3	9.3	9.3	9.3	9.3	9.7	9.7
Stable Urban + Stable other	55.2	59.0	59.6	59.6	57.1	56.5	56.1
Stable pasture-cropland	14.9	14.6	14.2	13.6	12.8	12.4	11.7
Stable secondary forest	27.8	26.2	24.4	25.0	25.0	26.7	32.3
Stable water	14.3	14.2	14.3	14.3	14.4	14.5	14.4
Forest to pasture	93.0	100.7	108.6	85.6	91.9	78.0	81.6
Forest to secondary forest	130.3	128.7	155.3	84.0	113.1		121.6
Gain of secondary forest	196.0	137.6	137.2	178.5	196.0		148.6
Loss of secondary forest	196.0	115.7		136.5	96.3	163.0	98.8

Table C-7. Margin of error estimated from a single sample. (Margin of error = half width of confidence interval / area estimate).

BIBLIOGRAPHY

Achard, F., Beuchle, R., Mayaux, P., Stibig, H.-J., Bodart, C., Brink, A., Carboni, S., Desclée, B., Donnay, F., Eva, H.D., Lupi, A., Raši, R., Seliger, R., Simonetti, D., 2014. Determination of tropical deforestation rates and related carbon losses from 1990 to 2010. Global Change Biology 20, 2540–2554. https://doi.org/10.1111/gcb.12605

Achard, F., Eva, H.D., Stibig, H.-J., Mayaux, P., Gallego, J., Richards, T., Malingreau, J.-P., 2002. Determination of Deforestation Rates of the World's Humid Tropical Forests. Science 297, 999–1002. https://doi.org/10.1126/science.1070656

Aide, T.M., Clark, M.L., Grau, H.R., López-Carr, D., Levy, M.A., Redo, D., Bonilla-Moheno, M., Riner, G., Andrade-Núñez, M.J., Muñiz, M., 2013. Deforestation and Reforestation of Latin America and the Caribbean (2001–2010). Biotropica 45, 262–271. https://doi.org/10.1111/j.1744-7429.2012.00908.x

Alvarez, E., Duque, A., Saldarriaga, J., Cabrera, K., de las Salas, G., del Valle, I., Lema, A., Moreno, F., Orrego, S., Rodríguez, L., 2012. Tree above-ground biomass allometries for carbon stocks estimation in the natural forests of Colombia. Forest Ecology and Management 267, 297–308. https://doi.org/10.1016/j.foreco.2011.12.013

Anaya, J.A., Chuvieco, E., Palacios-Orueta, A., 2009. Aboveground biomass assessment in Colombia: A remote sensing approach. Forest Ecology and Management 257, 1237–1246. https://doi.org/10.1016/j.foreco.2008.11.016

Andersen, L.E., Doyle, A.S., Granado, S. del, Ledezma, J.C., Medinaceli, A., Valdivia, M., Weinhold, D., 2016. Net Carbon Emissions from Deforestation in Bolivia during 1990-2000 and 2000-2010: Results from a Carbon Bookkeeping Model. PLoS ONE 11, e0151241. https://doi.org/10.1371/journal.pone.0151241

Arévalo, P., Olofsson, P., Woodcock, C.E., 2019. Continuous monitoring of land change activities and post-disturbance dynamics from Landsat time series: A test methodology for REDD+ reporting. Remote Sensing of Environment. https://doi.org/10.1016/j.rse.2019.01.013

Armenteras, D., Barreto, J.S., Tabor, K., Molowny-Horas, R., Retana, J., 2017. Changing patterns of fire occurrence in proximity to forest edges, roads and rivers between NW Amazonian countries. Biogeosciences 14, 2755–2765. https://doi.org/10.5194/bg-14-2755-2017

Armenteras, D., González, T.M., Retana, J., 2013. Forest fragmentation and edge influence on fire occurrence and intensity under different management types in Amazon forests. Biological Conservation 159, 73–79. https://doi.org/10.1016/j.biocon.2012.10.026

Armenteras, D., Rudas, G., Rodriguez, N., Sua, S., Romero, M., 2006. Patterns and causes of deforestation in the Colombian Amazon. Ecological Indicators 6, 353–368.

Arneth, A., Sitch, S., Pongratz, J., Stocker, B.D., Ciais, P., Poulter, B., Bayer, A.D., Bondeau, A., Calle, L., Chini, L.P., Gasser, T., Fader, M., Friedlingstein, P., Kato, E., Li, W., Lindeskog, M., Nabel, J.E.M.S., Pugh, T. a. M., Robertson, E., Viovy, N., Yue, C., Zaehle, S., 2017. Historical carbon dioxide emissions caused by land-use changes are possibly larger than assumed. Nature Geosci 10, 79–84. https://doi.org/10.1038/ngeo2882

Asner, G.P., Clark, J.K., Mascaro, J., Galindo García, G.A., Chadwick, K.D., Navarrete Encinales, D.A., Paez-Acosta, G., Cabrera Montenegro, E., Kennedy-Bowdoin, T., Duque, á., Balaji, A., von Hildebrand, P., Maatoug, L., Phillips Bernal, J.F., Yepes Quintero, A.P., Knapp, D.E., García Dávila, M.C., Jacobson, J., Ordóñez, M.F., 2012. High-resolution mapping of forest carbon stocks in the Colombian Amazon. Biogeosciences 9, 2683–2696. https://doi.org/10.5194/bg-9-2683-2012

Australian Government, 2017. FullCAM [WWW Document]. URL http://www.fullcam.com/FullCAMServer/Help/index.htm (accessed 7.22.17).

Baccini, A., Goetz, S.J., Walker, W.S., Laporte, N.T., Sun, M., Sulla-Menashe, D., Hackler, J., Beck, P.S.A., Dubayah, R., Friedl, M.A., Samanta, S., Houghton, R.A., 2012a. Estimated carbon dioxide emissions from tropical deforestation improved by carbon-density maps. Nature Climate Change 2, 182–185. https://doi.org/10.1038/nclimate1354

Baccini, A., Goetz, S.J., Walker, W.S., Laporte, N.T., Sun, M., Sulla-Menashe, D., Hackler, J., Beck, P.S.A., Dubayah, R., Friedl, M.A., Samanta, S., Houghton, R.A., 2012b. Estimated carbon dioxide emissions from tropical deforestation improved by carbon-density maps. Nature Climate Change 2, 182–185. https://doi.org/10.1038/nclimate1354

Baccini, A., Walker, W., Carvalho, L., Farina, M., Sulla-Menashe, D., Houghton, R.A., 2017. Tropical forests are a net carbon source based on aboveground measurements of gain and loss. Science eaam5962. https://doi.org/10.1126/science.aam5962

Baccini, A., Walker, W., Farina, M., Houghton, R.A., 2018. Estimated Deforested Area Biomass, Tropical America, Africa, and Asia, 2000.

Bai, J., Perron, P., 2003. Computation and analysis of multiple structural change models. Journal of Applied Econometrics 18, 1–22. https://doi.org/10.1002/jae.659

Baumann, M., Gasparri, I., Piquer-Rodríguez, M., Gavier Pizarro, G., Griffiths, P., Hostert, P., Kuemmerle, T., 2017. Carbon emissions from agricultural expansion and intensification in the Chaco. Global Change Biology 23, 1902–1916. https://doi.org/10.1111/gcb.13521

Breiman, L., 2001. Random Forests. Machine Learning 45, 5–32. https://doi.org/10.1023/A:1010933404324

Brown, K.M., Foody, G.M., Atkinson, P.M., 2009. Estimating per-pixel thematic uncertainty in remote sensing classifications. International Journal of Remote Sensing 30, 209–229. https://doi.org/10.1080/01431160802290568

Brown, R.L., Durbin, J., Evans, J.M., 1975. Techniques for Testing the Constancy of Regression Relationships Over Time. Journal of the Royal Statistical Society: Series B (Methodological) 37, 149–163. https://doi.org/10.1111/j.2517-6161.1975.tb01532.x

Brown, S., 1997a. Estimating biomass and biomass change of tropical forests: a primer, FAO forestry paper. Food and Agriculture Organization of the United Nations, Rome.

Brown, S., 1997b. Estimating biomass and biomass change of tropical forests: a primer, FAO forestry paper. Food and Agriculture Organization of the United Nations, Rome.

Bullock, E.L., Woodcock, C.E., Holden, C.E., 2019. Improved change monitoring using an ensemble of time series algorithms. Remote Sensing of Environment. https://doi.org/10.1016/j.rse.2019.04.018

Bullock, E.L., Woodcock, C.E., Olofsson, P., 2018. Monitoring tropical forest degradation using spectral unmixing and Landsat time series analysis. Remote Sensing of Environment 110968. https://doi.org/10.1016/j.rse.2018.11.011

Burnicki, A.C., 2011. Modeling the Probability of Misclassification in a Map of Land Cover Change [WWW Document]. https://doi.org/info:doi/10.14358/PERS.77.1.39

Cabrera, E., Vargas, D., Galindo, G., García, M.C., Ordoñez, M.F., Vergara, L., Pacheco, A., Rubiano, J., Giraldo, P., IDEAM, 2011. Memoria técnica de la cuantificación de la deforestación histórica nacional – escalas gruesa y fina.

Carlson, K.M., Curran, L.M., Asner, G.P., Pittman, A.M., Trigg, S.N., Marion Adeney, J., 2012. Carbon emissions from forest conversion by Kalimantan oil palm plantations. Nature Climate Change 3, 283–287. https://doi.org/10.1038/nclimate1702

Carmel, Y., 2004. Characterizing location and classification error patterns in time-series thematic maps. IEEE Geoscience and Remote Sensing Letters 1, 11–14. https://doi.org/10.1109/LGRS.2003.821696

Carvalho, J.A., Higuchi, N., Araújo, T.M., Santos, J.C., 1998. Combustion completeness in a rainforest clearing experiment in Manaus, Brazil. Journal of Geophysical Research: Atmospheres 103, 13195–13199. https://doi.org/10.1029/98JD00172

Chow, G.C., 1960. Tests of Equality Between Sets of Coefficients in Two Linear Regressions. Econometrica 28, 591–605. https://doi.org/10.2307/1910133

Cochran, W.G., 1977. Sampling Techniques, 3rd Edition, 3rd edition. ed. John Wiley & Sons, New York.

Cockx, K., Van de Voorde, T., Canters, F., 2014. Quantifying uncertainty in remote sensing-based urban land-use mapping. International Journal of Applied Earth Observation and Geoinformation 31, 154–166. https://doi.org/10.1016/j.jag.2014.03.016

Cohen, W.B., Yang, Z., Stehman, S.V., Schroeder, T.A., Bell, D.M., Masek, J.G., Huang, C., Meigs, G.W., 2016. Forest disturbance across the conterminous United States from 1985–2012: The emerging dominance of forest decline. Forest Ecology and Management, Special Section: Forest Management for Climate Change 360, 242–252. https://doi.org/10.1016/j.foreco.2015.10.042

Comber, A., Fisher, P., Brunsdon, C., Khmag, A., 2012. Spatial analysis of remote sensing image classification accuracy. Remote Sensing of Environment 127, 237–246. https://doi.org/10.1016/j.rse.2012.09.005

Comber, A.J., 2013. Geographically weighted methods for estimating local surfaces of overall, user and producer accuracies. Remote Sensing Letters 4, 373–380. https://doi.org/10.1080/2150704X.2012.736694

Davis, S.J., Burney, J.A., Pongratz, J., Caldeira, K., 2014. Methods for attributing land-use emissions to products. Carbon Management 5, 233–245. https://doi.org/10.1080/17583004.2014.913867

DeFries, R.S., Houghton, R.A., Hansen, M.C., Field, C.B., Skole, D., Townshend, J., 2002. Carbon emissions from tropical deforestation and regrowth based on satellite observations for the 1980s and 1990s. Proceedings of the National Academy of Sciences, U.S.A. 99, 14256-14261. https://doi.org/10.1073/pnas.182560099

Dehghan, H., Ghassemian, H., 2006. Measurement of uncertainty by the entropy: application to the classification of MSS data. International Journal of Remote Sensing 27, 4005–4014. https://doi.org/10.1080/01431160600647225

DeVries, B., Decuyper, M., Verbesselt, J., Zeileis, A., Herold, M., Joseph, S., 2015. Tracking disturbance-regrowth dynamics in tropical forests using structural change detection and Landsat time series. Remote Sensing of Environment 169, 320–334. https://doi.org/10.1016/j.rse.2015.08.020

Dubayah, R., 2018. The Global Ecosystem Dynamics Investigation: Current Status, in: AGU Fall Meeting Abstracts. pp. B44E-15.

Duivenvoorden, J.F., 1996. Patterns of Tree Species Richness in Rain Forests of the Middle Caqueta Area, Colombia, NW Amazonia. Biotropica 28, 142–158. https://doi.org/10.2307/2389070

Espejo, A., Jonckheere, I., 2017. Proceedings: Technical Workshop on Lessons learned from Accuracy Assessments in the context of REDD+. FAO, Rome.

Etter, A., McAlpine, C., Phinn, S., Pullar, D., Possingham, H., 2006a. Unplanned land clearing of Colombian rainforests: Spreading like disease? Landscape and Urban Planning 77, 240–254.

Etter, A., McAlpine, C., Wilson, K., Phinn, S., 2006b. Regional patterns of agricultural land use and deforestation in Colombia. Agriculture, Ecosystems & Environment 114, 369–386. https://doi.org/16/j.agee.2005.11.013

FAO, 2010. Global Forest Resources Assessment 2010. Food and Agriculture Organization of the United Nations, Rome.

FAO (Ed.), 1993. Forest resources assessment 1990: tropical countries, FAO forestry paper. Food and Agriculture Organization of the United Nations, Rome.

Fearnside, P.M., Leal, N., Fernandes, F.M., 1993. Rainforest burning and the global carbon budget: Biomass, combustion efficiency, and charcoal formation in the Brazilian Amazon. Journal of Geophysical Research: Atmospheres 98, 16733–16743. https://doi.org/10.1029/93JD01140

Fisher, J.B., Huntzinger, D.N., Schwalm, C.R., Sitch, S., 2014. Modeling the Terrestrial Biosphere. Annual Review of Environment and Resources 39, 91–123. https://doi.org/10.1146/annurev-environ-012913-093456

Foody, G.M., 2008. RVM-based multi-class classification of remotely sensed data. International Journal of Remote Sensing 29, 1817–1823. https://doi.org/10.1080/01431160701822115

Foody, G.M., 2005. Local characterization of thematic classification accuracy through spatially constrained confusion matrices. International Journal of Remote Sensing 26, 1217–1228. https://doi.org/10.1080/01431160512331326521

Foody, G.M., 1992. Derrivation and applications of probablistic measures of class membership from maximum-likelihood classification. Photogrammetric Engineering & Remote Sensing 58, 1335–1341. https://doi.org/10.3851/IMP1936

Friedl, M.A., McIver, D.K., Hodges, J.C.F., Zhang, X.Y., Muchoney, D., Strahler, A.H., Woodcock, C.E., Gopal, S., Schneider, A., Cooper, A., Baccini, A., Gao, F., Schaaf, C., 2002. Global land cover mapping from MODIS: algorithms and early results. Remote

Sensing of Environment, The Moderate Resolution Imaging Spectroradiometer (MODIS): a new generation of Land Surface Monitoring 83, 287–302. https://doi.org/10.1016/S0034-4257(02)00078-0

Friedl, M.A., Sulla-Menashe, D., Tan, B., Schneider, A., Ramankutty, N., Sibley, A., Huang, X., 2010. MODIS Collection 5 global land cover: Algorithm refinements and characterization of new datasets. Remote Sensing of Environment 114, 168–182. https://doi.org/10.1016/j.rse.2009.08.016

Friedlingstein, P., Cox, P., Betts, R., Bopp, L., von Bloh, W., Brovkin, V., Cadule, P., Doney, S., Eby, M., Fung, I., Bala, G., John, J., Jones, C., Joos, F., Kato, T., Kawamiya, M., Knorr, W., Lindsay, K., Matthews, H.D., Raddatz, T., Rayner, P., Reick, C., Roeckner, E., Schnitzler, K.-G., Schnur, R., Strassmann, K., Weaver, A.J., Yoshikawa, C., Zeng, N., 2006. Climate–Carbon Cycle Feedback Analysis: Results from the C4MIP Model Intercomparison. Journal of Climate 19, 3337–3353. https://doi.org/10.1175/JCLI3800.1

Galindo, G., Espejo, O.J., Ramirez, J.P., Forero, C., Valbuena, C.A., Rubiano, J.C., Lozano, R.H., Vargas, K.M., Palacios, A., Palacios, S., Franco, C.A., Granados, E.I., Vergara, L.K., Cabrera, E., 2014. Memoria técnica de la Cuantificación de la superficie de bosque natural y deforestación a nivel nacional. Actualización Periodo 2012 – 2013. Bogota, D.C.

Gebhardt, S., Wehrmann, T., Ruiz, M.A.M., Maeda, P., Bishop, J., Schramm, M., Kopeinig, R., Cartus, O., Kellndorfer, J., Ressl, R., Santos, L.A., Schmidt, M., 2014. MAD-MEX: Automatic Wall-to-Wall Land Cover Monitoring for the Mexican REDD-MRV Program Using All Landsat Data. Remote Sensing 6, 3923–3943. https://doi.org/10.3390/rs6053923

GFOI, 2016. Integrating remote-sensing and ground-based observations for estimation of emissions and removals of greenhouse gases in forests: Methods and Guidance from the Global Forest Observations Initiative., 2nd ed. Food and Agriculture Organization of the United Nations, Rome.

GFOI, 2014. Integrating remote-sensing and ground-based observations for estimation of emissions and removals of greenhouse gases in forests: Methods and Guidance from the Global Forest Observations Initiative., 1st ed. Group on Earth Observations, Geneva.

Giacco, F., Thiel, C., Pugliese, L., Scarpetta, S., Marinaro, M., 2010. Uncertainty Analysis for the Classification of Multispectral Satellite Images Using SVMs and SOMs. IEEE Transactions on Geoscience and Remote Sensing 48, 3769–3779. https://doi.org/10.1109/TGRS.2010.2047863

Gillespie, T.W., Willis, K.S., Ostermann-Kelm, S., 2015. Spaceborne remote sensing of the world's protected areas. Progress in Physical Geography: Earth and Environment 39, 388–404. https://doi.org/10.1177/0309133314561648

Goetz, S.J., Hansen, M., Houghton, R.A., Walker, W., Laporte, N., Busch, J., 2015. Measurement and monitoring needs, capabilities and potential for addressing reduced emissions from deforestation and forest degradation under REDD+. Environmental Research Letters 10, 123001. https://doi.org/10.1088/1748-9326/10/12/123001

Griffiths, P., Kuemmerle, T., Baumann, M., Radeloff, V.C., Abrudan, I.V., Lieskovsky, J., Munteanu, C., Ostapowicz, K., Hostert, P., 2014. Forest disturbances, forest recovery, and changes in forest types across the Carpathian ecoregion from 1985 to 2010 based on Landsat image composites. Remote Sensing of Environment, Special Issue on 2012 ForestSAT 151, 72–88. https://doi.org/10.1016/j.rse.2013.04.022

Hansen, M.C., Egorov, A., Potapov, P.V., Stehman, S.V., Tyukavina, A., Turubanova, S.A., Roy, D.P., Goetz, S.J., Loveland, T.R., Ju, J., Kommareddy, A., Kovalskyy, V., Forsyth, C., Bents, T., 2014. Monitoring conterminous United States (CONUS) land cover change with Web-Enabled Landsat Data (WELD). Remote Sensing of Environment 140, 466–484. https://doi.org/10.1016/j.rse.2013.08.014

Hansen, M.C., Potapov, P.V., Moore, R., Hancher, M., Turubanova, S.A., Tyukavina, A., Thau, D., Stehman, S.V., Goetz, S.J., Loveland, T.R., Kommareddy, A., Egorov, A., Chini, L., Justice, C.O., Townshend, J.R.G., 2013. High-Resolution Global Maps of 21st-Century Forest Cover Change. Science 342, 850–853. https://doi.org/10.1126/science.1244693

Hansis, E., Davis, S.J., Pongratz, J., 2015. Relevance of methodological choices for accounting of land use change carbon fluxes: accounting of land use carbon fluxes. Global Biogeochemical Cycles 29, 1230–1246. https://doi.org/10.1002/2014GB004997

Harris, N.L., Brown, S., Hagen, S.C., Saatchi, S.S., Petrova, S., Salas, W., Hansen, M.C., Potapov, P.V., Lotsch, A., 2012. Baseline Map of Carbon Emissions from Deforestation in Tropical Regions. Science 336, 1573–1576. https://doi.org/10.1126/science.1217962

Holden, C., 2016a. yatsm: Yet Another Time Series Model (YATSM): v0.6.1. https://doi.org/10.5281/zenodo.51336

Holden, C., 2016b. TSTools: TSTools: v1.1.1. https://doi.org/10.5281/zenodo.55045

Houghton, R.A., Hackler, J.L., 2006. Emissions of carbon from land use change in sub-Saharan Africa. J. Geophys. Res. 111, G02003. https://doi.org/10.1029/2005JG000076

Houghton, R.A., Hobbie, J.E., Melillo, J.M., Moore, B., Peterson, B.J., Shaver, G.R., Woodwell, G.M., 1983. Changes in the Carbon Content of Terrestrial Biota and Soils between 1860 and 1980: A Net Release of CO"2 to the Atmosphere. Ecological Monographs 53, 235–262. https://doi.org/10.2307/1942531

Houghton, R.A., House, J.I., Pongratz, J., van der Werf, G.R., DeFries, R.S., Hansen, M.C., Le Quéré, C., Ramankutty, N., 2012. Carbon emissions from land use and land-cover change. Biogeosciences 9, 5125–5142. https://doi.org/10.5194/bg-9-5125-2012

Houghton, R.A., Nassikas, A.A., 2017. Global and regional fluxes of carbon from land use and land cover change 1850–2015. Global Biogeochemical Cycles 31, 456–472. https://doi.org/10.1002/2016GB005546

Houghton, R.A., Skole, D.L., Nobre, C.A., Hackler, J.L., Lawrence, K.T., Chomentowski, W.H., 2000. Annual fluxes of carbon from deforestation and regrowth in the Brazilian Amazon. Nature 403, 301. https://doi.org/10.1038/35002062

Huang, C., Goward, S.N., Masek, J.G., Thomas, N., Zhu, Z., Vogelmann, J.E., 2010. An automated approach for reconstructing recent forest disturbance history using dense Landsat time series stacks. Remote Sensing of Environment 114, 183–198. https://doi.org/10.1016/j.rse.2009.08.017

IDEAM, 2016. Sexto Boletín de Alertas Tempranas de Deforestación (AT-D). Segundo semestre 2015.

Instituto Nacional de Pesquisas Espaciais (INPE), 2016. Deforestation estimates in the Brazilian Amazon [WWW Document]. URL http://www.obt.inpe.br/prodes/index.php (accessed 8.29.16).

IPCC, 2006. 2006 IPCC guidelines for national greenhouse gas inventories.

Kennedy, R.E., Yang, Z., Cohen, W.B., 2010. Detecting trends in forest disturbance and recovery using yearly Landsat time series: 1. LandTrendr — Temporal segmentation algorithms. Remote Sensing of Environment 114, 2897–2910. https://doi.org/10.1016/j.rse.2010.07.008

Khatami, R., Mountrakis, G., Stehman, S.V., 2017a. Mapping per-pixel predicted accuracy of classified remote sensing images. Remote Sensing of Environment 191, 156–167. https://doi.org/10.1016/j.rse.2017.01.025

Khatami, R., Mountrakis, G., Stehman, S.V., 2017b. Predicting individual pixel error in remote sensing soft classification. Remote Sensing of Environment 199, 401–414. https://doi.org/10.1016/j.rse.2017.07.028

Kim, D.-H., Sexton, J.O., Noojipady, P., Huang, C., Anand, A., Channan, S., Feng, M., Townshend, J.R., 2014. Global, Landsat-based forest-cover change from 1990 to 2000. Remote Sensing of Environment 155, 178–193. https://doi.org/10.1016/j.rse.2014.08.017

Kim, O.S., 2010. An Assessment of Deforestation Models for Reducing Emissions from Deforestation and Forest Degradation (REDD). Transactions in GIS 14, 631–654. https://doi.org/10.1111/j.1467-9671.2010.01227.x

Kuemmerle, T., Olofsson, P., Chaskovskyy, O., Baumann, M., Ostapowicz, K., Woodcock, C.E., Houghton, R.A., Hostert, P., Keeton, W.S., Radeloff, V.C., 2011. Post-Soviet farmland abandonment, forest recovery, and carbon sequestration in western Ukraine. Global Change Biology 17, 1335–1349. https://doi.org/10.1111/j.1365-2486.2010.02333.x

Kurz, W., Dymond, C., White, T., Stinson, G., Shaw, C., Rampley, G., Smyth, C., Simpson, B., Neilson, E., Trofymow, J., others, 2009. CBM-CFS3: a model of carbon-dynamics in forestry and land-use change implementing IPCC standards. Ecological Modelling 220, 480–504.

Le Quéré, C., Raupach, M.R., Canadell, J.G., Marland et al., G., Le Quéré et al., C., Le Quéré et al., C., Raupach, M.R., Canadell, J.G., Marland, G., Bopp, L., Ciais, P., Conway, T.J., Doney, S.C., Feely, R.A., Foster, P., Friedlingstein, P., Gurney, K., Houghton, R.A., House, J.I., Huntingford, C., Levy, P.E., Lomas, M.R., Majkut, J., Metzl, N., Ometto, J.P., Peters, G.P., Prentice, I.C., Randerson, J.T., Running, S.W., Sarmiento, J.L., Schuster, U., Sitch, S., Takahashi, T., Viovy, N., van der Werf, G.R., Woodward, F.I., 2009. Trends in the sources and sinks of carbon dioxide. Nature Geoscience 2, 831–836. https://doi.org/10.1038/ngeo689

Le Toan, T., Quegan, S., Davidson, M.W.J., Balzter, H., Paillou, P., Papathanassiou, K., Plummer, S., Rocca, F., Saatchi, S., Shugart, H., Ulander, L., 2011. The BIOMASS mission: Mapping global forest biomass to better understand the terrestrial carbon cycle. Remote Sensing of Environment, DESDynI VEG-3D Special Issue 115, 2850–2860. https://doi.org/10.1016/j.rse.2011.03.020

Liu, W., Gopal, S., Woodcock, C.E., 2004. Uncertainty and Confidence in Land Cover Classification Using a Hybrid Classifier Approach. Photogrammetric Engineering & Remote Sensing 70, 963–971. https://doi.org/10.14358/PERS.70.8.963

Loarie, S.R., Asner, G.P., Field, C.B., 2009. Boosted carbon emissions from Amazon deforestation. Geophys. Res. Lett. 36, L14810. https://doi.org/10.1029/2009GL037526

Loosvelt, L., Peters, J., Skriver, H., Lievens, H., Coillie, F.M.B.V., Baets, B.D., Verhoest, N.E.C., 2012. Random Forests as a tool for estimating uncertainty at pixel-level in SAR image classification. International Journal of Applied Earth Observation and Geoinformation 19, 173–184. https://doi.org/10.1016/j.jag.2012.05.011

MADS, IDEAM, 2014. Proposed Forest Reference Emission Level for deforestation in the Colombian Amazon Biome for results–based payments for REDD+ under the UNFCCC. Ministry of Environmentand Sustainable Development.

Mascorro, V.S., Coops, N.C., Kurz, W.A., Olguín, M., 2015. Choice of satellite imagery and attribution of changes to disturbance type strongly affects forest carbon balance estimates. Carbon Balance & Management 10, 30. https://doi.org/10.1186/s13021-015-0041-6

Masek, J.G., Goward, S.N., Kennedy, R.E., Cohen, W.B., Moisen, G.G., Schleeweis, K., Huang, C., 2013. United States Forest Disturbance Trends Observed Using Landsat Time Series. Ecosystems 16, 1087–1104. https://doi.org/10.1007/s10021-013-9669-9

McIver, D.K., Friedl, M.A., 2001. Estimating pixel-scale land cover classification confidence using nonparametric machine learning methods. IEEE Transactions on Geoscience and Remote Sensing 39, 1959–1968. https://doi.org/10.1109/36.951086

McRoberts, R.E., 2011. Satellite image-based maps: Scientific inference or pretty pictures? Remote Sensing of Environment 115, 715–724. https://doi.org/10.1016/j.rse.2010.10.013

McRoberts, R.E., Walters, B.F., 2012. Statistical inference for remote sensing-based estimates of net deforestation. Remote Sensing of Environment 124, 394–401. https://doi.org/10.1016/j.rse.2012.05.011

Meyer, V., Saatchi, S., Ferraz, A., Xu, L., Duque, A., García, M., Chave, J., 2019. Forest degradation and biomass loss along the Chocó region of Colombia. Carbon Balance and Management 14, 2. https://doi.org/10.1186/s13021-019-0117-9

Miller, J., Franklin, J., Aspinall, R., 2007. Incorporating spatial dependence in predictive vegetation models. Ecological Modelling 202, 225–242.

Mitchard, E.T., Saatchi, S.S., Baccini, A., Asner, G.P., Goetz, S.J., Harris, N.L., Brown, S., 2013. Uncertainty in the spatial distribution of tropical forest biomass: a comparison of pan-tropical maps. Carbon Balance and Management 8, 10. https://doi.org/10.1186/1750-0680-8-10

Moore, B., Boone, R., Hobbie, J., Houghton, R., Melillo, J., Peterson, B., Shaver, G., Vorosmarty, C., Woodwell, G., 1981. A simple model for analysis of the role of terrestrial ecosystems in the global carbon budget. Modelling the Global Carbon Cycle, SCOPE Report No 16.

Mosquera, O., Buurman, P., Ramirez, B.L., Amezquita, M.C., 2012a. Carbon stocks and dynamics under improved tropical pasture and silvopastoral systems in Colombian Amazonia. Geoderma 189–190, 81–86. https://doi.org/10.1016/j.geoderma.2012.04.022

Mosquera, O., Buurman, P., Ramirez, B.L., Amezquita, M.C., 2012b. Carbon replacement and stability changes in short-term silvo-pastoral experiments in Colombian Amazonia. Geoderma 170, 56–63. https://doi.org/10.1016/j.geoderma.2011.09.016

Navarrete, D., Sitch, S., Aragão, L.E.O.C., Pedroni, L., Duque, A., 2016. Conversion from forests to pastures in the Colombian Amazon leads to differences in dead wood dynamics depending on land management practices. Journal of Environmental Management 171, 42–51. https://doi.org/10.1016/j.jenvman.2016.01.037

Numata, I., Cochrane, M.A., Roberts, D.A., Soares, J.V., Souza, C.M., Sales, M.H., 2010. Biomass collapse and carbon emissions from forest fragmentation in the Brazilian Amazon Journal of Geophysical Research 115, G03027. https://doi.org/10.1029/2009JG001198

O'Connor, B., Secades, C., Penner, J., Sonnenschein, R., Skidmore, A., Burgess, N.D., Hutton, J.M., 2015. Earth observation as a tool for tracking progress towards the Aichi Biodiversity Targets. Remote Sensing in Ecology and Conservation 1, 19–28. https://doi.org/10.1002/rse2.4

Olofsson, P., Foody, G.M., Herold, M., Stehman, S.V., Woodcock, C.E., Wulder, M.A., 2014. Good practices for estimating area and assessing accuracy of land change. Remote Sensing of Environment 148, 42–57. https://doi.org/10.1016/j.rse.2014.02.015

Olofsson, P., Foody, G.M., Stehman, S.V., Woodcock, C.E., 2013. Making better use of accuracy data in land change studies: Estimating accuracy and area and quantifying uncertainty using stratified estimation. Remote Sensing of Environment 129, 122–131. https://doi.org/10.1016/j.rse.2012.10.031

Olofsson, P., Kuemmerle, T., Griffiths, P., Knorn, J., Baccini, A., Gancz, V., Blujdea, V., Houghton, R.A., Abrudan, I.V., Woodcock, C.E., 2011. Carbon implications of forest restitution in post-socialist Romania. Environmental Research Letters 6, 045202. https://doi.org/10.1088/1748-9326/6/4/045202

Olofsson, P., Torchinava, P., Woodcock, C.E., Baccini, A., Houghton, R.A., Ozdogan, M., Zhao, F., Yang, X., 2010. Implications of land use change on the national terrestrial carbon budget of Georgia. Carbon Balance and Management 5, 4. https://doi.org/10.1186/1750-0680-5-4

Olson, D.M., Dinerstein, E., 2002. The Global 200: Priority Ecoregions for Global Conservation. Annals of the Missouri Botanical Garden 89, 199–224. https://doi.org/10.2307/3298564

Orme, C.D.L., Davies, R.G., Burgess, M., Eigenbrod, F., Pickup, N., Olson, V.A., Webster, A.J., Ding, T.-S., Rasmussen, P.C., Ridgely, R.S., Stattersfield, A.J., Bennett, P.M., Blackburn, T.M., Gaston, K.J., Owens, I.P.F., 2005. Global hotspots of species richness are not congruent with endemism or threat. Nature 436, 1016–1019. https://doi.org/10.1038/nature03850

Pasquarella, V.J., Holden, C.E., Kaufman, L., Woodcock, C.E., 2016. From imagery to ecology: leveraging time series of all available Landsat observations to map and monitor

ecosystem state and dynamics. Remote Sensing in Ecology and Conservation 2, 152–170. https://doi.org/10.1002/rse2.24

Pasquarella, V.J., Holden, C.E., Woodcock, C.E., 2018. Improved mapping of forest type using spectral-temporal Landsat features. Remote Sensing of Environment 210, 193–207. https://doi.org/10.1016/j.rse.2018.02.064

Pearson, T.R.H., Brown, S., Murray, L., Sidman, G., 2017. Greenhouse gas emissions from tropical forest degradation: an underestimated source. Carbon Balance and Management 12, 3. https://doi.org/10.1186/s13021-017-0072-2

Pedregosa, F., Varoquaux, G., Gramfort, A., Michel, V., Thirion, B., Grisel, O., Blondel, M., Prettenhofer, P., Weiss, R., Dubourg, V., Vanderplas, J., Passos, A., Cournapeau, D., Brucher, M., Perrot, M., Duchesnay, E., 2011. Scikit-learn: Machine Learning in Python. Journal of Machine Learning Research 12, 2825–2830.

Phillips, J., Duque, Á., Scott, C., Wayson, C., Galindo, G., Cabrera, E., Chave, J., Peña, M., Álvarez, E., Cárdenas, D., Duivenvoorden, J., Hildebrand, P., Stevenson, P., Ramírez, S., Yepes, A., 2016. Live aboveground carbon stocks in natural forests of Colombia. Forest Ecology and Management 374, 119–128. https://doi.org/10.1016/j.foreco.2016.05.009

Phillips, J.F., Duque, A.J., Cabrera, K.R., Yepes, A.P., Navarrete, D.A., García, M.C., Álvarez, E., Cabrera, E., Cárdenas, D., Galindo, G., Ordoñez, M.F., Rodríguez, M.L., Vargas, D.M., 2011a. Estimación de las reservas potenciales de carbono almacenadas en la biomasa aérea en bosques naturales de Colombia.

Phillips, J.F., Duque, A.J., Yepes, A.P., Cabrera, E., García, M.C., Navarrete, D.A., Álvarez, E., Cárdenas, D., 2011b. Estimación de las reservas actuales (2010) de carbono almacenadas en la biomasa aérea en bosques naturales de Colombia: Estratificación, alometría y métodos analíticos.

Piao, S., Ciais, P., Friedlingstein, P., de Noblet-Ducoudré, N., Cadule, P., Viovy, N., Wang, T., 2009. Spatiotemporal patterns of terrestrial carbon cycle during the 20th century. Global Biogeochemical Cycles 23, n/a-n/a. https://doi.org/10.1029/2008GB003339

Ploberger, W., Krämer, W., 1992. The Cusum Test with Ols Residuals. Econometrica 60, 271–285. https://doi.org/10.2307/2951597

Pongratz, J., Reick, C.H., Raddatz, T., Claussen, M., 2009. Effects of anthropogenic land cover change on the carbon cycle of the last millennium. Global Biogeochemical Cycles 23. https://doi.org/10.1029/2009GB003488

Poorter, L., Bongers, F., Aide, T.M., Almeyda Zambrano, A.M., Balvanera, P., Becknell, J.M., Boukili, V., Brancalion, P.H.S., Broadbent, E.N., Chazdon, R.L., Craven, D., de Almeida-Cortez, J.S., Cabral, G.A.L., de Jong, B.H.J., Denslow, J.S., Dent, D.H., DeWalt, S.J., Dupuy, J.M., Durán, S.M., Espírito-Santo, M.M., Fandino, M.C., César, R.G., Hall, J.S., Hernandez-Stefanoni, J.L., Jakovac, C.C., Junqueira, A.B., Kennard, D., Letcher, S.G., Licona, J.-C., Lohbeck, M., Marín-Spiotta, E., Martínez-Ramos, M., Massoca, P., Meave, J.A., Mesquita, R., Mora, F., Muñoz, R., Muscarella, R., Nunes, Y.R.F., Ochoa-Gaona, S., de Oliveira, A.A., Orihuela-Belmonte, E., Peña-Claros, M., Pérez-García, E.A., Piotto, D., Powers, J.S., Rodríguez-Velázquez, J., Romero-Pérez, I.E., Ruíz, J., Saldarriaga, J.G., Sanchez-Azofeifa, A., Schwartz, N.B., Steininger, M.K., Swenson, N.G., Toledo, M., Uriarte, M., van Breugel, M., van der Wal, H., Veloso, M.D.M., Vester, H.F.M., Vicentini, A., Vieira, I.C.G., Bentos, T.V., Williamson, G.B., Rozendaal, D.M.A., 2016. Biomass resilience of Neotropical secondary forests. Nature 530, 211–214. https://doi.org/10.1038/nature16512

Potapov, P., Siddiqui, B.N., Iqbal, Z., Aziz, T., Zzaman, B., Islam, A., Pickens, A., Talero, Y., Tyukavina, A., Turubanova, S., Hansen, M.C., 2017. Comprehensive monitoring of Bangladesh tree cover inside and outside of forests, 2000–2014. Environmental Research Letters 12, 104015. https://doi.org/10.1088/1748-9326/aa84bb

Potapov, P.V., Dempewolf, J., Talero, Y., Hansen, M.C., Stehman, S.V., Vargas, C., Rojas, E.J., Castillo, D., Mendoza, E., A Calderón, Giudice, R., Malaga, N., Zutta, B.R., 2014. National satellite-based humid tropical forest change assessment in Peru in support of REDD+ implementation. Environmental Research Letters 9, 124012. https://doi.org/10.1088/1748-9326/9/12/124012

Prasad, M.S.G., Arora, M.K., 2014. A simple measure of confidence for fuzzy land-cover classification from remote-sensing data. International Journal of Remote Sensing 35, 8122–8137. https://doi.org/10.1080/01431161.2014.979303

Pugh, T.A.M., Lindeskog, M., Smith, B., Poulter, B., Arneth, A., Haverd, V., Calle, L., 2019. Role of forest regrowth in global carbon sink dynamics. Proceedings of the National Academy of Sciences 201810512. https://doi.org/10.1073/pnas.1810512116

QGIS Development Team, 2009. QGIS Geographic Information System. Open Source Geospatial Foundation.

Quaife, T., Quegan, S., Disney, M., Lewis, P., Lomas, M., Woodward, F.I., 2008. Impact of land cover uncertainties on estimates of biospheric carbon fluxes: IMPACT OF LAND COVER ON C FLUXES. Global Biogeochemical Cycles 22, n/a-n/a. https://doi.org/10.1029/2007GB003097

Quéré, C.L., Andrew, R.M., Friedlingstein, P., Sitch, S., Hauck, J., Pongratz, J., Pickers, P.A., Korsbakken, J.I., Peters, G.P., Canadell, J.G., Arneth, A., Arora, V.K., Barbero, L., Bastos, A., Bopp, L., Chevallier, F., Chini, L.P., Ciais, P., Doney, S.C., Gkritzalis, T.,

Goll, D.S., Harris, I., Haverd, V., Hoffman, F.M., Hoppema, M., Houghton, R.A., Hurtt, G., Ilyina, T., Jain, A.K., Johannessen, T., Jones, C.D., Kato, E., Keeling, R.F., Goldewijk, K.K., Landschützer, P., Lefèvre, N., Lienert, S., Liu, Z., Lombardozzi, D., Metzl, N., Munro, D.R., Nabel, J.E.M.S., Nakaoka, S., Neill, C., Olsen, A., Ono, T., Patra, P., Peregon, A., Peters, W., Peylin, P., Pfeil, B., Pierrot, D., Poulter, B., Rehder, G., Resplandy, L., Robertson, E., Rocher, M., Rödenbeck, C., Schuster, U., Schwinger, J., Séférian, R., Skjelvan, I., Steinhoff, T., Sutton, A., Tans, P.P., Tian, H., Tilbrook, B., Tubiello, F.N., Laan-Luijkx, I.T. van der, Werf, G.R. van der, Viovy, N., Walker, A.P., Wiltshire, A.J., Wright, R., Zaehle, S., Zheng, B., 2018. Global Carbon Budget 2018. Earth System Science Data 10, 2141–2194. https://doi.org/10.5194/essd-10-2141-2018

Ramírez-Delgado, J.P., Galindo, G.A., Yepes, A.P., Cabrera, E., 2018. Estimación de la degradación de bosques de Colombia a través de un análisis de fragmentación. Instituto de Hidrología, Meteorología y Estudios Ambientales - IDEAM, Ministerio de Ambiente y Desarrollo sostenible - MADS, Programa ONU-REDD Colombia, Bogota, D.C.

Reinmann, A.B., Hutyra, L.R., Trlica, A., Olofsson, P., 2016. Assessing the global warming potential of human settlement expansion in a mesic temperate landscape from 2005 to 2050. Science of The Total Environment 545–546, 512–524. https://doi.org/10.1016/j.scitotenv.2015.12.033

Robbins, M., Gallagher, C., Lund, R., Aue, A., 2011. Mean shift testing in correlated data. Journal of Time Series Analysis 32, 498–511. https://doi.org/10.1111/j.1467-9892.2010.00707.x

Rodríguez-Veiga, P., Barbosa-Herrera, A.P., Barreto-Silva, J.S., Bispo, P.C., Cabrera, E., Capachero, C., Galindo, G., Gou, Y., Moreno, L.M., Louis, V., Lozano, P., Pacheco-Pascagaza, A.M., Pachon-Cendales, I.P., Phillips-Bernal, J.F., Roberts, J., Salinas, N.R., Vergara, L., Zuluaga, A.C., Balzter, H., 2019. Mapping the spatial distribution of colombia's forest aboveground biomass using SAR and optical data. ISPRS - International Archives of the Photogrammetry, Remote Sensing and Spatial Information Sciences XLII-3/W7, 57–60. https://doi.org/10.5194/isprs-archives-XLII-3-W7-57-2019

Saatchi, S.S., Harris, N.L., Brown, S., Lefsky, M., Mitchard, E.T.A., Salas, W., Zutta, B.R., Buermann, W., Lewis, S.L., Hagen, S., Petrova, S., White, L., Silman, M., Morel, A., 2011. Benchmark map of forest carbon stocks in tropical regions across three continents. Proceedings of the National Academy of Sciences U. S. A. 108, 9899–9904. https://doi.org/10.1073/pnas.1019576108

Saldarriaga, J.G., West, D.C., Tharp, M.L., Uhl, C., 1988. Long-Term Chronosequence of Forest Succession in the Upper Rio Negro of Colombia and Venezuela. Journal of Ecology 76, 938–958. https://doi.org/10.2307/2260625

Sánchez-Cuervo, A.M., Aide, T.M., Clark, M.L., Etter, A., 2012. Land Cover Change in Colombia: Surprising Forest Recovery Trends between 2001 and 2010. PLoS ONE 7, e43943. https://doi.org/10.1371/journal.pone.0043943

Seabold, S., Perktold, J., 2010. Statsmodels: Econometric and statistical modeling with python, in: 9th Python in Science Conference.

Shadman Roodposhti, M., Aryal, J., Lucieer, A., Bryan, B.A., 2019. Uncertainty Assessment of Hyperspectral Image Classification: Deep Learning vs. Random Forest. Entropy 21, 78. https://doi.org/10.3390/e21010078

Sleeter, B.M., Sohl, T.L., Loveland, T.R., Auch, R.F., Acevedo, W., Drummond, M.A., Sayler, K.L., Stehman, S.V., 2013. Land-cover change in the conterminous United States from 1973 to 2000. Global Environmental Change 23, 733–748. https://doi.org/10.1016/j.gloenvcha.2013.03.006

Smith, I.A., Hutyra, L.R., Reinmann, A.B., Marrs, J.K., Thompson, J.R., 2018. Piecing together the fragments: elucidating edge effects on forest carbon dynamics. Frontiers in Ecology and the Environment 16, 213–221. https://doi.org/10.1002/fee.1793

Stehman, S.V., 2014. Estimating area and map accuracy for stratified random sampling when the strata are different from the map classes. International Journal of Remote Sensing 35, 4923–4939. https://doi.org/10.1080/01431161.2014.930207

Stehman, S.V., 2013. Estimating area from an accuracy assessment error matrix. Remote Sensing of Environment 132, 202–211. https://doi.org/10.1016/j.rse.2013.01.016

Stehman, S.V., 2012. Impact of sample size allocation when using stratified random sampling to estimate accuracy and area of land-cover change. Remote Sensing Letters 3, 111–120. https://doi.org/10.1080/01431161.2010.541950

Stehman, S.V., 2000. Practical Implications of Design-Based Sampling Inference for Thematic Map Accuracy Assessment. Remote Sensing of Environment 72, 35–45. https://doi.org/10.1016/S0034-4257(99)00090-5

Stysley, P.R., Coyle, D.B., Clarke, G.B., Frese, E., Blalock, G., Morey, P., Kay, R.B., Poulios, D., Hersh, M., 2016. Laser production for NASA's Global Ecosystem Dynamics Investigation (GEDI) lidar. Proeedings of SPIE 9832, id. 983207. doi:10.1117/12.2239889.

Sy, V.D., Herold, M., Achard, F., Beuchle, R., Clevers, J.G.P.W., Lindquist, E., Verchot, L., 2015. Land use patterns and related carbon losses following deforestation in South America. Environmental Research Letters 10, 124004. https://doi.org/10.1088/1748-9326/10/12/124004

Toomey, M., Roberts, D.A., Caviglia-Harris, J., Cochrane, M.A., Dewes, C.F., Harris, D., Numata, I., Sales, M.H., Sills, E., Souza, C.M., 2013. Long-term, high-spatial resolution carbon balance monitoring of the Amazonian frontier: Predisturbance and postdisturbance carbon emissions and uptake. Journal of Geophysical Research. Biogeosciences 118, 400-411. https://doi.org/10.1002/jgrg.20033

Tyukavina, A., Baccini, A., Hansen, M.C., Potapov, P.V., Stehman, S.V., Houghton, R.A., Krylov, A.M., Turubanova, S., Goetz, S.J., 2015. Aboveground carbon loss in natural and managed tropical forests from 2000 to 2012. Environmental Research Letters 10, 074002. https://doi.org/10.1088/1748-9326/10/7/074002

UNFCCC, 2018. FOCUS: Mitigation - Reporting on national implementation and MRV | UNFCCC [WWW Document]. URL https://unfccc.int/topics/mitigation/workstreams/measurement--reporting-and-verification (accessed 10.9.18).

UNODC, 2016. Monitoreo de territorios afectados por cultivos ilícitos 2015. Government of Colombia/United Nations Office on Drugs and Crime., Bogotá.

UN-REDD, 2016. UN-REDD Programme [WWW Document]. UN-REDD Programme. URL http://www.un-redd.org/ (accessed 7.25.16).

USGS, 2010. ESPA [WWW Document]. URL http://espa.cr.usgs.gov/index/ (accessed 7.26.16).

Verbesselt, J., Hyndman, R., Newnham, G., Culvenor, D., 2010a. Detecting trend and seasonal changes in satellite image time series. Remote Sensing of Environment 114, 106–115. https://doi.org/10.1016/j.rse.2009.08.014

Verbesselt, J., Hyndman, R., Zeileis, A., Culvenor, D., 2010b. Phenological change detection while accounting for abrupt and gradual trends in satellite image time series. Remote Sensing of Environment 114, 2970–2980. https://doi.org/10.1016/j.rse.2010.08.003

Woodcock, C.E., Allen, R., Anderson, M., Belward, A., Bindschadler, R., Cohen, W., Gao, F., Goward, S.N., Helder, D., Helmer, E., Nemani, R., Oreopoulos, L., Schott, J., Thenkabail, P.S., Vermote, E.F., Vogelmann, J., Wulder, M.A., Wynne, R., 2008. Free Access to Landsat Imagery. Science 320, 1011–1011. https://doi.org/10.1126/science.320.5879.1011a

Yepes, A., Navarrete, D., Phillips, J., Duque, A., Cabrera, E., Galindo, G., Vargas, D., García, M., Ordoñez, M., 2011. Estimación de las emisiones de dióxido de carbono generadas por deforestación durante el periodo 2005-2010. Instituto de Hidrología, Meteorología, y Estudios Ambientales-IDEAM-. Bogotá DC, Colombia.

Yin, H., Pflugmacher, D., Kennedy, R.E., Sulla-Menashe, D., Hostert, P., 2014. Mapping Annual Land Use and Land Cover Changes Using MODIS Time Series. IEEE Journal of Selected Topics in Applied Earth Observations and Remote Sensing 7, 3421–3427. https://doi.org/10.1109/JSTARS.2014.2348411

Zhu, Z., 2017. Change detection using landsat time series: A review of frequencies, preprocessing, algorithms, and applications. ISPRS Journal of Photogrammetry and Remote Sensing 130, 370–384. https://doi.org/10.1016/j.isprsjprs.2017.06.013

Zhu, Z., Woodcock, C.E., 2014a. Continuous change detection and classification of land cover using all available Landsat data. Remote Sensing of Environment 144, 152–171. https://doi.org/10.1016/j.rse.2014.01.011

Zhu, Z., Woodcock, C.E., 2014b. Automated cloud, cloud shadow, and snow detection in multitemporal Landsat data: An algorithm designed specifically for monitoring land cover change. Remote Sensing of Environment 152, 217–234. https://doi.org/10.1016/j.rse.2014.06.012

Zhu, Z., Woodcock, C.E., 2012. Object-based cloud and cloud shadow detection in Landsat imagery. Remote Sensing of Environment 118, 83–94. https://doi.org/10.1016/j.rse.2011.10.028

Zhu, Z., Woodcock, C.E., Olofsson, P., 2012. Continuous monitoring of forest disturbance using all available Landsat imagery. Remote Sensing of Environment, Landsat Legacy Special Issue 122, 75–91. https://doi.org/10.1016/j.rse.2011.10.030

CURRICULUM VITAE